Modeling Biological Oscillations

Hermann Riecke

Engineering Sciences and Applied Mathematics

Northwestern University

h-riecke@northwestern.edu

June 4, 2018

Contents

[1] (Turchin, 2003), online version at (after logging in): https://ebookcentral.proquest.com/lib/northwestern/detail.action?docID=

[2] Lotka points out that a large part of Volterra's results had already appeared earlier in Lotka's book Lotka (1920); Volterra (1926); Lotka (1927, 1925)

[3] (Turchin and Hanski, 1997; Turchin and Ellner, 2000; Turchin, 2003)

[4] (Fall et al., 2002) Ch.5

References

References

Aranson I.S., and Kramer L. (2002). The world of the complex Ginzburg-Landau equation. Rev. Mod. Phys. *74*, 99.

Aschoff J., and Wever R. (1962). Spontanperiodik des menschen bei ausschluss aller zeitgeber. Naturwissenschaften *49*, 337–&.

Barraquand F., Louca S., Abbott K.C., Cobbold C.A., Cordoleani F., DeAngelis D.L., Elderd B.D., Fox J.W., Greenwood P., Hilker F.M., Murray D.L., Stieha C.R., Taylor R.A., Vitense K., Wolkowicz G.S.K., and Tyson R.C. (2017). Moving forward in circles: challenges and opportunities in modelling population cycles. Ecology letters *20*, 1074–1092.

Berridge M.J., Lipp P., and Bootman M.D. (2000). The versatility and universality of calcium signalling. Nature Reviews Molecular Cell Biology *1*, 11–21.

Bliss R.D., Painter P.R., and Marr A.G. (1982). Role of feedback inhibition in stabilizing the classical operon. Journal of Theoretical Biology *97*, 177–193.

BUSS L.W., and JACKSON J.B.C. (1979). Competitive networks - non-transitive competitive relationships in cryptic coral-reef environments. American Naturalist *113*, 223–234.

Chaté H., and Manneville P. (1996). Phase diagram of the two-dimensional complex Ginzburg-Landau equation. Physica A *224*, 348.

Davidson A.J., Sellix M.T., Daniel J., Yamazaki S., Menaker M., and Block G.D. (2006). Chronic jet-lag increases mortality in aged mice. Current Biology *16*, R914–R916.

Dykhuizen D.E. (1998). Santa rosalia revisited: Why are there so many species of bacteria? Antonie Van Leeuwenhoek International Journal of General and Molecular Microbiology *73*, 25–33.

Eberhardt L.L. (1997). Is wolf predation ratio-dependent? Canadian Journal of Zoology-revue Canadienne De Zoologie *75*, 1940–1944.

Edery I., Zwiebel L.J., Dembinska M.E., and Rosbash M. (1994). Temporal phosphorylation of the drosophila period protein. Proceedings of the National Academy of Sciences of the United States of America *91*, 2260–2264.

Elowitz M.B., and Leibler S. (2000). A synthetic oscillatory network of transcriptional regulators. Nature *403*, 335–338.

Elton C., and Nicholson M. (1942). The ten-year cycle in numbers of the lynx in canada. Journal of Animal Ecology *11*, 215–244.

Erlinge S. (1974). Distribution, territoriality and numbers of the weasel mustela nivalis in relation to prey abundance. Oikos *25*, 308–314.

Fall C., Marland E., Wagner J., and Tyson J., eds. (2002). Computational Cell Biology (Springer).

Fraser A.M., and Swinney H.L. (1986). Independent coordinates for strange attractors from mutual information. Phys. Rev. A *33*, 1134–1140.

Frean M., and Abraham E.R. (2001). Rock-scissors-paper and the survival of the weakest. Proceedings of the Royal Society B-biological Sciences *268*, 1323–1327.

Friel D.D., and Tsien R.W. (1992). Phase-dependent contributions from ca2+ entry and ca2+ release to caffeine-induced [ca2+]i oscillations in bullfrog sympathetic neurons. Neuron *8*, 1109–1125.

Goldbeter A. (1995). A model for circadian oscillations in the drosophila period protein (per). Proceedings of the Royal Society B-biological Sciences *261*, 319–324.

Goodwin B. (1963). Temporal organization in cells (Academic Press).

Goodwin B.C. (1965). Oscillatory behavior in enzymatic control processes. Advances in enzyme regulation *3*, 425–438.

Goyal A., and Maslov S. (2018). Diversity, stability, and reproducibility in stochastically assembled microbial ecosystems. Phys. Rev. Lett. *120*, 158102.

Griffith J.S. (1968). Mathematics of cellular control processes .i. negative feedback to 1 gene. Journal of Theoretical Biology *20*, 202–&.

Gyorke S., and Fill M. (1993). Ryanodine receptor adaptation - control mechanism of ca2+-induced ca2+ release in heart. Science *260*, 807–809.

Hall J.C., and Rosbash M. (1987). Genes and biological rhythms. Trends in Genetics *3*, 185–191.

HANSKI I., HANSSON L., and HENTTONEN H. (1991). Specialist predators, generalist predators, and the microtine rodent cycle. Journal of Animal Ecology *60*, 353–367.

Hanski I., and Korpimaki E. (1995). Microtine rodent dynamics in northern europe: parameterized models for the predator-prey interaction. Ecology .

Hardin P.E., Hall J.C., and Rosbash M. (1990). Feedback of the drosophila period gene-product on circadian cycling of its messenger-rna levels. Nature *343*, 536–540.

Harrison G.W. (1995). Comparing predator-prey models to luckinbills experiment with didinium and paramecium. Ecology *76*, 357–374.

Henttonen H., and Hanski I. (2000). Chaos in real data. The analysis of non-linear dynamics from short ecological time series (Kluwer), chap. Population dynamics of small rodents in northern Fennoscandia, p. 73.

Holling C.S. (1965). The functional response of predators to prey density and its role in mimicry and population regulation. Memoirs of the Entomological Society of Canada *97*, 5.

Holling C.S. (1966). The functional response of invertebrate predators to prey density. Memoirs of the Entomological Society of Canada *98*, 5–86.

HUTCHINSON G.E. (1961). The paradox of the plankton. American Naturalist *95*, 137–145.

Joly E. (2017). Baseball and jet lag: Correlation does not imply causation. Proceedings of the National Academy of Sciences of the United States of America *114*, E3168–E3168.

Keizer J., and Levine L. (1996). Ryanodine receptor adaptation and ca2+-induced ca2+ release-dependent ca2+ oscillations. Biophysical Journal *71*, 3477–3487.

Kerr B., Riley M.A., Feldman M.W., and Bohannan B.J.M. (2002). Local dispersal promotes biodiversity in a real-life game of rock-paper-scissors. Nature *418*, 171–174.

Klarsfeld A. (2013). At the dawn of chronobiology. https://sites.google.com/site/klarsfeldandre/les-horloges-du-vivant .

Konopka R.J., and Benzer S. (1971). Clock mutants of drosophila-melanogaster. Proceedings of the National Academy of Sciences of the United States of America *68*, 2112–+.

Kuba K., and Nishi S. (1976). Rhythmic hyperpolarizations and depolarization of sympathetic-ganglion cells induced by caffeine. Journal of Neurophysiology *39*, 547–563.

Lechleiter J., Girard S., Peralta E., and Clapham D. (1991). Spiral calcium wave-propagation and annihilation in xenopus-laevis oocytes. Science *252*, 123–126.

Lee C.G., Parikh V., Itsukaichi T., Bae K., and Edery I. (1996). Resetting the drosophila clock by photic regulation of per and a per-tim complex. Science *271*, 1740–1744.

Leloup J.C., and Goldbeter A. (1998). A model for circadian rhythms in drosophila incorporating the formation of a complex between the per and tim proteins. Journal of Biological Rhythms *13*, 70–87.

LESLIE P.H. (1948). Some further notes on the use of matrices in population mathematics. Biometrika *35*, 213–245.

Leybaert L., and Sanderson M.J. (2012). Intercellular ca(2+) waves: mechanisms and function. Physiological reviews *92*, 1359–1392.

Lotka A. (1925). Elements of Physical Biology (Williams and Wilkins).

Lotka A.J. (1920). Analytical note on certain rhythmic relations in organic systems. Proceedings of the National Academy of Sciences of the United States of America *6*, 410–415.

Lotka A.J. (1927). Fluctuations in the abundance of a species considered mathematically. Nature *119*, 12–12.

LUCKINBILL L.S. (1973). Coexistence in laboratory populations of paramecium-aurelia and its predator didinium-nasutum. Ecology *54*, 1320–1327.

McGeown J.G. (2010). Seeing is believing! imaging ca2+-signalling events in living cells. Experimental Physiology *95*, 1049–1060.

Myers M.P., WagerSmith K., RothenfluhHilfiker A., and Young M.W. (1996). Light-induced degradation of timeless and entrainment of the drosophila circadian clock. Science *271*, 1736–1740.

Recht L.D., Lew R.A., and Schwartz W.J. (1995). Baseball teams beaten by jet-lag. Nature *377*, 583–583.

Reinberg A., and Halberg F. (1971). Circadian chironopharmacology. Annual Review of Pharmacology *11*, 455–+.

ROSENZWEIG M.L., and MACARTHUR R.H. (1963). Graphical representation and stability conditions of predator-prey interactions. American Naturalist *97*, 209–+.

Sinervo B., and Lively C.M. (1996). The rock-paper-scissors game and the evolution of alternative male strategies. Nature *380*, 240–243.

Song A., Severini T., and Allada R. (2017). How jet lag impairs major league baseball performance. Proceedings of the National Academy of Sciences of the United States of America *114*, 1407–1412.

Strogatz S. (2015). Nonlinear Dynamics and Chaos (Westview Press).

Szczesny B., Mobilia M., and Rucklidge A.M. (2013). When does cyclic dominance lead to stable spiral waves? Epl *102*, 28012.

Turchin P. (2003). Complex Population Dynamics (Princeton).

Turchin P., and Ellner S.P. (2000). Living on the edge of chaos: Population dynamics of fennoscandian voles. Ecology *81*, 3099–3116.

Turchin P., and Hanski I. (1997). An empirically based model for latitudinal gradient in vole population dynamics. American Naturalist *149*, 842–874.

Turchin P., Lorio P.L., Taylor A.D., and Billings R.F. (1991). Why do populations of southern pine beetles (coleoptera, scolytidae) fluctuate. Environmental Entomology *20*, 401–409.

Turchin P., and Ostfeld R.S. (1997). Effects of density and season on the population rate of change in the meadow vole. Oikos *78*, 355–361.

Tyson J.J., Hong C.I., Thron C.D., and Novak B. (1999). A simple model of circadian rhythms based on dimerization and proteolysis of per and tim. Biophysical Journal *77*, 2411–2417.

Volterra V. (1926). Fluctuations in the abundance of a species considered mathematically. Nature *118*, 558–560.

Yang G.R., Chen L.H., Grant G.R., Paschos G., Song W.L., Musiek E.S., Lee V., McLoughlin S.C., Grosser T., Cotsarelis G., and FitzGerald G.A. (2016). Timing of expression of the core clock gene bmal1 influences its effects on aging and survival. Science Translational Medicine *8*, 324ra16.

Yodzi P. (1989). Introduction to Theoretical Ecology (Harper and Row).

1 Introduction

Oscillations and more complex dynamics arise in a wide range or biological systems, differing widely in scale, ranging from the population dynamics of hares and voles, the circadian rhythms in animals and humans, to the competition between 'warfaring' bacteria and calcium oscillations within individual cells.

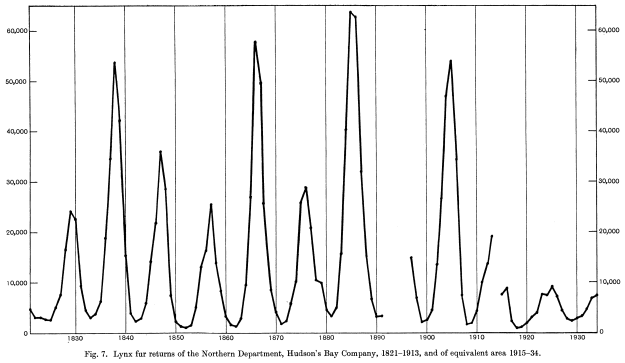

Fig. 7. Lynx fur returns of the Northern Department, Hudson's Bay Company, 1821–1913, and of equivalent area 1915–34.

Figure 1: 10-year lynx cycle in Northern Canada, based on fir catches/sales reported by the Hudson'ts Bay Company (Elton and Nicholson, 1942).

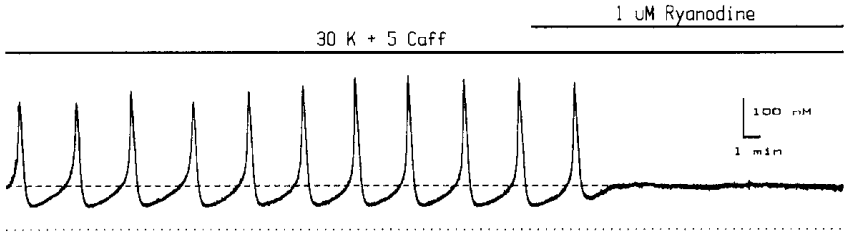

Figure 2: Calcium oscillations in bullfrog sympathetic neuron Friel and Tsien (1992). These oscillations arise in response to caffeine.

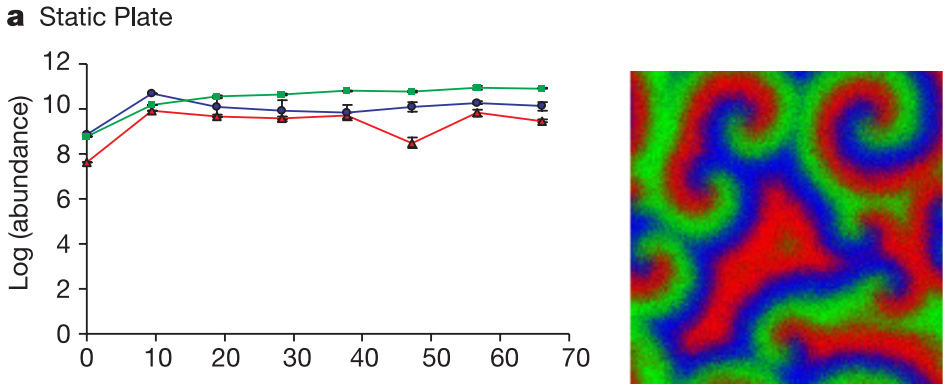

Figure 3: Competition between three strains of bacteria: killer bacteria, resistant bacteria, and susceptible bacteria Kerr et al. (2002); Szczesny et al. (2013).

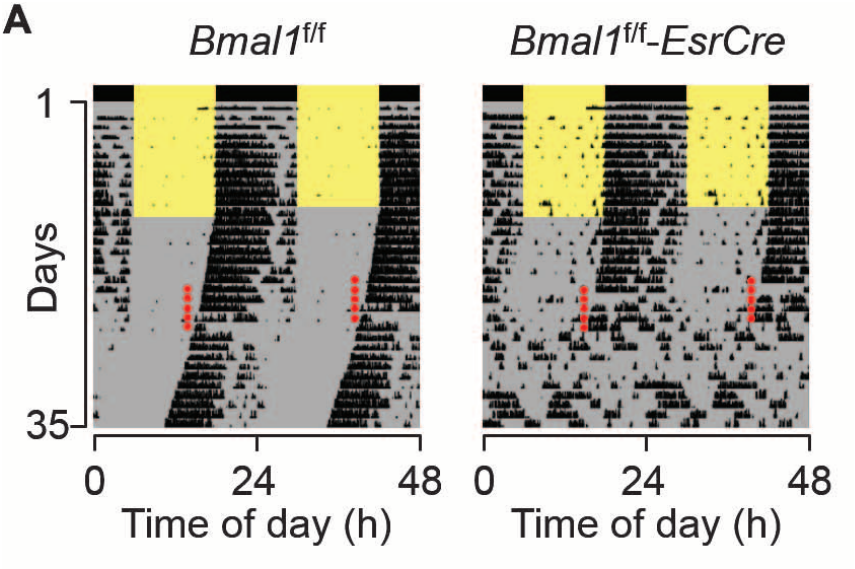

Figure 4: Circadian rhythms in mice (and other animals) are driven by genetic oscillators. Mutants lacking the *Bmal1* 'clock gene' (gene loss triggered at red bars) lose the circadian rhythm (Yang et al., 2016).

2 Population Oscillations[5]

2.1 General Considerations

Population dynamics is one of those examples that are always used in introductory classes on differential equations. How useful is mathematical modeling for population dynamics beyond that very basic level? Can it capture convincingly more complex dynamics than exponential growth and saturation?

Quite a few ecological systems exhibit non-trivial dynamics like oscillations:

- lynx-hare
- voles preyed upon by weasels and birds
- competition between bacteria
- ciliate *Didinium nasutum* preying on ciliate *Paramecium* [6]

[5] (Turchin, 2003), online version at (after logging in): https://ebookcentral.proquest.com/lib/northwestern/detail.action?docID=

[6] By Barfooz at the English Wikipedia. - Originally uploaded to the English Wikipedia, where it was made by Barfooz., CC BY-SA 3.0, https://commons.wikimedia.org/w/index.php?curid=172055

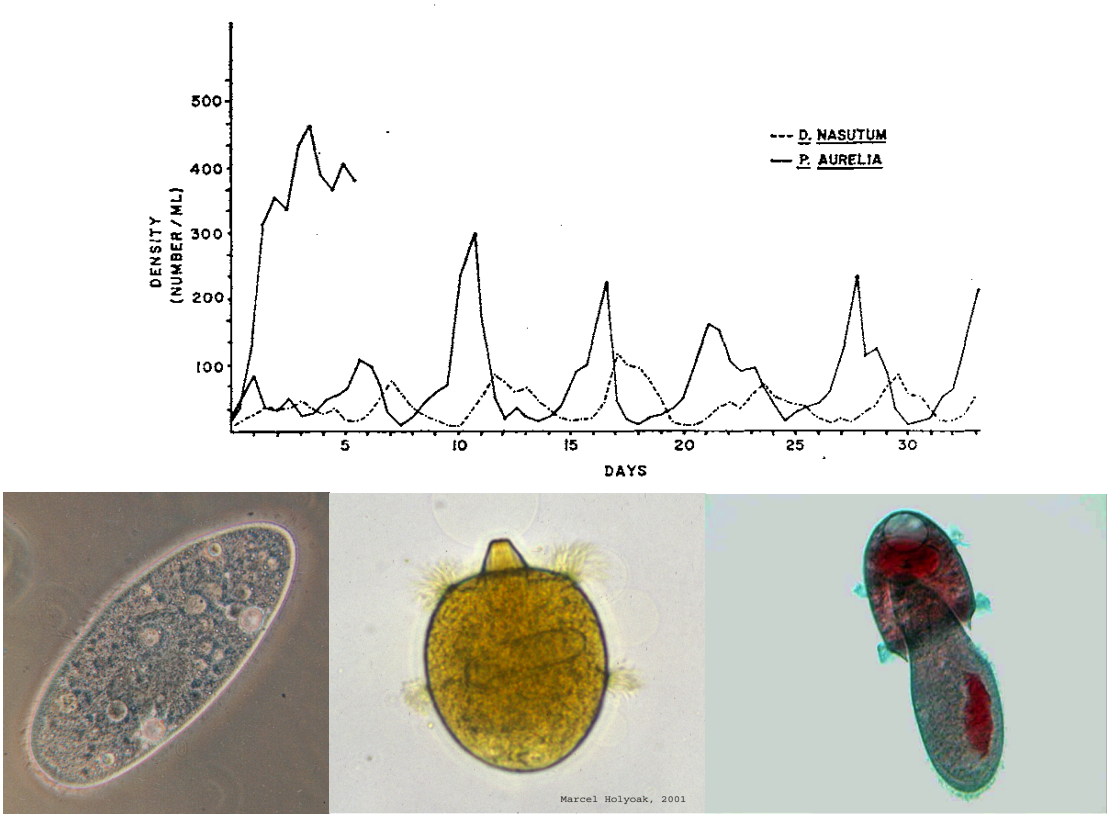

Figure 5: a) *Didinium nasutum* preying on *Paramecium LUCKINBILL (1973).*

What types of models might be useful in population modeling?

- Agent based modeling:
  Since all population dynamics consist of a change in the number and possibly age and other properties of individual animals one could aim at model each of these individuals
  - interactions like predation or competition for food can be modeled quite explicitly
  - agents age with time. This can capture aspects like
    * delay in reproduction, change in fertility
    * change in resilience with respect to environmental changes or predators (pups vs. mature vs. old animals)
  - spatial dependence: allows migration of the agents
  - when the biological system has relatively small popluations, the discreteness of the number of agents can be important
    * an individual cannot 'die partially', at the time of its death the population suddenly changes
    * the timing of that death is typically not deterministic: the discreteness introduces noise into the system
    * when the last individuum of a population dies, that population goes extinct.

  - when the biological system consists of a large number of individuals, the computational effort may be too large.
  - analytical methods are of limited use

- Population models: describe only the density or total population size
  - need the continuum limit in the number of agents by assuming a large number of individuals
  - continuum limit allows the use of differential equations
  - spatial aspects can be captured with partial differential equations: migration, 'clumping'
  - to capture age structure one would need multiple coupled differential equations, one for each age group
  - interactions like predation have to be treated using some effective interaction like mass action: assume the probability of an interaction is proportional to the density. The classic Lotka-Volterra model is a minimal model of that from.
  - Temporal evolution
    * assuming smooth changes in the densities: differential equation
    * population dynamics can be seasonal: e.g. hatching every spring. Then discrete maps from one year to the next could be more suitable.
    * if the available data are only semi-annually (e.g. spring/fall), it may more appropriate to map spring $\rightarrow$ spring or fall $\rightarrow$ fall.

General conditions for oscillations

- Autonomous differential equations:
  - in 1 dimension the solution either converges to a fixed points or goes to infinity during an oscillation the time derivative has to have opposite signs when the solution goes through any specific value $\hat{y}$ sequentially

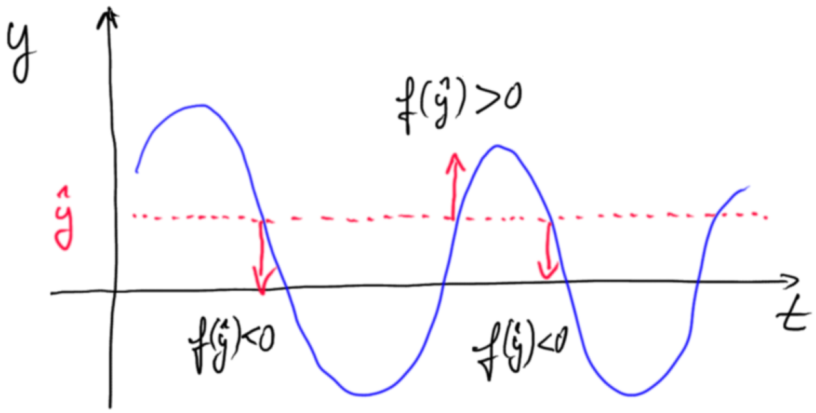

Figure 6: Sketch of phase line: impossibility of oscillations. For any

- we need at least 2 dimensions, i.e. 2^{nd}-order differential equation or a system of 2 1^{st}-order equations

- Maps:

$$y_{n+1} = f(y_n)$$

  - a fixed point in the map need not correspond to a fixed point in the full system: it could be periodic with a period that is a fraction of the time between iterates of the map.
  - in 1 dimension the solution need not go to a fixed point: it can jump between multiple points.
    If there are only a finite number of such points, the solution of the underlying system has a period that is rationally related to the time between iterates of the map.
    The solution can also be chaotic with infinitely many such points.

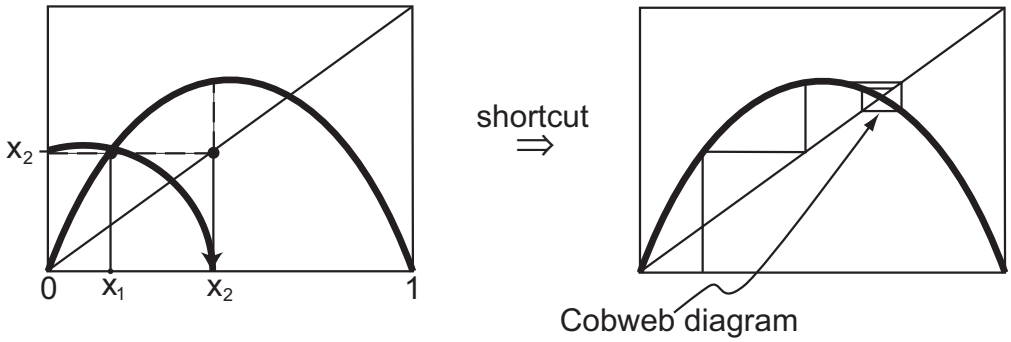

Figure 7: Sketch of cobweb diagram for period 2.

2.2 Time-Series Methods for Oscillations

We will first look at a number of ways to represent dynamical behavior and characterize oscillations.

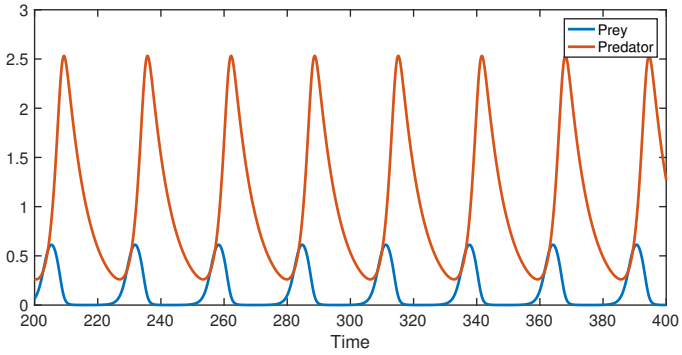

Figure 8: Temporal evolution of prey and predator in a model (Rosenzweig-MacArthur model).

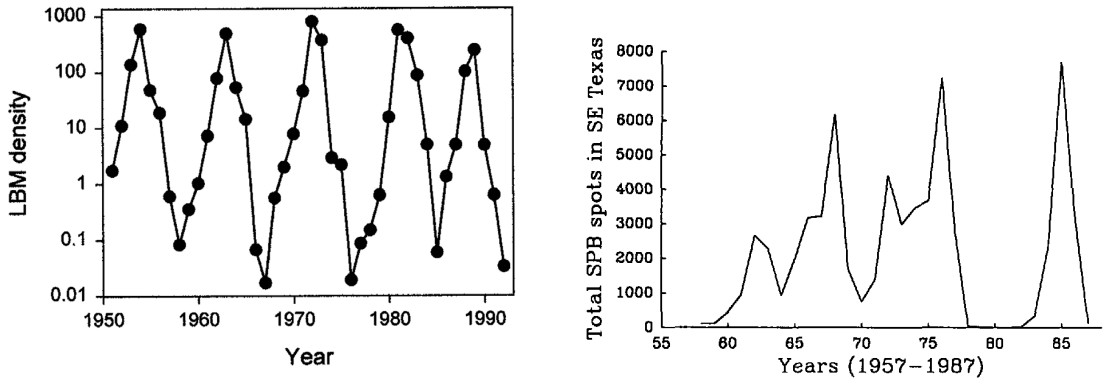

Figure 9: Time series. a) Oscillations in the larch budmoth (larva/kg of larch branches) Turchin (2003). b) Oscillatory behavior in the population of the Southern Pine beetle Turchin et al. (1991).

Notes

- Aspects that often arise in the data for population dynamics:
  - not many oscillations are captured: the periods are often on the order of a few years
  - data are quite noisy, since the investigated populations are under the influence of many environmental factors (other species, weather,...)
  - the hares are eaten by predators: often only a single species is measured, although oscillations typically require more than a single species.
  - how reliable and precise are the measurements?

- counting lynx via counting number of furs returned for sale is a relatively indirect measurement

Fourier Spectrum

For oscillations given by $y(t)$ it is very natural to characterize them using their Fourier spectrum

$$\hat{y}(\omega) = \int_{-\infty}^{+\infty} y(t)\, e^{-i\omega t} dt.$$

However, we have data only for a finite time interval, which implies a lowest non-zero frequency of $\frac{2\pi}{t_{max}}$,

$$\hat{y}_n = \int_0^{t_{max}} y(t)\, e^{-i\frac{2\pi}{t_{max}}nt} dt \qquad n \text{ integer},$$

and therefore the Fourier spectrum consists of a discrete set Fourier modes with frequencies given by $\frac{2\pi}{t_{max}}n$.

The Fourier decomposition effectively assumes that the data $y(t)$ have a period of t_{max}, i.e. the Fourier decomposition of $y(t)$ is the same as that of a function that is a periodic continuation of $y(t)$ with period tax.

However:

- the experimental data will in general not have a period that is an integer fraction of the duration of the experiment $\Rightarrow$ the periodic continuation that the Fourier decomposition automatically assumes generates in general a function that is not continuous from $t = t_{max}$ to $t = 0$.

Consider a simple example $y(t) = \cos\omega t$

$$\hat{y}_n = \int_0^{t_{max}} \cos\omega t\, e^{-i\frac{2\pi}{t_{max}}nt} dt$$

For $\omega = \frac{2\pi}{t_{max}}m$ one has the orthogonality of the Fourier modes $e^{i\frac{2\pi}{T}nt}$ and $e^{i\frac{2\pi}{T}mt}$ when $n \neq m$ yielding only a single non-zero Fourier component,

$$\hat{y}_n = \begin{cases} \frac{1}{2}t_{max} & \text{for} \quad n = m \\ 0 & \text{for} \quad n \neq m \end{cases}$$

For general frequencies ω this is not the case, even though $y(t)$ is a simple trig function: its periodic continuation beyond the interval $[0, t_{max}]$ is not continuous.

For simplicity consider $\omega = \frac{2\pi}{t_{max}}\left(m + \frac{1}{2}\right)$

$$\begin{aligned} \hat{y}_n &= \frac{1}{2}\int_0^{t_{max}} e^{i\left(\frac{2\pi}{t_{max}}m + \frac{\pi}{t_{max}} - \frac{2\pi}{t_{max}}n\right)t} dt + \frac{1}{2}\int_0^{t_{max}} e^{i\left(-\frac{2\pi}{t_{max}}m - \frac{\pi}{t_{max}} - \frac{2\pi}{t_{max}}n\right)t} dt \\ &= \cdots \\ &= \frac{4in}{-4n^2 + (1+2m)^2}\frac{t_{max}}{\pi} \end{aligned}$$

Notes:

- all Fourier modes are now non-zero, even though the true signal only has a single Fourier mode.
- the magnitude of the Fourier modes decays like $\frac{1}{n}$ for large n, which represents a relatively slow decay (compared to an exponential decay, say).

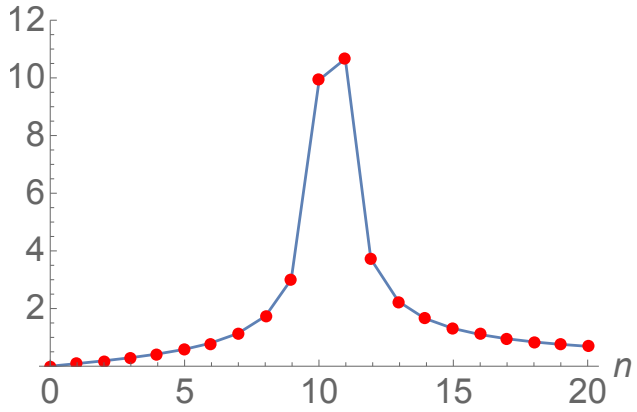

Figure 10: Fourier spectrum of $y(t) = \cos\left(\frac{2\pi}{t_{max}}\left(m + \frac{1}{2}\right)t\right)$ showing the broadening of the spectral peak due to the mismatch between the period of the oscillation and the duration of the time series.

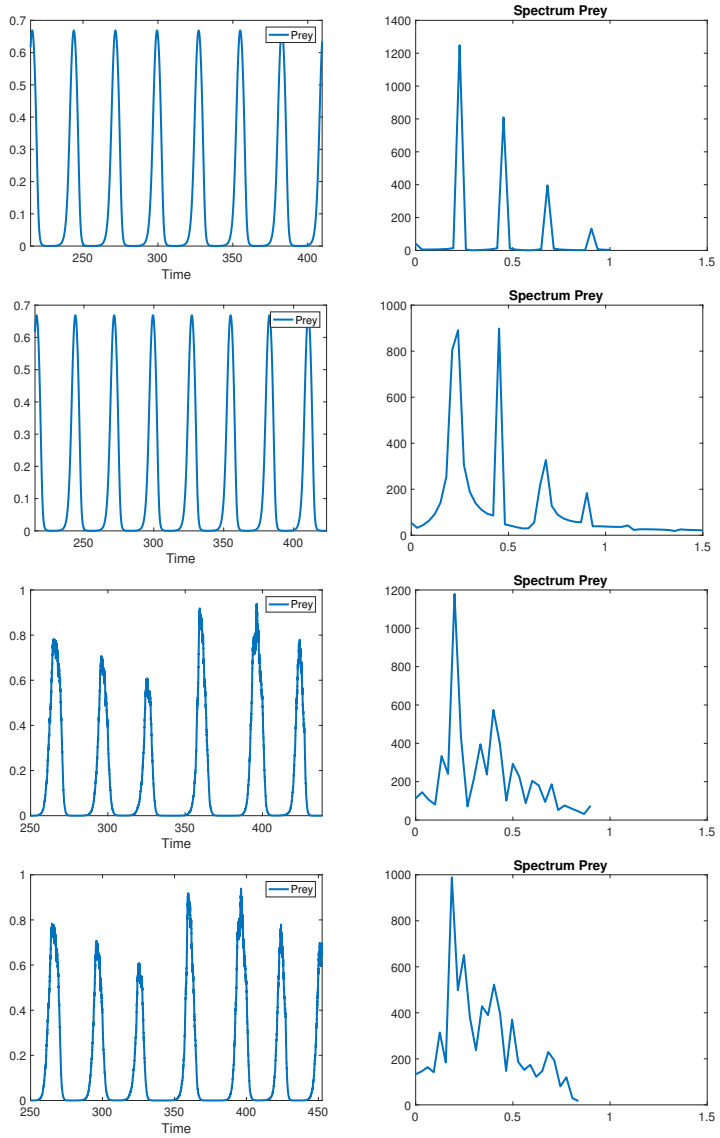

Figure 11: Prey evolution and Fourier spectrum of its mean-subtracted time series. a) no noise, $t_{max} = 194.6$. b) no noise. $t_{max} = 208.6$. c) $\sigma_\zeta = 0.1$, $t_{max} = 188.6$, d) $\sigma_\zeta = 0.1$, $t_{max} = 202.6$. Mismatch and noise both lead to a broadening of the spectral peaks, making it difficult to assess whether a peak is 'real' or only due to the finite duration of the time series.

Notes:

- In real data one could omit data at the end points, but when the data are not very clean it is not clear how many to drop.
- It is typically useful to compute the spectrum after subtracting the mean to avoid a large peak at $\omega = 0$.

Autocorrelation Function

A quantitative measure for the duration over which oscillations are coherent or persist is the autocorrelation function

$$C_{yy}(\tau) = \frac{\int_{-\infty}^{\infty} y(t')\, y(t'-\tau)\, dt'}{\int_{-\infty}^{\infty} y(t')^2\, dt'} \equiv \langle y(t) y(t-\tau) \rangle.$$

The autocorrelation function can also be obtained from the Fourier spectrum

$$\begin{aligned} \int_{-\infty}^{\infty} y(t')\, y(t'-\tau)\, d\tau \qquad &= \qquad \int dt' \int d\omega' \int d\omega'\, y(\omega)\, y(\omega')\, e^{i\omega t' + i\omega'(t'-\tau)} \\ \underbrace{=}_{\text{orthogonality}} \qquad & 2\pi \int d\omega\, y(\omega)\, \underbrace{y(-\omega)}_{y^*(\omega)}\, e^{i\omega\tau} \\ & 2\pi \int d\omega\ |y(\omega)|^2\, e^{i\omega\tau} \end{aligned}$$

The orthogonality used is

$$\int_{-\infty}^{+\infty} e^{i\omega t} dt = 2\pi\delta(\omega)$$

where $\delta(\omega)$ is the Dirac δ-function defined via

$$\delta(x) = 0 \quad \text{for} \quad x \neq 0 \qquad \int_{-\epsilon}^{+\epsilon} \delta(x)\, dx = 1.$$

Thus, the autocorrelation function is essentially given by the Fourier transform of the power spectrum (Wiener-Khinchin theorem).

For discrete, finite data set

$$\hat{C}_{yy}(m) = \frac{1}{N-|m|} \sum_{n=0}^{N-m-1} y_{n+m} y_n \qquad |m| \leq N-1 \tag{1}$$

$$C_{yy}(m) = \frac{\hat{C}_{yy}(m)}{\hat{C}_{yy}(0)}.$$

Note:

- The normalization in the discrete version takes into account that with increasing values of m the number of terms in the sum decreases.
- In Matlab the discrete version (1) is obtained with `xcorr` with option `'unbiased'`
- For a strictly periodic function with period T the autocorrelation function is also periodic with that period.
- For irregular/noisy oscillations the envelope of $C_{yy}(t)$ decays with time. The amount by which it decays in one period is a quantitative measure of the irregularity of the oscillations.

- When calculating the autocorrelation using the Fourier transform on the finite interval, the duration of the interval can significantly affect the results. When using the direct sum, changing the finite length has less of an impact.

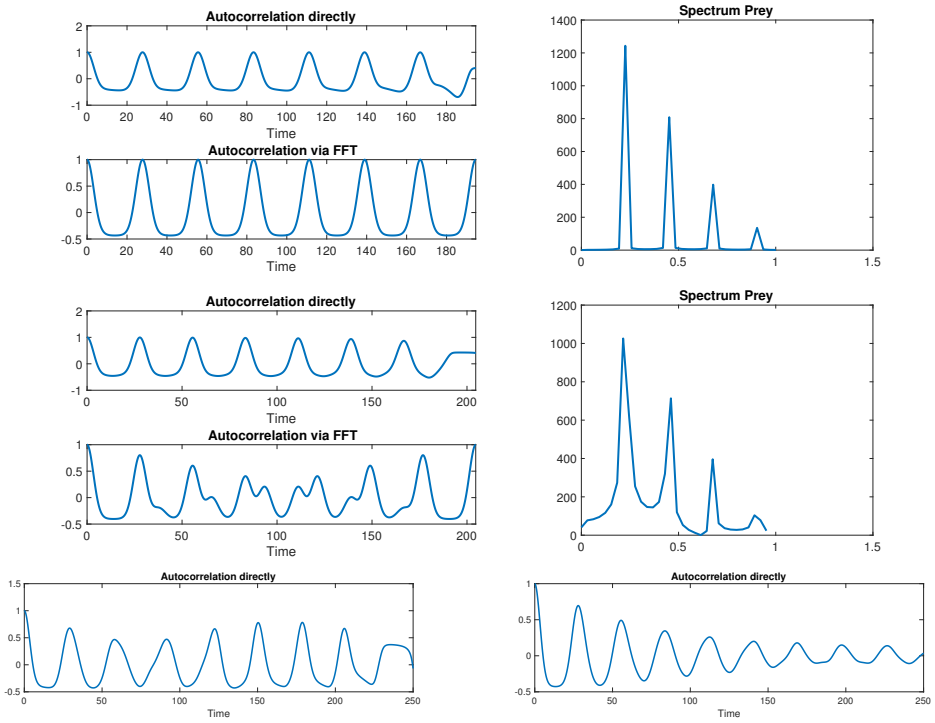

Figure 12: Autocorrelation function without and with noise from simulation data. a) For different durations via (1) and via FFT for $t_{max} = 194.6$ and $t_{max} = 204.6$. c) Autocorrelation with noise $\sigma_\zeta = 0.05$ with $t_{max} = 250$ and $t_{max} = 5000$.

More generally, it is also useful to introduce the cross-correlation function between two different variables

$$C_{xy}(\tau) = \frac{\int x(t')\, y(t'-\tau)\, dt'}{\sqrt{\int x(t')^2\, dt'}\sqrt{\int y(t')^2\, dt'}}.$$

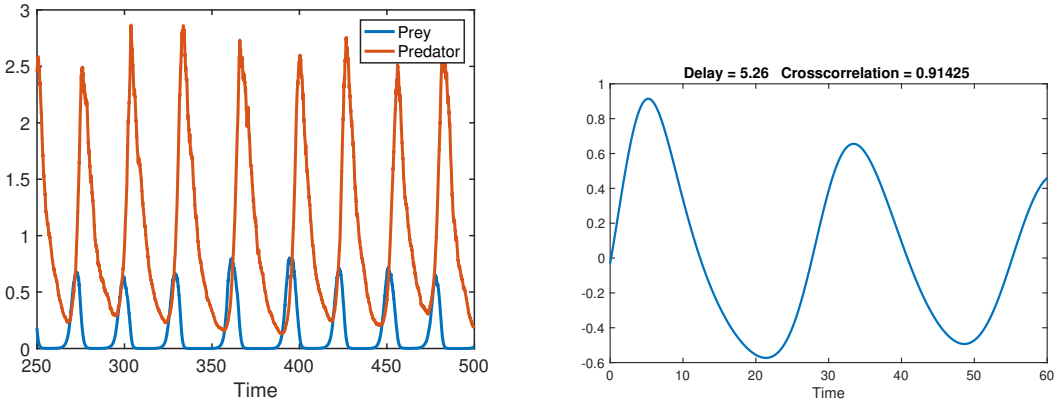

Figure 13: The cross-correlation between predator and prey shows how the predator dynamics is lagging that of the prey. $\sigma_\zeta = 0.05$.

Phase Plane Analysis

In dynamical systems it is often very useful to visualize the dynamics geometrically. For simple oscillations in 2 variables this can be done in the phase plane.

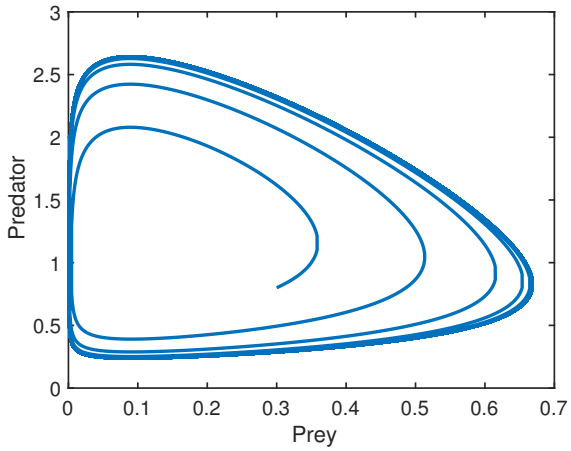

Figure 14: Prey-predator phase plane.

Goal of a phase plane/space representation

- Representation in which the evolution of the system is represented as a *flow*.
  - This requires, in particular, that for any point in that phase space the future evolution is unique. Thus, at each point a vector is defined that shows the time derivative of that point, i.e. the dynamics is to define a *vector field*.
  - Trajectories cannot intersect in phase space. Trajectories can come together only at fixed points: the vector field vanishes at those points and the dynamics

do not go through the fixed point.

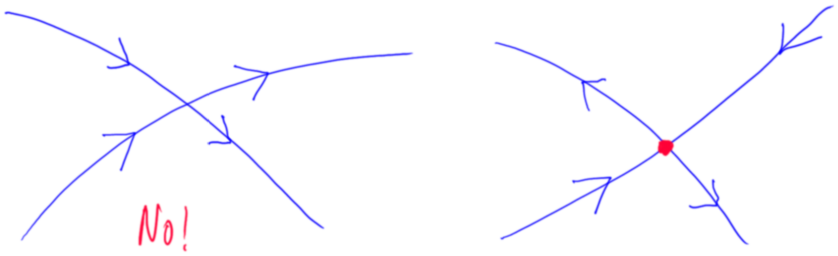

However

- In population dynamics often only data on one species are available, i.e. only a single variable is measured.

As a motivation, consider instead of n first-order equations a single n^{th}-order equation. Then any initial condition $(y(t_i), \dot{y}(t_i), \ddot{y}(t_i), \ldots, \frac{d^n y}{dt^n}|_{t_i})$ defines a unique solution. Instead of using n variables one could imagine using y and its first $n-1$ derivatives as the coordinates for the phase space. From any point in this space a unique solution would arise. Starting from experimental data, we have only $y(t_j)$ at discrete time points, but no derivatives. If the time points were sufficiently close one could obtain the derivatives approximatively using finite differences. To obtain the point in phase space that corresponds to the solution at time t_0 this would involve not only $y(t_i)$ but also y at time points around t_i. This suggests using directly $y(t_i)$ and y at a number of earlier times, $y(t_{i-k})$, $k = 1 \ldots n-1$.

Takens Embedding Theorem

- Floris Takens: a d-dimensional attractor of a dynamical system can *always* be embedded in Euclidean space using *at most* $k = 2d+1$ time-delay coordinates.
  For a periodic orbit therefore $k \leq 3$.

Therefore we can in general represent the dynamics of the system by using sufficiently many delay coordinates.

How should the delay be picked?

- To approximate derivatives one would need to pick a short delay, the shorter the better the approximation.
  However, then $y(t)$ and $y(t-\tau)$ are very close: the points fall very close to the diagonal, amounting to poor visualization of the attractor.
- For long delays $y(t)$ will have 'forgotten' the value of $y(t-\tau)$ and $y(t)$ will depend very little on $y(t-\tau)$

We want:

- Compared to $y(t)$ the earlier value $y(t-\tau)$ should provide *additional* information about the current state
  $\Rightarrow y(t)$ and $y(t-\tau)$ should not be correlated or anti-correlated
  Pick the smallest value of τ for which

$$C_{yy}(\tau) = 0.$$

- If the oscillations are about a large value, C_{yy} may not vanish for any delay:
  - Need to subtract the mean before computing the correlation, i.e. compute the covariance.

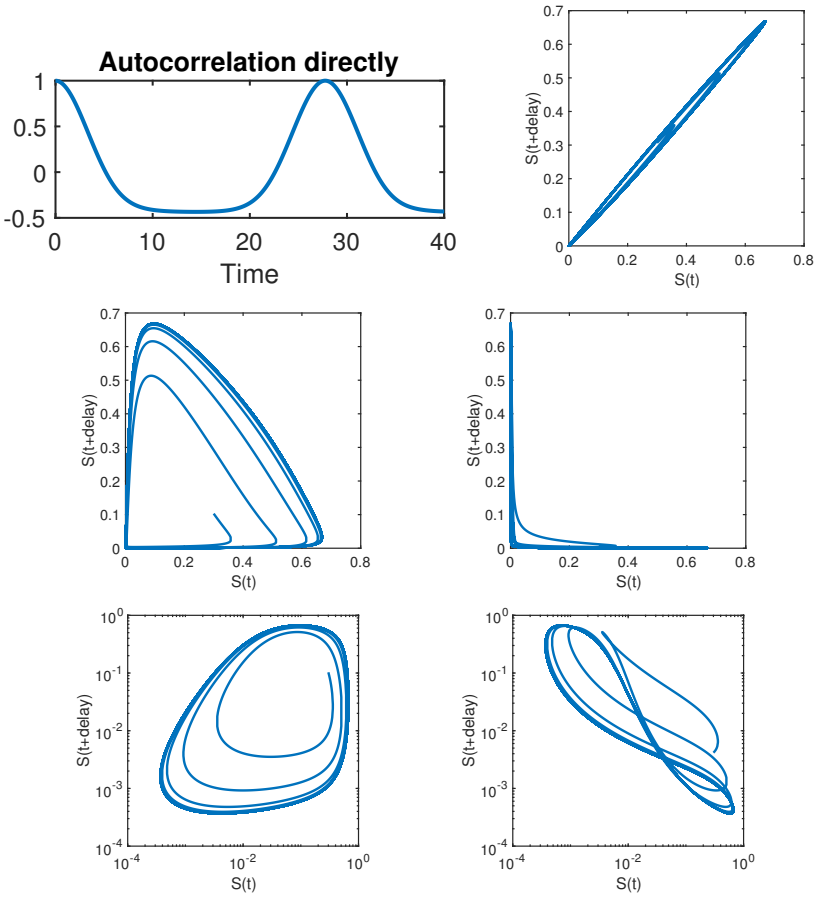

Figure 15: Time delay embedding of model data for different values of the delay. a) Autocorrelation function. b) $\tau = 0.1$. c) $\tau = 5$. d) $\tau = 13$, e) $\tau = 5$, logarithmic scale, f) $\tau = 13$, logarithmic scale; note that in this 2-dimensional embedding the trajectory intersects itself!

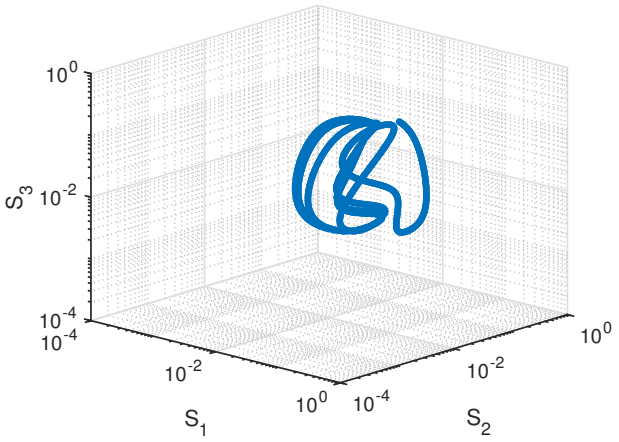

Figure 16: The self-intersections of the trajectory in the 2d embedding are removed in 3d (cf. Takens embedding theorem). (cf. movie`Figures/attractor_video_etaexp0.8_delta0.15_psi2_delay13.mp4`)

Notes:

- In general, even if $C_{yy}(\tau) = 0$ higher-order correlations like $C_{yyy}(\tau_1, \tau_2)$ can be non-zero. To implement the notion that $y(t-\tau)$ should provide as much additional information about the current state as possible it would therefore be better to minimize the *mutual information* between $y(t)$ and $y(t-\tau)$ Fraser and Swinney (1986). The measurement of mutual information requires, however, a large amount of data, which are usually not available for population dynamics.
- If the data are strongly affected by seasonal effects, it is good to consider the *stroboscopic* map and take the delay a multiple of a year. But this is only reasonable if the generation time of the population is at least a year. Otherwise one needs to include the seasonal effects in the model.

2.2.1 Black-Box Models

One important goal of modeling is to predict the future state of the system. Can we directly predict the state based on the time series without prior knowledge of the workings of the system and without building a mechanistic model, i.e. purely 'data-driven'?

If we have data only at multiples of τ we would want to determine F such that

$$y(t) = F\left(y(t-\tau), y(t-2\tau), \ldots\right).$$

If the attractor reconstruction works well in 2 dimensions, we would expect that plotting $y(t)$ vs $y(t-\tau)$ and $y(t-2\tau)$ should give a reasonable *response surface*.

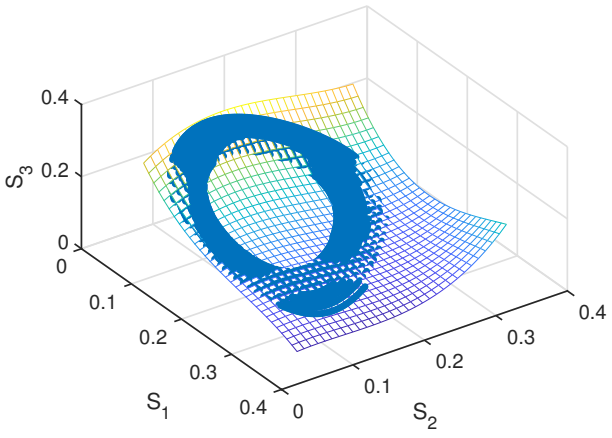

Figure 17: Response surface in terms of the delayed coordinates $S_1 \equiv S(t-2\tau)$, $S_2 \equiv S(t-\tau)$, $S_3 = S(t)$ for the signal $S(t)$.

How to quantify the response surface?

A simple approach is to approximate the surface with low-order polynomials

$$F(y_1, y_2) = \sum_{n=0}^{q} \sum_{m=0}^{n} a_{m,n-m} y_1^m y_2^{n-m}$$

with $y_1 = y(t-\tau)$ and $y_2 = y(t-2\tau)$. Using the data $y(t_i)$ we get then

$$y(t_i) = \sum_{n=0}^{q} \sum_{m=0}^{n} a_{m,n-m} y(t_{i-1})^m y(t_{i-2})^{n-m} \qquad i = 1 \dots N$$

Notes:

- Notation: q is the maximal order of the polynomial
- This is a linear system in the unknown coefficients a_{mn}.
- For N large enough these equations can be solved by linear regression

Example

$q = 1$

$$y(t_i) = a_{00} + a_{10} y(t_{i-1}) + a_{01} y(t_{i-2})$$

Write this as

$$\begin{pmatrix} 1 & y(t_2) & y(t_1) \\ 1 & y(t_3) & y(t_2) \\ \dots & \dots & \dots \\ & & \\ 1 & y(t_{N-1}) & y(t_{N-2}) \end{pmatrix} \begin{pmatrix} a_{00} \\ a_{10} \\ a_{01} \end{pmatrix} = \begin{pmatrix} y(t_3) \\ y(t_4) \\ \dots \\ \\ y(t_N) \end{pmatrix}$$

i.e.

$$\mathbf{M}\mathbf{x} = \mathbf{b}.$$

To get a least-squares approximation we minimize the residual R,

$$R = \|\mathbf{M}\mathbf{x} - \mathbf{b}\|^2 = \sum_i \left(\sum_j M_{ij} x_j - b_i \right)^2,$$

i.e.

$$\begin{aligned} 0 = \frac{1}{2}\frac{\partial R}{\partial x_l} &= \sum_i \left(\sum_j M_{ij} x_j - b_i \right) \frac{\partial}{\partial x_l} \left(\sum_k M_{ik} x_k - b_i \right) \\ &= \sum_i \left(\sum_j M_{ij} x_j - b_i \right) \sum_k M_{ik} \delta_{lk} \\ &= \sum_i \left(\sum_j M_{ij} x_j - b_i \right) M_{il} \\ &= \sum_{ij} \left(\mathbf{M}^t\right)_{li} M_{ij} x_j - \sum_i \left(\mathbf{M}^t\right)_{li} b_i. \end{aligned}$$

Here δ_{lk} is the Kronecker δ

$$\delta_{lk} = \begin{cases} 1 & \text{for } l = k \\ 0 & \text{for } l \neq k \end{cases}.$$

Thus, the equation for $\mathbf{x}$ becomes

$$\mathbf{M}^t\mathbf{M}\mathbf{x} = \mathbf{M}^t\mathbf{b}.$$

Note:

- Instead of a polynomial approximation one can also do non-parametric fits, e.g. kernel regression

$$F(y_1, y_2) = \frac{\sum_j e^{-\frac{1}{\sigma^2}\left((y_1 - y(t_{j-1}))^2 + (y_2 - y(t_{j-2}))^2\right)} y(t_j)}{\sum_j e^{-\frac{1}{\sigma^2}\left((y_1 - y(t_{j-1}))^2 + (y_2 - y(t_{j-2}))^2\right)}}$$

  The only parameter is σ, which characterizes the smoothing done by this fit.
  With many data points the evaluation of the sum can become slow.

In this procedure we made two fundamental choices:

- embedding dimension: so far we chose $p = 2$ assuming that the attractor is well embedded that way.
- order q of the polynomial approximation of the response surface

How do we choose p and q? How well should we approximate the data points?

Issues

- If p is too small the attractor cannot be captured adequately.
- If p is too large, the number of coefficients in the approximation of the response surface becomes too large.
- Large q also leads to too many unknowns.

Moreover, in general there are two issues:

- High-order polynmials oscillate between data points $\rightarrow$ predictions are bad for intermediate times
  in a map this may not be so much of an issue, since the intermediate times are never included. E.g. mapping populations from 1 spring to the next do not need to be able to predict summer populations.
- The data are noisy and we are assuming that the deterministic aspect of the system is smooth
  - the response surface should also be smooth and should not follow the data in all its noisy aspects

  - do not use polynomials of high order q to capture the noisy details
  - **Do not fit the noise.**

How do we know whether our approximation is already fitting the noise rather than the underlying dynamics?

If we ran the system another time with different noise but identical parameters otherwise, we would get a different solution. Our approximate model should capture that solution with similar quality as the solution on which it was based:

- the model should **generalize** beyond the specific data that were used in building the model.

Cross-Validation of the Black-Box Model

How do we assess the quality of the prediction based on the response surface?

We can measure the error in the prediction of the data that were used for obtaining the model. But this does not address the possibility that the model is fitting the noise rather than the underlying system. We need to use *new data* to test the model.

When given experimental data, we may not have the option to ask for another set of data with the same parameters, i.e. another trial.

Instead, to test the ability of the model generalize, do not use all the available data for building the model and use the left-out data to validate it.

Omitting data in building the model will, in principle, deteriorate the model:

- If we have a lot of data, we can simply omit half of them and will still have enough to get a good model, while using the other half for validation.
- If we have only few data, we do not want to omit that many data points. Instead we can omit a single data point and test the model on that data point. Performing only one such test is not very conclusive. Instead:
  - repeatedly omit one data point, obtain the corresponding model and measure its prediction error for this one data point.
  - each omitted data point leads to a different model, i.e. a different approximation for the response surface
    * if these models differ substantially from each other, the models cannot really be trusted.
    * if these models are similar it is good to take the 'average' model, i.e. average the coefficients across the different models.
    * Averaging over the different models may improve the model.
      Since the averaged model is using effectively all data points in its training data, one cannot assess its predictive power based on these data. One would have to use a new set of data for that.

Even if overfitting the data is not an issue, one may be interested in obtaining a model that matches the data 'optimally' in a sense that compares the number of unknown parameters that need to be fitted and the quality of the resulting fit.

Often one is interested in a 'parsimonious' model, i.e. a model that captures the essential aspects of the system with only few assumptions, i.e. few unknowns:

- if adding further terms leads only to a marginal improvement in the fit the additional terms presumably are not essential

A quantitative measure for the balance between fit quality and complexity of the model is the Akaike information criterion

$$AIC = 2k - \ln \mathcal{L}_{max}$$

where k is the number of parameters of the model and $\mathcal{L}_{max}$ is the likelihood of the parameters of the best fit given the data. Broadly speaking, in a least-squares approach the likelihood of the parameters decreases with increasing residual.
Thus, to justify an increase in the number of parameters k the residual has to decrease sufficiently to decrease AIC.

The overall procedure is then:

- measure average prediction error across a set of test data for increasing values of p and q and compare it with a default prediction: if the system had no significant deterministic dynamics and all variability was just coming from noise a reasonable prediction would be simply the temporal average $\bar{y} = \frac{1}{N}\sum_{j=1}^{N} y_j$ of the signal. Therefore measure

$$R_2 = 1 - \frac{\sum_{j=1}^{N} \left(y_{fit}(t_j) - y_j\right)^2}{\sum_{j=1}^{N} \left(\bar{y} - y_j\right)^2},$$

  where $y_{fit}(t_j)$ is the prediction obtained from the fit (model) to the data that had omitted $y(t_j)$.

Note:

- Here we consider situations where we only have a single time series, i.e. we have no direct way of measuring the variability of y at a given time. Therefore we cannot compare the quality of the prediction at a given time point with the variance in the data at that time point.

Thus,

- if R_2 is close to 1 the prediction is good.
- if R_2 is close to 0 the prediction is no better than just taking the overall average of the data
- if R_2 is negative the prediction is utmost bad.

Investigate the black-box approach using a non-trivial model for a prey N and a predator P (see Sec.2.4.1),

$$\frac{dN}{dt} = N\,(1-N) - \frac{1}{1+\eta N}\,N\,P \tag{2}$$

$$\frac{dP}{dt} = -\delta P + \psi\frac{N}{1+\eta N}\,P \tag{3}$$

In these simulations we can generate a lot of data. For the cross-validation we therefore simply take half of the data y_{2i}, $i = 1 \ldots N/2$, to fit the model and the other half of the data, y_{2i+1}, $i = 1 \ldots N/2$, to test the generalization of the model.

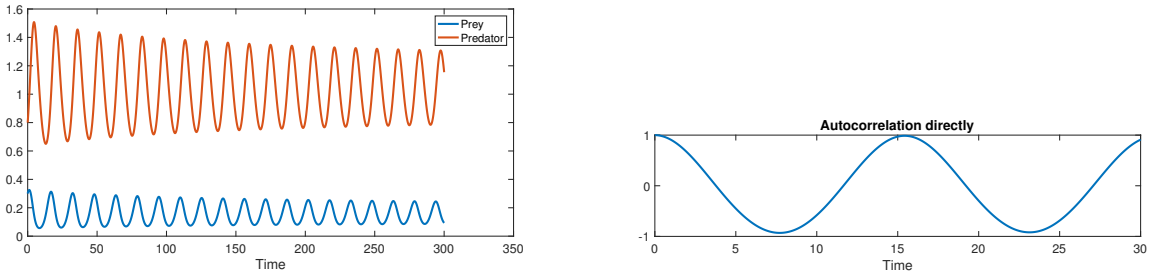

Figure 18: $\eta = e^{0.35}$, initial conditions $(0.3, 0.8)$, $\delta = 0.25$, $\psi = 2$, $t_{max} = 300$. a) Noiseless trajectoy. b) Autocorrelation function.

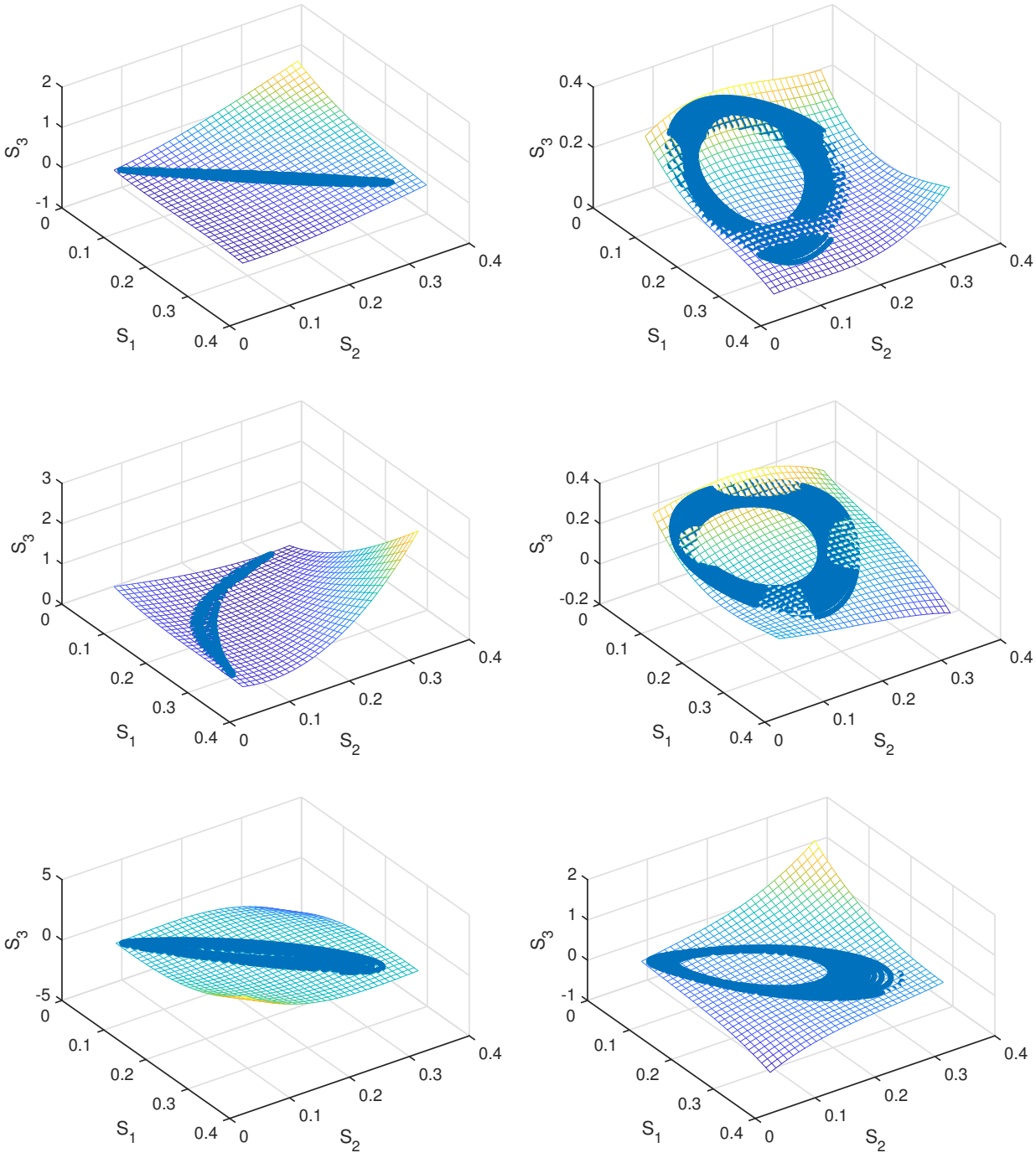

Figure 19: Embedding via delay coordinates and a response surface. a) $\tau = 0.2$ b) $\tau = 4$ c) $\tau = 8$, d) $\tau = 12$, e) $\tau = 15$, f) $\tau = 17$.

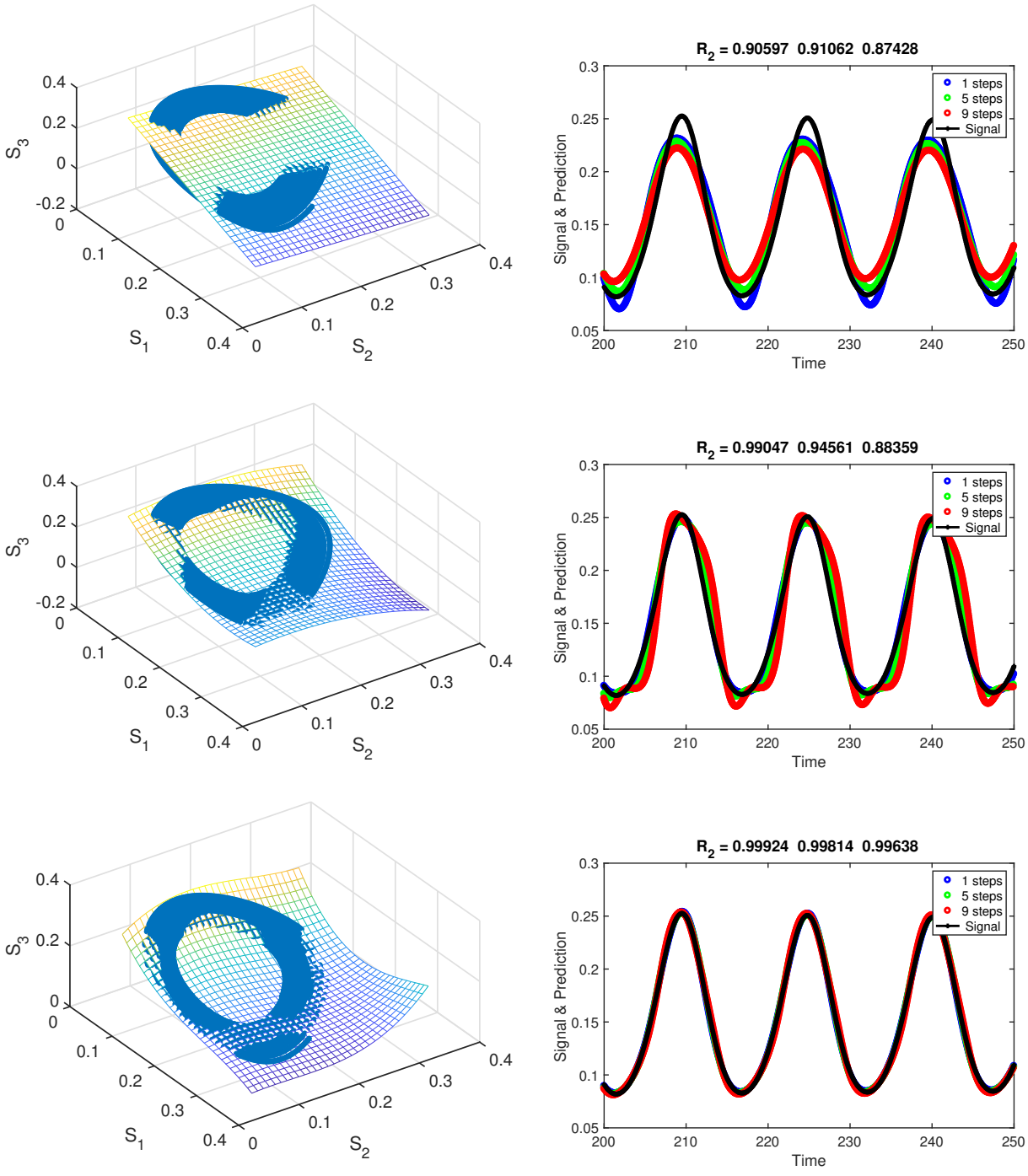

Figure 20: Response surface and predictions 1, 5, and 9 steps ahead for $\tau = 4$, $\eta = e^{0.35}$. a) linear approximation to the response surface, b) quadratic, c) cubic. Initial conditions $(0.3, 0.8)$, $\delta = 0.25$, $\psi = 2$. The resulting error R_2 is listed as the title. Note: the period of the oscillations is about 15, i.e. a 9-step prediction with $\tau = 4$ predicts 2 periods. Note that the estimate of the prediction error is not precise enough to warrant 5 digits; there should be at most 2 digits.

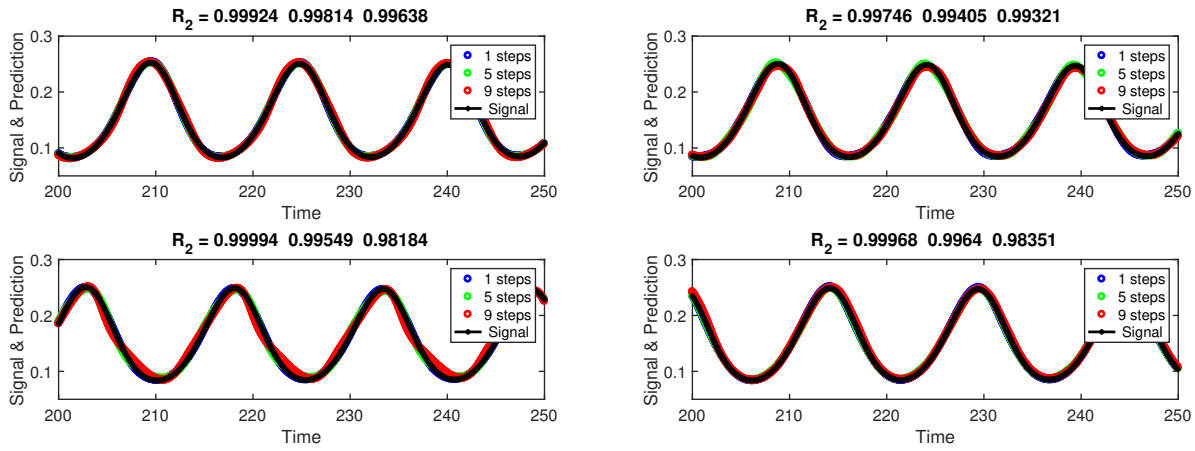

Figure 21: Prediction for different delays with cubic response surface. No noise. $\tau = 4$, $\tau = 12$, $\tau = 15$, $\tau = 17$. The predictions are slightly worse for $\tau = 15$ than for $\tau = 12$ and $\tau = 17$, reflecting possibly the worse reconstruction of the attractor for $\tau = 15$.

Increasing η increases the impact of the denominator, the nonlinearity of the differential equation bercomes 'less polynomial'. The approximations for the response surface are not as good for larger η and the predictions become quite bad. In fact, for yet larger η the predictions often diverge. Possibly, higher-order polynomials would still improve the approximation. Given the nonlinearity in the differential equations a more general nonlinearity might be better or using a kernel regression.

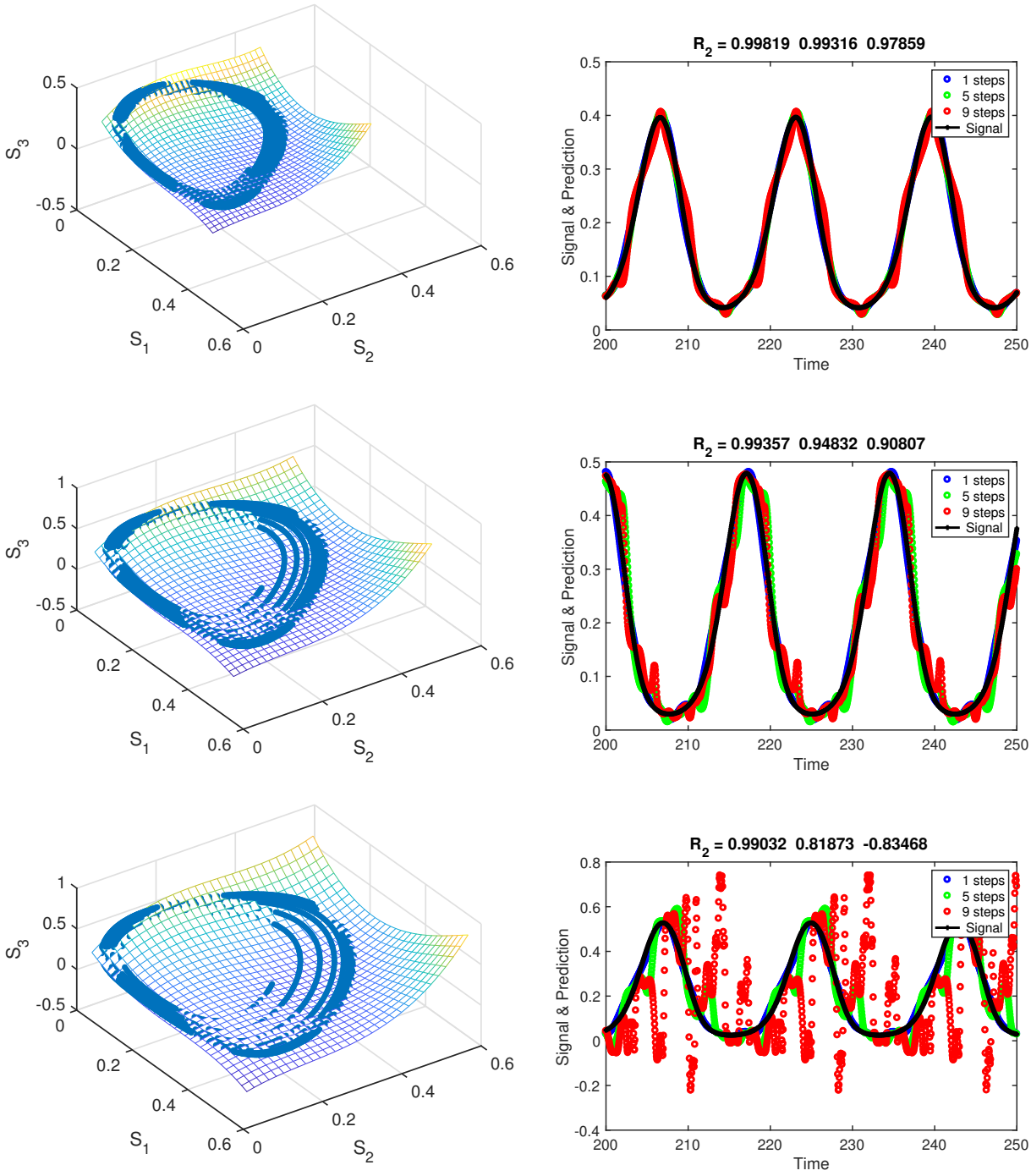

Figure 22: Cubic response surface and prediction. Initial condition $(0.3, 0.8)$, $\delta = 0.25$, $\psi = 2$, $\tau = 4$. a) $\eta = e^{0.5}$ b) $\eta = e^{0.6}$, c) $\eta = e^{0.67}$. Note the anharmonicity of the oscillation for $\eta = e^{0.67}$.

The real system is most likely noisy

$$\frac{dN}{dt} = N\,(1-N) - \frac{1}{1+\eta N}\,N\,P + N\zeta_N \tag{4}$$

$$\frac{dP}{dt} = -\delta P + \psi\frac{N}{1+\eta N}\,P + P\zeta_P \tag{5}$$

with ζ_α being a Gaussian random variable satisfying

$$\langle \zeta_\alpha(t) \rangle = 0 \quad \langle \zeta_\alpha(t)\zeta_\beta(t') \rangle = \sigma_\zeta^2 \delta(t-t')\delta_{\alpha\beta} \quad \text{with} \alpha, \beta \in \{N, P\}\,.$$

Note:

- The noise in (4,5) is multiplicative to avoid that the populations become negative.

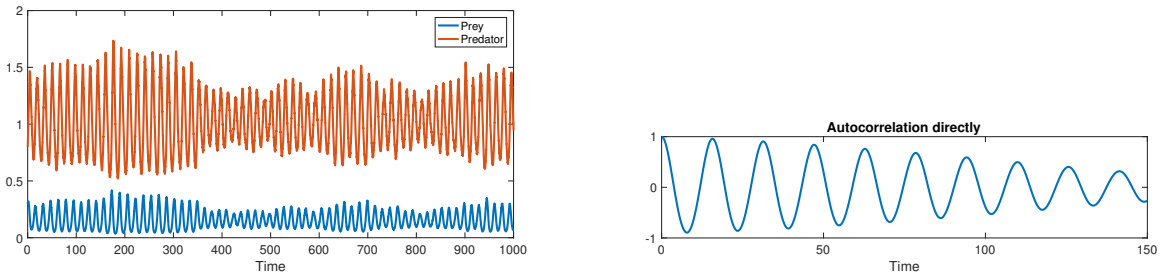

Figure 23: Noisy system $\sigma_\xi = 0.02$. Initial condition $(0.3, 0.8)$, $\delta = 0.25$, $\psi = 2$, $\tau = 4$. $\eta = e^{0.35}$, $t_{max} = 1000$.

The noise leads to strongly varying oscillation amplitudes and correspondingly a decaying autocorrelation function.

Of course, the prediction cannot take the noise into account that is different in each future step. This will impact particularly multi-step predictions. To assess the quality of the prediction one would also have to average the results over noise realizations. The response surface will also depend on the noise, since only a finite number of data point are available. To alleviate this, a longer time series is used in Fig.24 ($t_{max} = 2000$).

To assess the impact of the embedding delay on the prediction one needs to compare predictions for similar prediction times, i.e. the 1-step for $\tau = 12$ should be compared with the 3-step prediction for $\tau = 4$. Based on the individual examples in the figure, it seems that the 1-step predictions for larger τ are worse than the 3-step prediction for $\tau = 4$. However, no significant difference is apparent between the predictions for $\tau = 12$, $\tau = 15$, and $\tau = 17$, despite the worse embedding for $\tau = 15$ (cf. Fig.19).

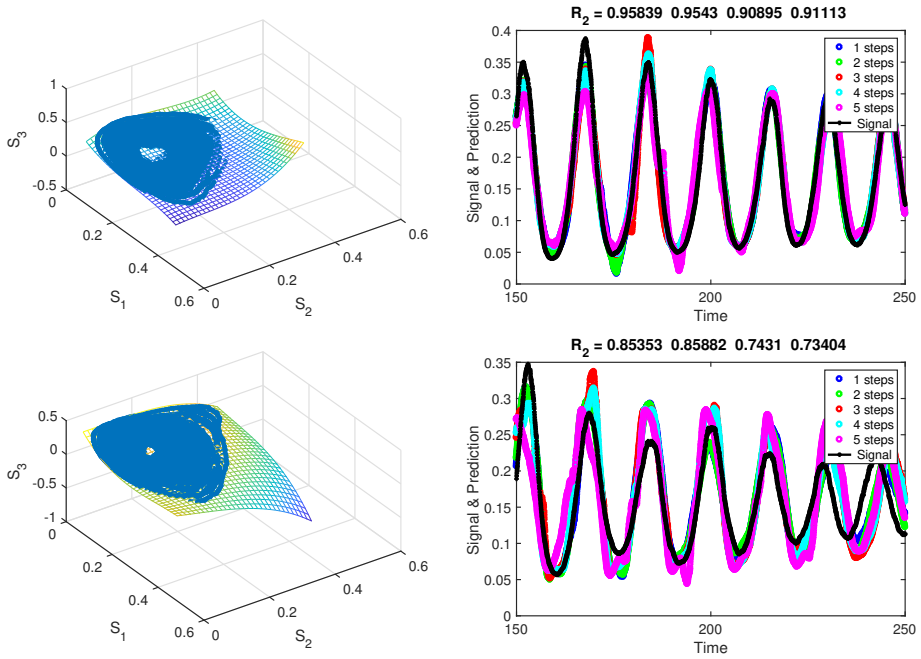

Figure 24: Noisy system $\sigma_\xi = 0.02$. Initial condition $(0.3, 0.8)$, $\delta = 0.25$, $\psi = 2$. $\eta = e^{0.35}$, $t_{max} = 2000$. top: $\tau = 4$, bottom: $\tau = 12$.

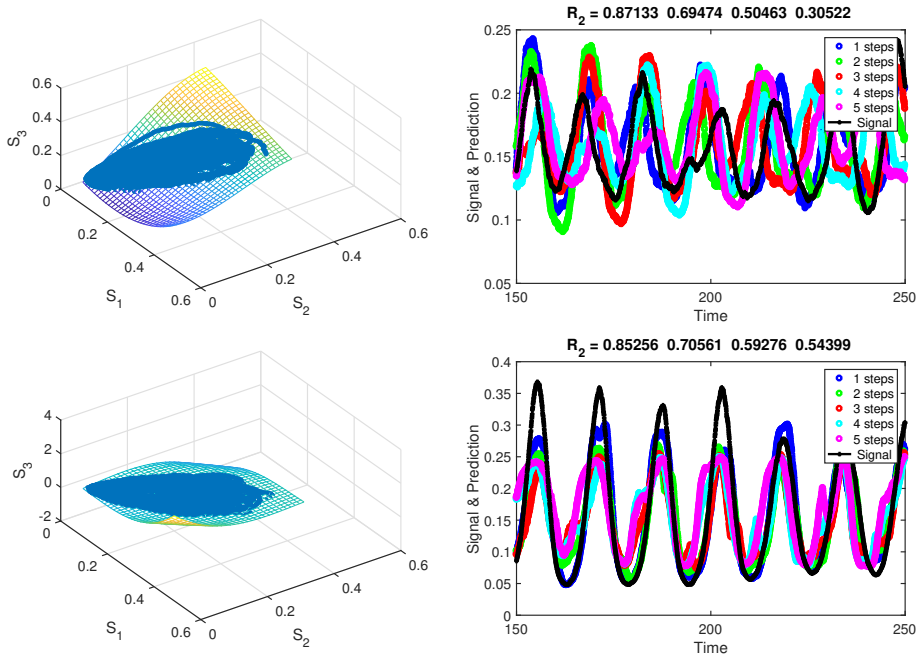

Figure 25: Noisy system $\sigma_\xi = 0.02$. Initial condition $(0.3, 0.8)$, $\delta = 0.25$, $\psi = 2$, $\tau = 4$. $\eta = e^{0.35}$, $t_{max} = 2000$. top: $\tau = 15$, bottom: $\tau = 17$.

These simulations suggest that the (slightly) worse embedding for $\tau = 15$, compared to $\tau = 12$, does not play a big role here (to assess in detail we would have to measure the error over many noise realizations and take the average).

Consider also the presence of measurement noise. Assume δ-correlated Gaussian noise

$$N(t) \to N(t) + \xi(t) \qquad \langle \xi(t) \rangle = 0 \quad \langle \xi(t)\xi(t') \rangle = \sigma_\xi^2 \delta(t - t')$$

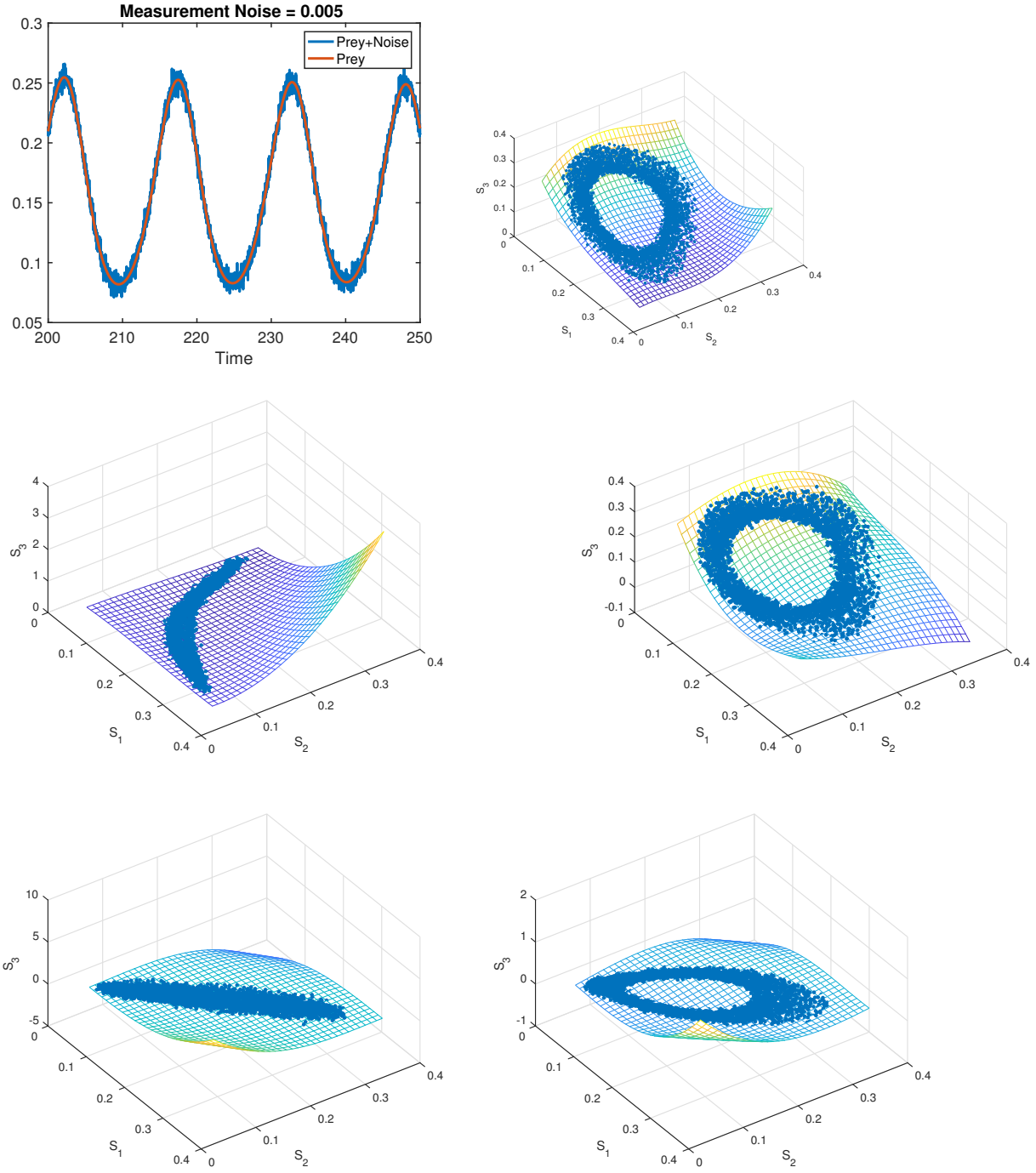

Figure 26: a) Prey with measurement noise (but no system noise). Embedding and response surface for data with measurement noise. b) $\tau = 4$ c) $\tau = 8$, d) $\tau = 12$, e) $\tau = 15$, f) $\tau = 17$.

With this noise the limit cycle is still much better defined for $\tau = 4, 12, 17$ than it is with

system noise (4,5), where the attractor was quite 'washed out' (Figs.24,25). However, for $\tau = 8$ and $\tau = 15$ no 'hole' is visible, which may lead to 'confusion' in the predictions.

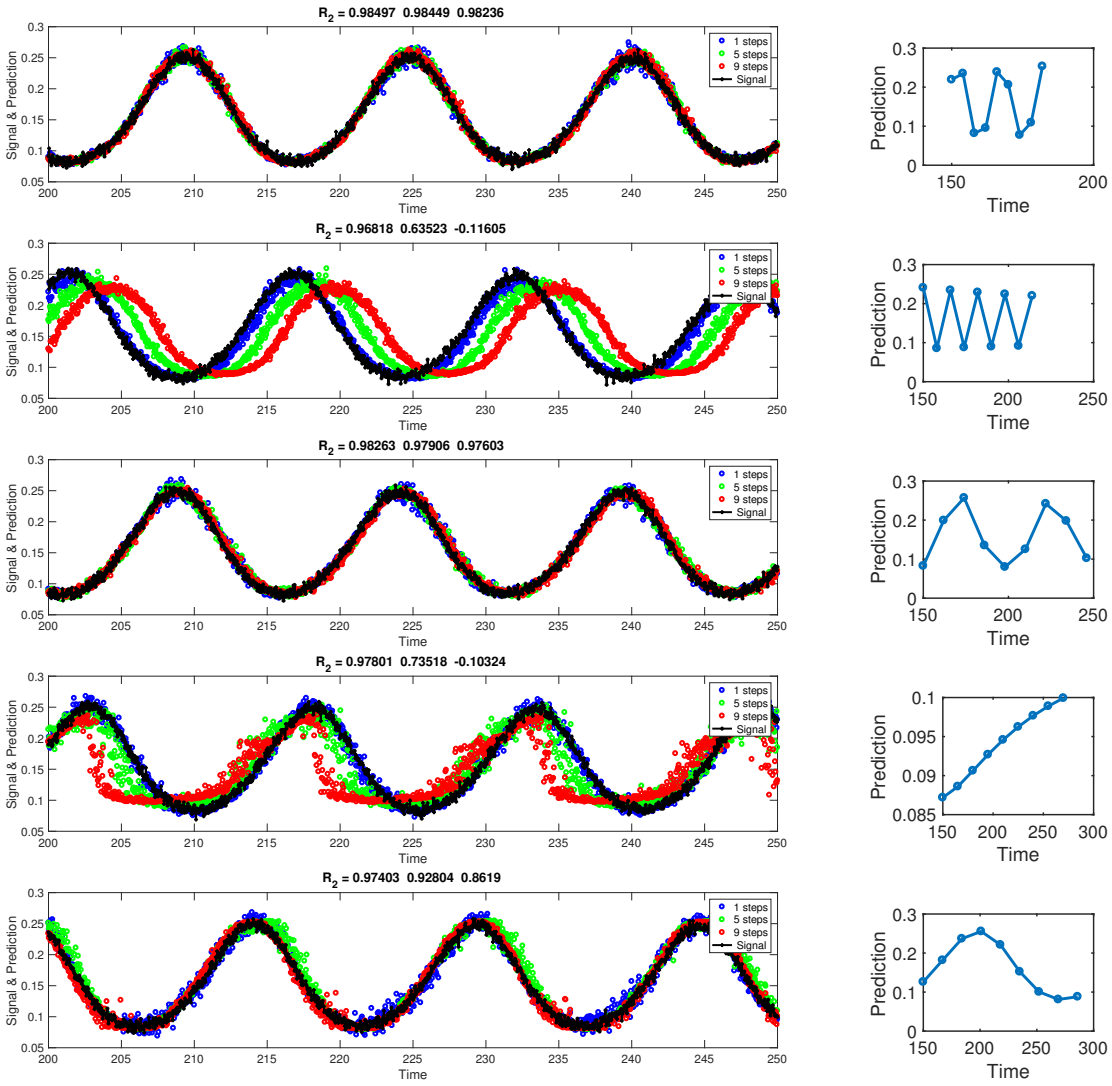

Figure 27: Prediction and error for data with measurement noise. Right column shows all n steps of the prediction starting from a fixed time point. a) $\tau = 4$ b) $\tau = 8$, c) $\tau = 12$, d) $\tau = 15$, e) $\tau = 17$. $\sigma_\xi = 0.005$.

Notes

- The predictions based on the poorly embedded attractor are substantially worse than for delays for which the autocorrelation function is close to 0.
- In the n-step prediction figures (right column in Fig.27) the individual oscillations are not resolved; their period is around 15.

Usefulness of the Black-Box Model Approach

- Predictions are possible without any detailed knowledge of the system at hand.
- Quantification of the type of dynamics observed by identification of optimal q
  - $q = 0$:
    - deterministic component in the mapping not significant
    - noisy fixed point
    - noisy periodic orbit with a period that is equal to the sampling time
    - to discriminate between these two possibilities: are data available with finer sampling time?
  - $q = 1$:
    - fixed point
    - oscillations with a period that is commensurate with the sampling time (e.g. oscillations in lock-step with seasonal changes)
    - certain type of chaotic dynamics, cf. the logistic map
  - $q = 2$:
    - fixed point
    - oscillations
    - chaotic dynamics
- Knowing q provides some guidance for developing mechanistic models
  - how many dynamical variables are needed? how many species are interacting?
- Interpolation between different parameter values if data are available for multiple sets of parameters.
  - possibly one could identify transition points between different types of dynamics, e.g. fixed point to oscillations.

Drawbacks of the Black_Box Model Approach

- In themselves the models do not provide mechanistic, intuitive insight into the system.

Notes:

- The same approach can be used to develop mechanistic models:
  - if data are available for multiple components participating in the dynamics
  - if functional forms for the evolution equations are suggested by the mechanistic framework
    (cf. Mangan's research on chemical reactions)
  - if the terms in the differential equations are to be recovered data are needed with fine time resolution.

2.3 Mechanistic Models: Introduce 'The Biology'

To really understand what is going on in the system we would like to have mechanistic models, i.e. we would like to udnerstand the mechanisms that are at work in the system:

- the dynamical variables include all the relevant 'players' of the system, e.g. food (grass), prey, predators
- the equations describe
  - the actions of the players, e.g. birth, death, movement
  - the interaction between the players, e.g. grazing, hunting

2.3.1 'Fundamental Laws'Turchin (2003)

Are there 'fundamental laws' that constrain or guide the formulation of the evolution equations?

Note:

- Such 'fundamental laws' are idealizations; real systems do not satisfy them exactly. But the idealization makes it easier to think about the system and identify relevant mechanisms that lead to deviations from the 'laws'.
- Turchin Turchin (2003) compares the situation with Newton's law of motion: in realistic systems the acceleration does not vanish in the absence of 'external forces': there is always friction. The idealization identifies friction as an additional force. This is useful because friction is not universally the same, but depends on the system, i.e. it needs to be modeled as well as the other 'external' forces. If friction was included in the 'fundamental law' one would have to have different fundamental laws for the motion of different wheels, bearings, tires,.....

FL 1: The size of a population changes by birth, death, emigration, or immigration.

Notes:

- This applies also to food, e.g. plants growing from seeds that can be dispersed by wind.
- We will ignore in the following the spatial aspects, i.e. we will assume that in the spatial domain in question the species are 'well-mixed'.

FL 2: Changes in the size of a population result from what happens with individuals.

Therefore the increase or decrease in a population is proportional to the size of the population

$$\frac{dN}{dt} = r\,N \qquad \Leftrightarrow \qquad \frac{d\ln N}{dt} = r.$$

Here r is the rate at which an individual propagates in the *current conditions*.

For constant conditions one therefore gets exponential growth or decay

$$N(t) = N(0)e^{rt}.$$

How can this be consistent with all the observed non-exponential behavior, like saturation, never mind oscillations?

The *current conditions* can and do change with the size of the population and, of course, with the overall availability of food and with the presence of other species.

Thus, the key modeling aspect pertains to describing deviations from the idealized case, i.e. to finding how the growth rates r_i of various species i depend on the conditions, which include the current sizes of other populations (food, predators, prey),

$$r_i = r_i\left(N_j(t), \ldots\right).$$

Note:

- In fact, the growth rate can also depend on previous population sizes, i.e. there can be a delayed impact, due to breeding, gestation, or maturation.
  Thus, r_i can depend on populations after a delay

  $$r_i(t) = r_i\left(N_j(t-\tau)\right),$$

  leading to delay-differential equations,
  or r_i can be a functional that depends on the whole functions $N_j(t')$, $-\infty < t' \leq t$,

  $$r_i = r_i\left\{N_j(t)\right\},$$

  leading to integral equations.
  We will mostly ignore such history effects, although they are very interesting. E.g. a delay can very easily lead to oscillations within a *single* species.

FL 3: Populations do not blow up: populations should exhibit self-limitation.

As a minimal condition one would require that the growth rate should decrease for large population sizes,

$$\frac{dr(N)}{dN} < 0 \qquad \text{for } N \to \infty.$$

A stronger condition one could require, would be

$$r(N) < 0 \qquad \text{for } N \to \infty.$$

Note:

- The first condition does not guarantee that the population does not blow up. Consider, e.g.,

  $$r(N) = N^{-\alpha} \qquad \text{with } \alpha > 0.$$

  Then

  $$\frac{1}{N}\frac{dN}{dt} = N^{-\alpha}$$

$$t + c = \int \frac{dN}{N^{1-\alpha}} = \frac{1}{\alpha} N^{\alpha}(t)$$

$$N(t) = (\alpha\,(t + c))^{\frac{1}{\alpha}}$$

For $\alpha > 0$ the population grows, but more slowly than exponential.

In view of our aim to study oscillations we will focus on populations that interact 'trophically', i.e. one population represents food for the other, we have consumers and resources.

FL 4: In the limit of low densities of the resource (prey) the functional response of the predator is linear in the prey density.

Notes:

- The *functional response* of the predator is defined as the rate at which 1 predator kills prey.
- This expresses something similar to the law of mass action in chemical reactions: the probability that a given predator will find and kill a prey is proportional to the density of the prey.

$$\frac{dN}{dt} = \ldots - \underbrace{N\,P\,k(N,P)}_{\text{trophic term}} \ldots \qquad k(N,P) \to \text{const. for } N \to 0,\ P \to 0.$$

- Deviations ($k(N,P) \neq$ const.) that need to be modeled then are, e.g.,
  - *Strength in* Numbers*:* for higher prey densities the prey may be able to defend themselves in a density-dependent fashion and the predator may not be able to catch all of the prey (cf. in schools of fish only a fraction of the fish get caught, i.e. k would decrease with increasing N).
  - for higher predator densities the predators may cooperate or compete.

FL 5: The amount of energy extracted from a resource is limited by the amount of the resource captured.

Notes:

- The law makes sense in terms of the biomass available.
- The fraction of energy used may not be constant. It could decrease with the density of the resource, e.g. a predator eats less of the prey (only the good parts) if there is a lot of prey to be had ('surplus killing').
- We need the *numerical response* of the predator, which is defined as the rate of change of the predator population.
- Often the reproduction rate of the predator is assumed to be proportional to the energy extracted from the prey,

$$\frac{dP}{dt} = \ldots + g(N)\,N\,P\,k(N,P) \ldots$$

- But:
  - The fraction of the energy needed for reproduction could represent only a small fraction of the total energy needed (heat generation, locomotion, predation). The reproduction rate would then not directly reflect the energy extracted (could involve, e.g., a threshold).
  - The reproduction rate could also be limited by other factors than food (maximal size of litter, gestation time).

FL 6: There is a maximal consumption rate.

Notes:

- Even with prey in abundance a predator can catch and digest only so much.
- Assuming food consumption and reproduction rates are directly related, this leads to a *maximal reproduction rate*.

2.3.2 The Lotka-Volterra Model[7]

Start with a minimal model for the trophic interaction of a predator with a prey.

The prey/resource gets its food from an abundant source and is consumed by the predator

$$\frac{dN}{dt} = rN - k\,NP$$

Dimensions:

- $[r] = \frac{1}{s}$, $[N] = prey$, $[P] = predator$, $[k] = \frac{1}{s}\frac{1}{predator}$
- r combines the reproduction and death rates in the absence of a predator. $r > 0$ to have the prey population grow in the absence of a predator

The predator can only reproduce if it catches prey

$$\frac{dP}{dt} = -dP + \chi\,k\,NP$$

Dimensions:

- $[d] = \frac{1}{s}$, $[\chi] = [\frac{1}{t\,k\,N}] = \frac{1}{s}s\,predator\,\frac{1}{prey} = \frac{predator}{prey}$
- χ gives the conversion from the rate at which prey is being killed to the rate at which predators propagate: how much does each prey contribute to the propagation of each predator.

[7] Lotka points out that a large part of Volterra's results had already appeared earlier in Lotka's book Lotka (1920); Volterra (1926); Lotka (1927, 1925)

To reduce the number of relevant parameters make the equations dimensionless:

$$\frac{1}{r}\frac{dN}{dt} = N - \frac{k}{r}NP$$

Introduce

$$\hat{t} = rt \qquad \hat{P} = \frac{k}{r}P \qquad \text{with} \quad [\hat{t}] = 1 \quad [\hat{P}] = 1$$

to get

$$\frac{dN}{d\hat{t}} = N - N\hat{P}$$

and

$$r\frac{r}{k}\frac{d\hat{P}}{d\hat{t}} = -\frac{dr}{k}\hat{P} + \chi\, k\, \frac{r}{k}N\hat{P}$$

$$\frac{d\hat{P}}{d\hat{t}} = -\frac{d}{r}\hat{P} + \chi\,\frac{k}{r}\,N\hat{P} \qquad \text{with} \quad [\chi\frac{k}{r}] = \frac{predator}{prey}\frac{s}{s \times predator} = \frac{1}{prey}$$

Introduce

$$\delta = \frac{d}{r} \qquad \hat{N} = \chi\frac{k}{r}N \qquad \text{with} \quad]\delta] = 1 \quad [\hat{N}] = 1$$

We are then left with

$$\begin{aligned}\frac{d\hat{N}}{d\hat{t}} &= \hat{N} - \hat{N}\hat{P} \\ \frac{d\hat{P}}{d\hat{t}} &= -\delta\hat{P} + \hat{N}\hat{P}\end{aligned}$$

Thus, we used a rescaling of the 3 variables of the equations to get rid of 3 parameters.

Notes:

- Only a single parameter determines the behavior of this system.
- Since we only allow positive populations and the dimensionless time is to increase with time, this reduction is only valid for a specific combination of the signs of the 4 coefficients.
- r, k, and χ cannot be 0, in fact, they need to be positive (since t should advance with time and populations are positive).

For simplicity drop the ˆ from the variables

$$\frac{dN}{dt} = N - NP \tag{6}$$

$$\frac{dP}{dt} = -\delta P + NP \tag{7}$$

Note:

- It is somewhat dangerous to 'drop the hat', because in subsequent results one has to remember that one is working with the rescaled variables and one has to remember which equations are using which variables.

How well do these equations match the 'fundamental laws' ?

- FL 1: yes
- FL 2: yes. r.h.s. of each each equation can be divided by the respective population
- FL 3: **no**. r.h.s are both linear in the respective populations, no decrease in the growth rate with increasing population
- FL 4: yes. it is linear in N for all N
- FL 5: yes. that is the factor χ.
- FL 6: **no**. the reproduction rate of the predator becomes arbitrarily large when the prey population becomes large.

Thus, from a biological perspective the model needs to be modified or extended. See below.

What dynamics does this model exhibit?

As for any nonlinear system, look first for simple solutions and then try to find suitable approximations to gain additional insight.

Steady States:

i) trivial state

$$N_0 = 0 = P_0$$

ii) For $N_0 \neq 0$ it follows that

$$P_0 = 1$$

For $P_0 \neq 0$ it follows that

$$N_0 = \delta \qquad \text{for } \delta \geq 0$$

Thus, the only non-trivial fixed point is $(N = \delta, P = 1)$.

Consider the linear stability of the fixed points with $\epsilon \ll 1$,

$$\begin{aligned} N(t) &= N_0 + \epsilon n(t) \\ P(t) &= P_0 + \epsilon p(t) \end{aligned}$$

i) $(N_0 = 0, P_0 = 0)$

$$\begin{aligned} \frac{dn}{dt} &= n \qquad n = n_0 e^t \\ \frac{dp}{dt} &= -\delta p \qquad p = p_0 e^{-\delta t} \end{aligned}$$

Thus, the trivial fixed point is a saddle point and linearly unstable with the unstable manifold given by the n-direction and the stable manifold by the p-direction.

ii) $(N_0 = \delta, P_0 = 1)$

$$\begin{pmatrix} \frac{dn}{dt} \\ \frac{dp}{dt} \end{pmatrix} = \begin{pmatrix} 1 - P_0 & -N_0 \\ P_0 & -\delta + N_0 \end{pmatrix} \begin{pmatrix} n \\ p \end{pmatrix} = \underbrace{\begin{pmatrix} 0 & -\delta \\ 1 & 0 \end{pmatrix}}_{\mathbf{M}} \begin{pmatrix} n \\ p \end{pmatrix}$$

Eigenvalues of $\mathbf{M}$

$$(-\lambda)^2 + \delta = 0 \qquad \lambda_{1,2} = i\sqrt{\delta}$$

The non-trivial fixed point is a center, since the eigenvalues are purely imaginary.

- (n, p) oscillates
- Within this approximation of the *linear* stability analysis the amplitude of the oscillations does not grow or shrink. What are the trajectories if nonlinear terms in the distance from the fixed point are included? With the nonlinearities included the center could turn into
  - a stable spiral $\rightarrow$ no persistent oscillations
  - an unstable spiral $\rightarrow$ possibly persistent oscillations if the growth saturates

One can easily see that even with the nonlinearities included there is a continuum of limit cycles in this simple model by expressing N in terms of P. Starting from (6,7)

$$\frac{dP}{dN} = \frac{P\,(-\delta + N)}{N\,(1 - P)}$$

Thus, the curve $P = P(N)$ has vertical tangents at $P = 1$ and horizontal slopes at $N = \delta$.

$$\frac{-\delta + N}{N} dN = \frac{1 - P}{P} dP$$

$$-\delta \ln N + N = \ln P - P + C$$

with C arbitrary. Expand around the fixed point

$$N = \delta + x \qquad P = 1 + y$$

we get

$$-\delta \underbrace{\ln\,(\delta + x)}_{\ln\left[\delta\left(1 + \frac{x}{\delta}\right)\right]} + \delta + x = \ln\,(1 + y) - 1 - y + C$$

Expand in x and y and using

$$\ln\,(1 + \epsilon) = \epsilon - \frac{1}{2}\epsilon^2 + \frac{1}{3}\epsilon^3 + \ldots$$

$$-\delta \ln \delta - \delta\frac{x}{\delta} + \delta\frac{1}{2}\frac{x^2}{\delta^2} + \mathcal{O}\left(x^3\right) + \delta + x = y - \frac{1}{2}y^2 + \mathcal{O}\left(y^3\right) - 1 - y + C$$

$$\frac{1}{2}\frac{1}{\delta}x^2 + \frac{1}{2}y^2 = C - 1 + \delta \ln \delta - \delta$$

Thus

- near the fixed point the trajectories are close to an ellipse
- C is arbitrary:
  there is a continuum of ellipses (or slightly deformed ellipses) of increasing size with increasing C

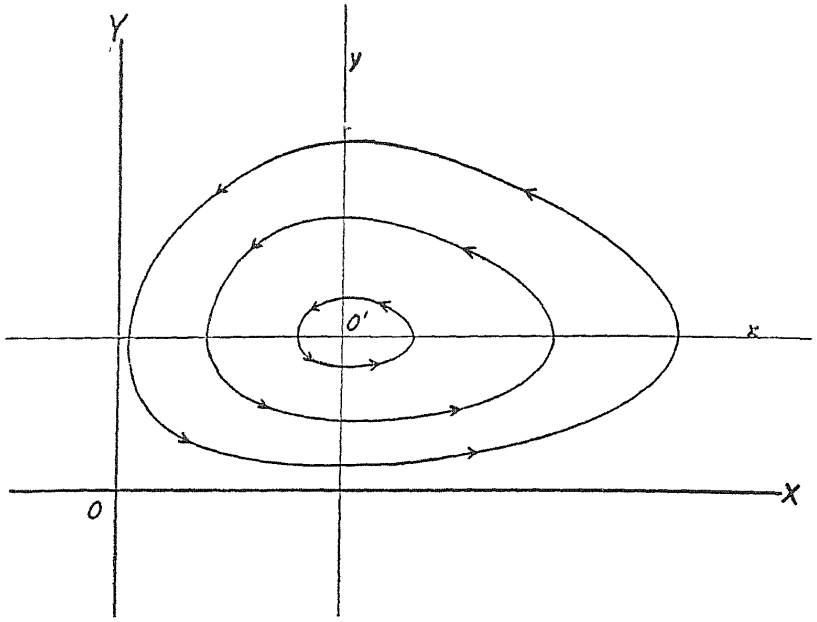

FIG. 13. COURSE OF PARASITIC INVASION OF INSECT SPECIES, ACCORDING TO LOTKA; ELEMENTARY TREATMENT

Figure 28: The limit cycles can have arbitrary amplitude Lotka (1925)

Note:

- Generically, fixed points are centers only for specific parameter values, i.e. at a Hopf bifurcation.
- In the Lotka-Volterra model the fixed point is a center for *all values* of δ(which is the only parameter in the system). This is not to be expected of a system, it is non-generic. It turns out, these equations are *structurally unstable*, i.e. even infinitesimally small additional terms in the equation can change the qualitative behavior of the system:
  - the center can turn into a stable or an unstable spiral, which would eliminate or stabilize the oscillations.

  - in numerical simulations the oscillation amplitude can change steadily if the time step is not small enough.

- Thus, we need to extend the Lotka based on
  - biology: it does not have self-limitation and limited reproduction rate
  - mathematics: the equations are not structurally stable

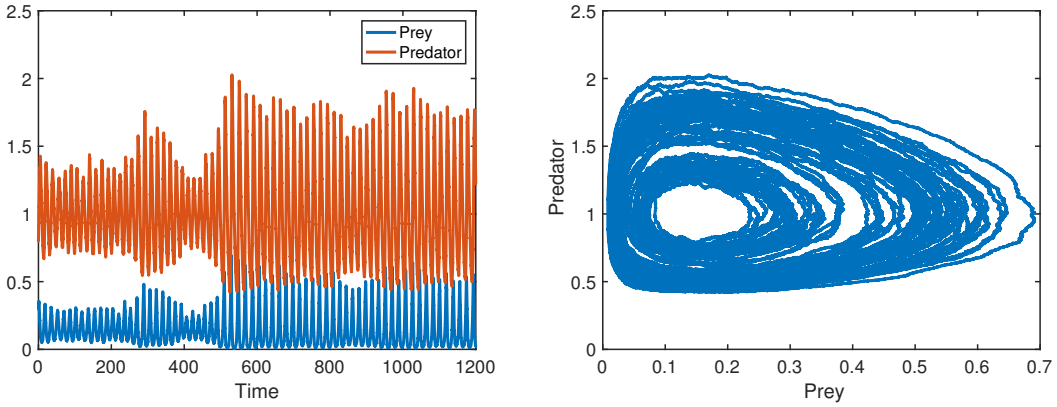

Figure 29: The continuum of oscillatory solutions allows noise to make the solution drift among solutions with different amplitudes, i.e. noise has a very strong effect.

Simple extension of Lotka-Volterra model

Include self-limitation of the prey via simple logistic term,

$$\begin{aligned} \frac{dN}{dt} &= N - \gamma N^2 - NP \\ \frac{dP}{dt} &= -\delta P + NP \end{aligned}$$

In the absence of a predator, the carrying capacity for the prey, i.e. the size of the prey population that this environment can sustain, is

$$N_c = \frac{1}{\gamma}.$$

Now the fixed points are given by

i) trivial fixed point $(0,0)$. Its instability is unchanged by the addition of a nonlinear term

ii) the nontrivial fixed point becomes $(\delta, 1-\gamma\delta)$

Linearization

$$\begin{aligned} \begin{pmatrix} \frac{dn}{dt} \\ \frac{dp}{dt} \end{pmatrix} &= \begin{pmatrix} 1 - P_0 - 2\gamma N_0 & -N_0 \\ P_0 & -\delta + N_0 \end{pmatrix} \begin{pmatrix} n \\ p \end{pmatrix} \\ &= \begin{pmatrix} 1 - (1-\gamma\delta) - 2\gamma\delta & -\delta \\ 1 - \gamma\delta & 0 \end{pmatrix} \begin{pmatrix} n \\ p \end{pmatrix} \\ &= \underbrace{\begin{pmatrix} -\gamma\delta & -\delta \\ 1 - \gamma\delta & 0 \end{pmatrix}}_{\boldsymbol{M}} \begin{pmatrix} n \\ p \end{pmatrix} \end{aligned}$$

Now the eigenvalues are

$$\lambda_{1,2} = \frac{1}{2}\left(trace(\boldsymbol{M}) \pm \sqrt{trace(\boldsymbol{M})^2 - 4\,det(\boldsymbol{M})}\right)$$

with

$$trace(\boldsymbol{M}) = -\gamma\delta < 0 \qquad det(\boldsymbol{M}) = \delta\,(1-\gamma\delta)$$

For oscillatory behavior we need

$$trace(\boldsymbol{M})^2 - 4\,det(\boldsymbol{M}) < 0 \qquad \gamma^2\delta^2 - 4\delta\,(1-\gamma\delta) = \gamma^2\delta^2 + 4\gamma\delta^2 - 4\delta < 0$$

The eigenvalues become real when the equality holds

$$\gamma_{1,2} = \frac{-4\delta^2 \pm \sqrt{16\delta^4 + 16\delta^3}}{2\delta^2} = -2 \pm 2\sqrt{1+\frac{1}{\delta}}$$

Since $\gamma_2 < 0$ we get for

$$\gamma < \gamma_1 \equiv 2\left(\sqrt{1+\frac{1}{\delta}} - 1\right)$$

the eigenvalues are complex and the fixed point is some kind of spiral. For $\gamma > \gamma_1$ the fixed point becomes a node $\Rightarrow$ no oscillatory behavior (not even decaying oscillations)

In the oscillatory regime the fixed point is linearly stable for

$$trace(\boldsymbol{M}) \equiv -\gamma\delta < 0$$

This is the case for *any* finite carrying capacity the fixed point becomes stable. The approach to the fixed point becomes very slow, however, when the carrying capacity is large.

Notes:

- Sufficiently small carrying capacity $\Rightarrow$ all oscillatory behavior disappears
- *Any,* even arbitrarily large, finite carrying capacity $\Rightarrow$ stabilizes the fixed point
  - this reflects the structural instability of the Lotka-Volterra equations
- Structurally unstable equations are poorly suited to make reliable predictions, unless
  - one knows that the real system cannot introduce perturbations to the model in the 'structurallly unstable direction' or
  - such perturbations are known to be small enough to not have a significant impact on the time scales that are relevant for the problem.
    E.g. if the carrying is so large that the decay of the oscillations occurs only over a time scale of many periods, the model may still be useful to understand real systems. However, to observe such oscillations they would have to be driven by some mechanism, which could be noise, or they would have to be the result of some special initial condition.

To get a system that spontaneously generates oscillations, i.e. not only decaying oscillations, we need to extend the Lotka-Volterra model in a different way.

How to improve the modeling of the functional and the numerical response? Simply allow higher-order polynomials as we did in the black-box model?

2.3.3 Modeling Functional Response. Generalist and Specialist Predators

Improve the modeling of the predation process, i.e. the functional response.

In population dynamics one tends to distinguish between *specialist* predators and *generalists.* Generalist predators prey on more than one species: if one prey species is rare they can focus on another one in their diet $\Rightarrow$ the population size of such a predator species may not vary as much with the density of a single prey species as a *specialist* predator who preys only on one species.

How to model the difference in the functional response? What do the data show?

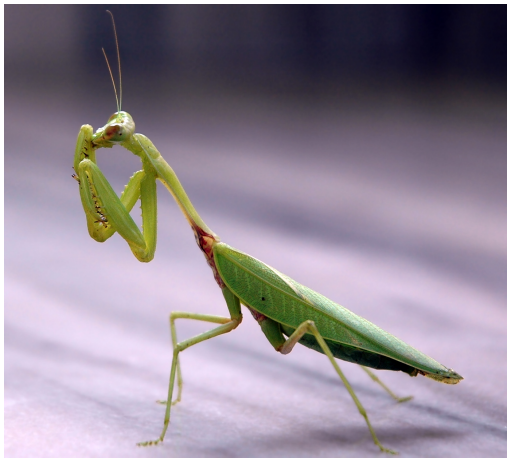

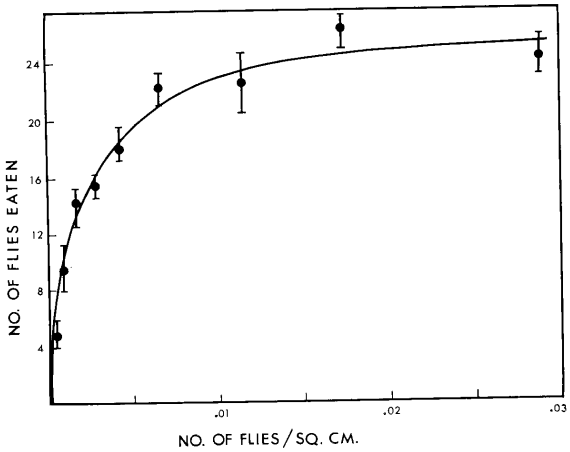

Figure 30: Praying mantis. Functional response of mantids to house flies. Plotted is the number of flies eaten within 8 hours by a mantis in a cage 119$\times$58cm after having been deprived of food for 36 hours. Each captured fly was replaced. At each fly density 3 experiments were performed Holling (1965).

[8]

Consider the number of prey attacked by a predator. A minimal model would be Holling (1965, 1966)

$$N_a = a\, T_T\, N$$

with N_A =number of prey attacked by a predator, a =rate of successful search, T_T =time predator is exposed to prey, N =prey density.

Consider units

$$[N_a] = prey \quad [T_T] = time \quad [N] = \frac{prey}{area} \quad \Rightarrow \quad [a] = \frac{area}{time}$$

Thus, a includes the range at which the predator strikes.

This minimal model leads to the Lotka-Volterra functional response term.

Possible refinements/extensions

[8] Photo of praying mantis by Shiva shankar - Taken at karkala, Karnataka as a praying mantis, CC BY-SA 2.0, https://commons.wikimedia.org/w/index.php?curid=244227

- the predator cannot spend all the time hunting, even if prey is available:
  - handling prey
  - digesting prey
- the rate of successful search depends on
  - the predator's range
  - the predator's 'motivation'=hunger: satiated, a predator may search/strike less

Assume predator needs a time T_H to handle each prey ($[T_H] = \frac{time}{prey}$), i.e. each prey handled takes away time from the hunting,

$$N_a = a\ (T_T - T_H N_a)\ N$$

i.e.

$$N_a = \frac{a\, T_T N}{1 + a T_H N.} \tag{8}$$

Using this functional response one gets then (written in dimensioned quantities again)

$$\frac{dN}{dt} = rN - \frac{a\, T_T N}{1 + a T_H N} P \tag{9}$$

$$\frac{dP}{dt} = -dP + \chi \frac{a\, T_T N}{1 + a T_H N} P \tag{10}$$

Note:

- This model has a functional response that is hyperbolic in N_a.
- It has a maximal reproduction rate.
- Only one type of resource/prey is available to the predator in this model: specialist predator.

In the spirit of the derivation (rational motivation) of (8) Holling has measured parameters in the predator-prey interaction extensively in mantids and included also a way of quantifying satiation/hunger and its impact on predator behavior. The resulting model is quite complicated, but gives a quite reasonable account of certain aspects of the predating behavior of mantids, considered as a model animal Holling (1966).

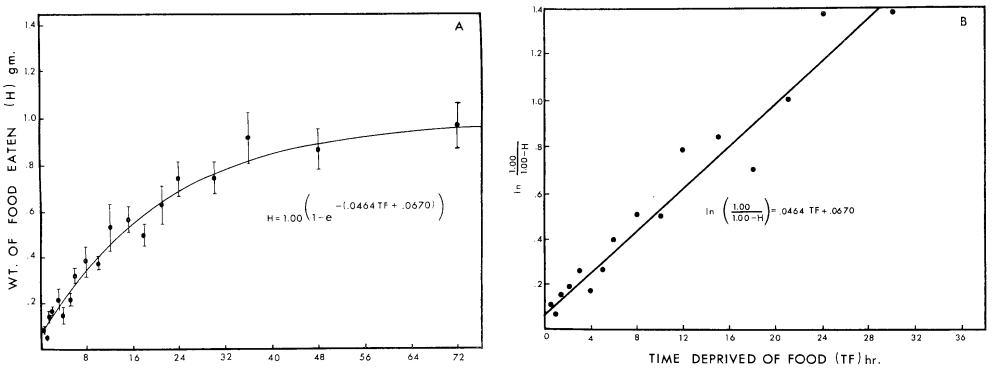

Figure 31: Measuring satiation/hunger in mantis in terms of the amount of food needed for satiation as a function of time after previous feeding to satiation. Satiation is modeled as decaying exponentially, which allows the introduction of a hunger variable that increases linearly in time. Holling (1966)

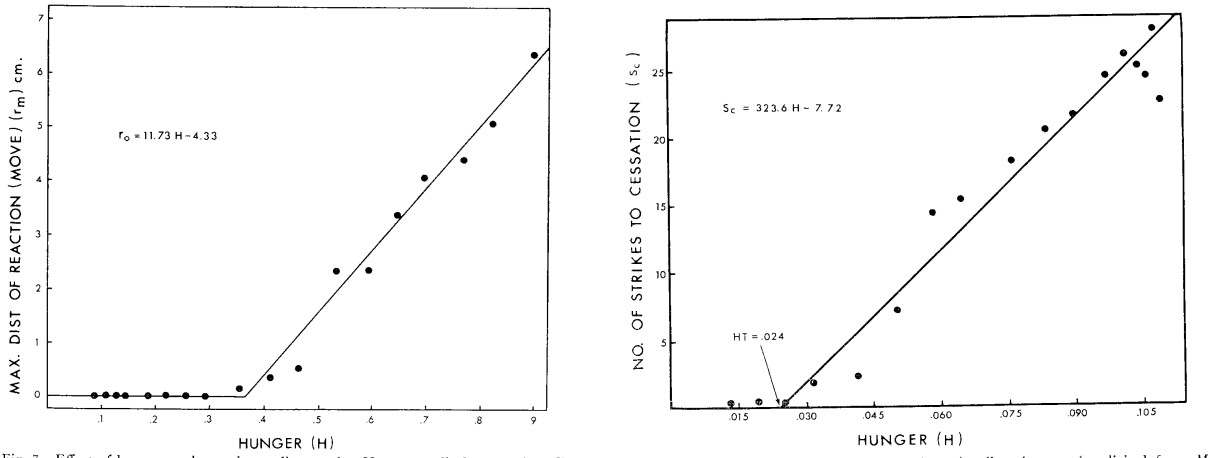

Fig. 7. Effect of hunger on the maximum distance that *H. crassa* stalked or struck at flies (average of 12 replicates).

Fig. 25. The effect of hunger on the number of strikes that can be elicited from *M. religiosa* by a fly dangled behind a glass barrier.

Figure 32: With increasing hunger the mantis is willing to strike at flies at a larger distance and more often (when the fly is unreachable behind a glass barrier) Holling (1966)

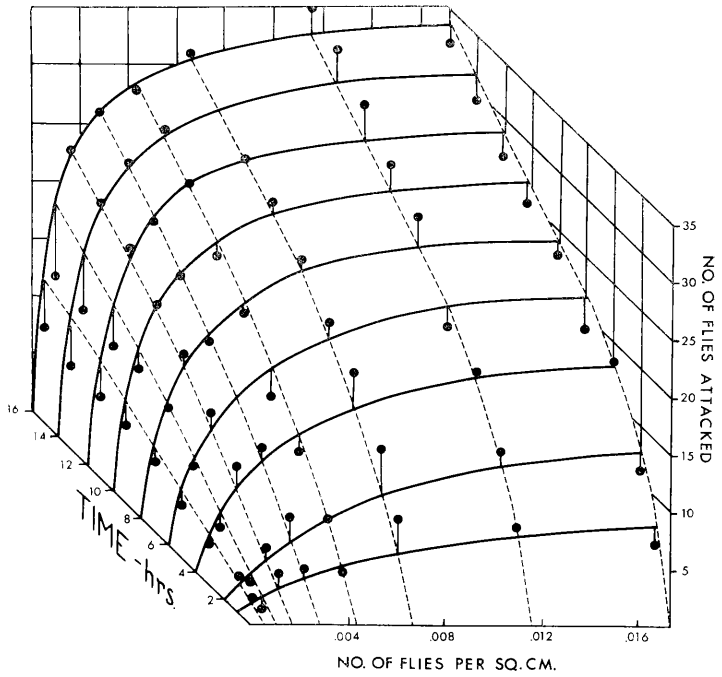

Fig. 29. Number of flies attacked by *H. crassa* at various prey densities and times. The points are actual data (averages of 3 replicates) and the lines are generated by the model.

Figure 33: Based on measurements like those in Figs.31,32 (and measurements of other quantities like mantid's prey awareness, striking success, and eating speed and their dependence on hunger) Holling comes up with a model that provides quite reasonable predictions for the number of flies attacked at a given time after the mantid has been fed to satiation (points are measurements, the surface is generated by the model Holling (1966).

How does the functional response change when multiple food sources are available?

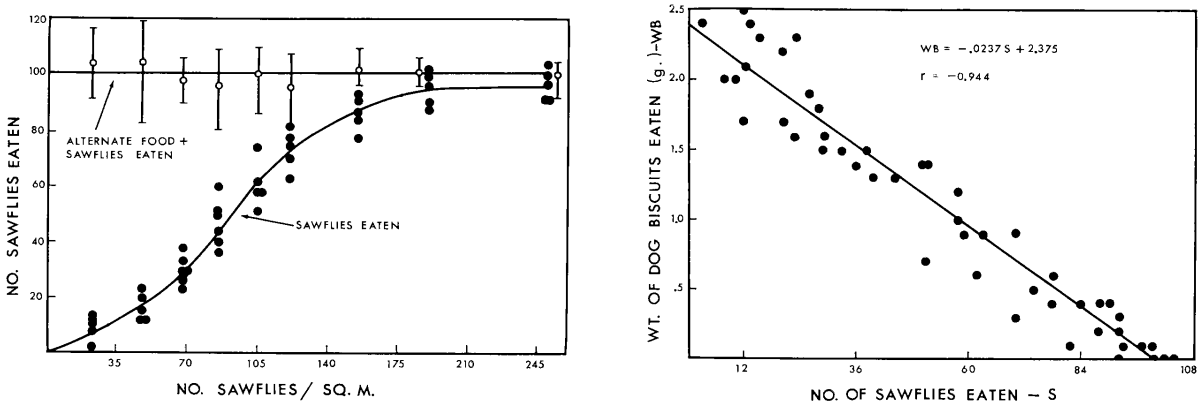

Figure 34: a) Functional response of deer mouse on sawfly prepupae. Sawfly cocoons are buried in the cage in a grid pattern and in addition dog biscuits are freely available. b) Dog biscuits vs prepupae of sawflies eaten Holling (1965).

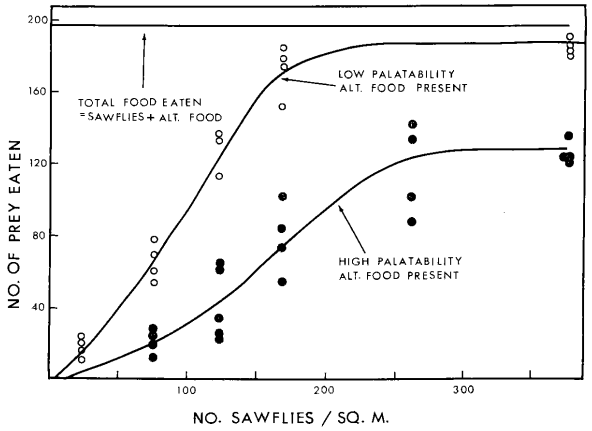

Figure 35: Palatibility of alternate food modifies fraction of prey (prepupae of sawflies) eaten by deer mouse. Low palatability food = dog biscuits, higher palatability food = sunflower seeds. Higher palatibility of alternate food $\rightarrow$ saw fly consumption saturates at lower value: mixed diet. Holling (1965)

Experiments suggest a sigmoidal functional response if an alternate abundant, but less palatable food source is available. Holling gives a detailed model for this scenario including effect of hunger and learning of the palatability Holling (1965).

One can motivate a sigmoidal-like form by assuming that the rate of successful searches increases with N, e.g. the predator weighs the additional effort required to get the better food compared to the easily available less palatable food,

$$a(N) = \frac{bN}{1+gN}.$$

This successful search rate saturates for large N. Inserting into N_a yields

$$N_a = \frac{T_T N}{\frac{1}{a(N)} + T_H N} = \frac{bT_T N^2}{1 + gN + bT_H N^2}$$

The parameter g does not have a strong influence on the overall shape of N_a: often it is simply set to 0 and one gets for the sigmoidal functional response mode for a generalist predator

$$N_a = \frac{bT_T N^2}{1 + bT_H N^2}$$

Notes:

- It is difficult to show that this is indeed the cause of the sigmoidal functional response.
- This model of the generalist predator does not model the alternate food source explicitly. Therefore within this framework the reproduction rate of this predator cannot really be modeled, since the amount of alternate food consumed is not known. This approach is reasonable if the amount of alternate food that is available is abundant and therefore the population of this predator is essentially constant, in particular, it does not vary with N.

2.4 Generalized Lotka-Volterra Models

2.4.1 Rosenzweig-MacArthur Model

Include the hyperbolic functional response function together with the finite carrying capacity N_c in the Lotka-Volterra equations ROSENZWEIG and MACARTHUR (1963); Harrison (1995)

$$\frac{dN}{dt} = rN\left(1 - \frac{N}{N_c}\right) - \frac{a\,T_T N}{1 + aT_H N} P \tag{11}$$

$$\frac{dP}{dt} = -dP + \chi \frac{a\,T_T N}{1 + aT_H N} P \tag{12}$$

Note:

- This is the model used for the discussion of the black-box approach.
- This model was first discussed in the context of graphical analysis of linear stability by Rosenzweig and MacArthur ROSENZWEIG and MACARTHUR (1963) and was later the starting point for Harrison's detailed analysis of Luckinbill's data on *Didinium nasutum* preying on *Paramecium* LUCKINBILL (1973) and his sequence of improved models Harrison (1995). Harrison's paper is worth looking at; it proceeds quite systematically in testing what changes of the model improve the agreement with the data. He finds the best agreement with a model that includes an additional differential equation for the energy acquired by eating (cf. satiation).

Introduce dimensionless quantities

$$\hat{t} = rt \qquad \hat{N} = \frac{N}{N_c}$$

$$\frac{d\hat{N}}{d\hat{t}} = \hat{N}\left(1-\hat{N}\right) - \frac{a\,T_T}{r}\frac{\hat{N}}{1+aT_H N_c\,\hat{N}}P$$

using

$$\hat{P} = \frac{aT_T}{r}P$$

we get

$$\frac{d\hat{N}}{d\hat{t}} = \hat{N}\left(1-\hat{N}\right) - \frac{1}{1+aT_H N_c\,\hat{N}}\,\hat{N}\,\hat{P}$$

and

$$r\frac{d\hat{P}}{d\hat{t}} = -d\hat{P} + \chi\frac{a\,T_T N_c\hat{N}}{1+aT_H N_c\hat{N}}\hat{P}$$

$$\frac{d\hat{P}}{d\hat{t}} = -\frac{d}{r}\hat{P} + \frac{\chi a\,T_T N_c}{r}\frac{\hat{N}}{1+aT_H N_c\hat{N}}\,\hat{P}$$

Introduce

$$\delta = \frac{d}{r} \qquad \eta = aT_H N_c \qquad \psi = \frac{\chi a T_T N_c}{r}$$

to get

$$\begin{aligned}\frac{d\hat{N}}{d\hat{t}} &= \hat{N}\left(1-\hat{N}\right) - \frac{1}{1+\eta\hat{N}}\,\hat{N}\,\hat{P}\\ \frac{d\hat{P}}{d\hat{t}} &= -\delta\hat{P} + \psi\frac{\hat{N}}{1+\eta\hat{N}}\,\hat{P}\end{aligned}$$

Again, dangerously omitting the ˆ, we get

$$\frac{dN}{dt} = N\,(1-N) - \frac{1}{1+\eta N}\,N\,P \tag{13}$$

$$\frac{dP}{dt} = -\delta P + \psi\frac{N}{1+\eta N}\,P \tag{14}$$

Notes:

- Here the prey density was made dimensionless in terms of its carrying capacity, whereas in the original Lotka-Volterra we used the conversion rate χ. Therefore the equations contain now a dimensionless conversion rate ψ.

Obtain the nontrivial fixed point:

For $P_0 \neq 0$ we get

$$-\delta\,(1+\eta N_0) + \psi N_0 = 0 \qquad N_0 = \frac{\delta}{\psi - \delta\eta}$$

and

$$P_0 = (1 - N_0)(1 + \eta N_0) = 1 - (1 - \eta)N_0 - \eta N_0^2$$

What happens at $\psi - \delta\eta = 0$? There $N_0 \to \infty$. Why that?

In the limit of large N_0 this solution becomes biologically meaningless, since P_0 becomes negative.

In fact, N_0 cannot exceed 1, i.e. the prey cannot exceed its carrying capacity. To reach $N_0 = 1$ the predator has to be extinct.

N_0 increases with increasing $\delta\eta$, i.e. when

- the death rate of the predator (relative to that of the prey) increases
- when the predator's hunting becomes ineffective, i.e. η large, because the handling time T_h is large

An increase in the search rate a, which also enters η does not increase N_0 since a also enters ψ; in fact, it decreases N_0.

Linear Stability of the fixed point (N_0, P_0):

Writing the equations as

$$\frac{dN}{dt} = F(N, P) \qquad \frac{dP}{dt} = G(N, P)$$

we get

$$\frac{\partial F}{\partial N} = 1 - 2N_0 - \left(\frac{1}{1 + \eta N_0} - \frac{N_0}{(1 + \eta N_0)^2}\eta\right) P_0 = 1 - 2N_0 - \frac{1}{(1 + \eta N_0)^2} P_0$$

$$\frac{\partial F}{\partial P} = -\frac{1}{1 + \eta N_0} N_0$$

$$\frac{\partial G}{\partial N} = \psi \frac{1}{(1 + \eta N_0)^2} P_0$$

$$\frac{\partial G}{\partial P} = -\delta + \psi \frac{N_0}{1 + \eta N_0}$$

Usually, we would at this point insert the expressions for N_0 and P_0 into this Jacobian and evaluate the eigenvalues. This looks like it is becoming very unwieldy. Instead, use N_0 and P_0 as independent parameters and solve the fixed-point equations for δ and η, since they show up only linearly in the equations,

$$1 + \eta N_0 = \frac{P_0}{1 - N_0} \qquad \delta = \frac{\psi N_0}{1 + \eta N_0} = \psi \frac{N_0 (1 - N_0)}{P_0}$$

We get then

$$\frac{\partial F}{\partial N} = 1 - 2N_0 - \frac{(1 - N_0)^2}{P_0^2} P_0 = \frac{1}{P_0}\left(P_0 (1 - 2N_0) - (1 - N_0)^2\right)$$

$$\frac{\partial F}{\partial P} = -\left(1-N_0\right)\frac{N_0}{P_0}$$
$$\frac{\partial G}{\partial N} = \psi\left(1-N_0\right)^2\frac{1}{P_0}$$
$$\frac{\partial G}{\partial P} = 0$$

Thus, we get for the trace and determinant of the Jacobian $\boldsymbol{M}$

$$trace(\boldsymbol{M}) = \frac{\partial F}{\partial N} + \frac{\partial G}{\partial P} = \frac{1}{P_0}\left(P_0\left(1-2N_0\right) - \left(1-N_0\right)^2\right)$$

$$det(\boldsymbol{M}) = -\frac{\partial F}{\partial P}\frac{\partial G}{\partial N} = \psi\left(1-N_0\right)^3\frac{N_0}{P_0^2}$$

Since $N_0 < 1$ we have $det(\boldsymbol{M}) > 0$, which implies that for $trace(\boldsymbol{M}) = 0$ we would get a Hopf bifurcation

$$trace(\boldsymbol{M}) = 0 \qquad \Rightarrow \qquad P_0^{(Hopf)} = \frac{\left(1-N_0\right)^2}{1-2N_0}$$

For a given fixed N_0 the fixed point becomes unstable to oscillations when the trace becomes positive,

$$P_0 > P_0^{(Hopf)}$$

Taking N_0 as a free parameter, we can insert $P_0^{(Hopf)}$ into δ and η we obtain a parametrization of the Hopf bifurcation in the (δ,η)-plane

$$\begin{aligned}\eta^{(Hopf)} &= \left(\frac{\left(1-N_0\right)^2}{1-2N_0}\frac{1}{1-N_0} - 1\right)\frac{1}{N_0} = \frac{1}{N_0}\left(\frac{1-N_0-1+2N_0}{1-2N_0}\right) = \frac{1}{1-2N_0}\\ \delta^{(Hopf)} &= \psi\frac{N_0}{1+\frac{N_0}{1-2N_0}} = \psi\frac{N_0\left(1-2N_0\right)}{1-N_0}\end{aligned}$$

On which side of the Hopf-bifurcation line is the fixed point unstable? We need to increasing P_0 beyond $P_0^{(Hopf)}$ at fixed N_0. This implies that both η and δ need to be changed: $\eta = \eta(P_0)$ and $\delta = \delta(P_0)$. We have

$$\frac{d\eta}{dP_0} = \frac{1}{N_0\left(1-N_0\right)} > 0 \qquad \frac{d\delta}{dP_0} = -\psi\frac{1}{P_0^2}N_0\left(1-N_0\right) < 0$$

Since the growth rate increases with increasing P_0 at fixed N_0 the fixed point becomes unstable as the Hopf bifurcation line is crossed from 'south-east' to 'north-west'.

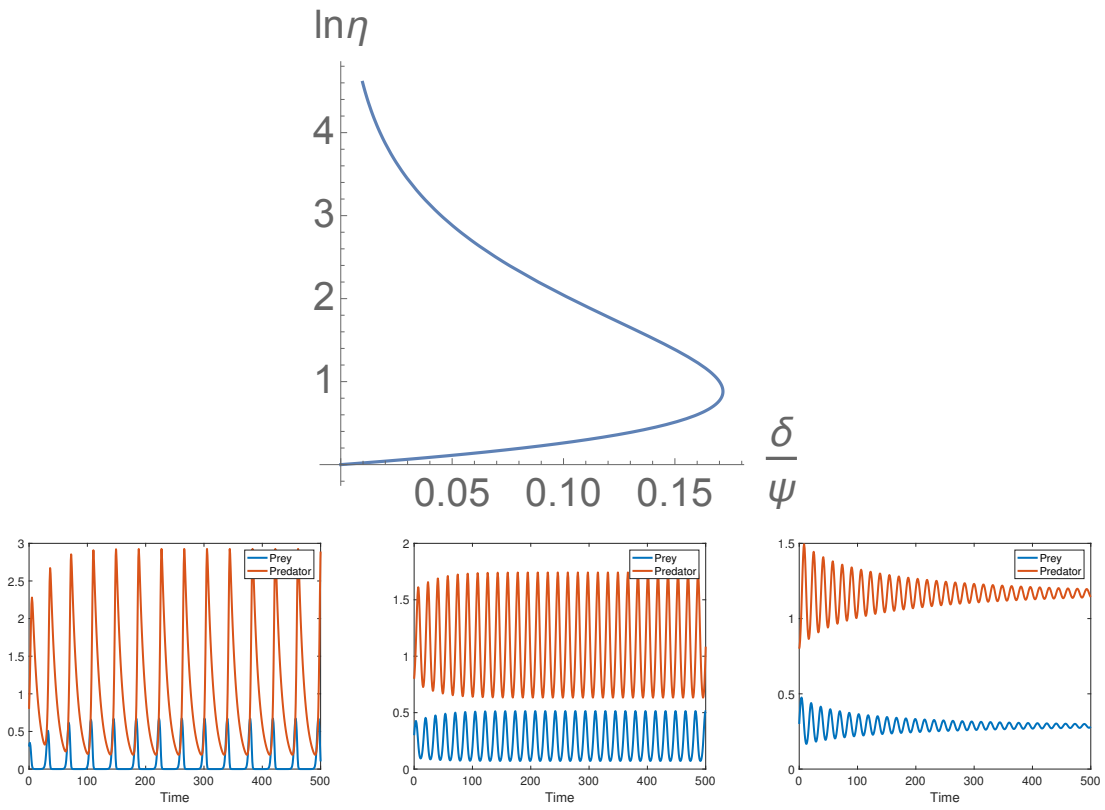

Figure 36: a) Phase diagram for the Rosenzweig-MacArthur model. b) Predator-prey dynamics for , $\delta = 0.1$, $\delta = 0.3$, $\delta = 0.35$ with $\eta = e^{0.8}$, $\psi = 2$.

Notes:

- As predicted by the linear stability analysis, oscillations arise at the stability limit as δ is decreased.
- Close to the onset of the oscillations they are harmonic. In this regime they can be described in a *weakly nonlinear* analysis

$$\begin{pmatrix} N \\ P \end{pmatrix} = \begin{pmatrix} N_0 \\ P_0 \end{pmatrix} + \epsilon \begin{pmatrix} n_1 \\ p_1 \end{pmatrix} A e^{i\omega t} + c.c. + \mathcal{O}(\epsilon^2) \qquad \epsilon \ll 1,$$

  where $\begin{pmatrix} n_1 \\ p_1 \end{pmatrix}$ is the complex eigenvector associated with the eigenvalue $\lambda = i\omega$ and A is a complex amplitude. The weakly nonlinear analysis yields a nonlinear (cubic) differential equation for A.
- Further above they become very anharmonic.
- The Rosenzweig-MacArthur model is consistent with our general rules and generates oscillations in a structurally stable way.

2.4.2 Brief Discussion of Other Models

Yodzis Model. The Rosenzweig-MacArthur model with its hyperbolic functional response assumes a specialist predator. How about introducing a generalist predator as in Yodzi (1989) (as cited in Turchin (2003)),

$$\begin{aligned} \frac{dN}{dt} &= N\,(1-N) - \frac{N^2}{1+\eta N^2}\,P \\ \frac{dP}{dt} &= -\delta P + \psi \frac{N^2}{1+\eta N^2}\,P \end{aligned}$$

It models that for low prey densities the predator reduces its effort to search for that prey and kills fewer of them.

But: Its reproduction rate is based purely on the intake from this prey and becomes very small for low N. If the predator really has no other food source, this reduction in effort would amount to the predator 'giving up on eating', which is not very realistic.

Possible changes

- include another food source
  - if that food source is abundant, the predator density may become relatively independent of N and its dynamics would not have to be modeled
  - if the alternate food source is scarce, it could be included in the model.
- predator goes into hibernation: reduce δ for low predation rate

Leslie Model. Motivated by the logistic population growth model one could argue that the influence of the prey density on the predator population is via the predator's carrying capacity, making the carrying capacity proportional to the prey density. That would lead in the simplest form to LESLIE (1948)

$$\begin{aligned} \frac{dN}{dt} &= N\,(1-N) - N\,P \\ \frac{dP}{dt} &= \sigma P \left(1 - \kappa \frac{P}{N}\right) \end{aligned}$$

What could be a mechanistic motivation for the logistic term in the predator equation?

Assume that there is competition between individual predators and that each dominating predator can defend an area $A_{territory}$ that is large enough to sustain it, $A_{territory}N = \kappa$. Then the density of predators, i.e. the carrying capacity, is $1/A_{territory} = N/\kappa$.

But: If the predator density is small compared to the prey density the reproduction rate of the predator would be independent of the functional response, i.e. independent of the food intake of the predator, even if the amount of prey is very small. Where does the biomass come from to provide the growth when there is almost no food? The amount of biomass generated per P by reproduction is constant, while that available is proportional to N.

A constant reproduction rate of the predator would be obtained in a systematic way, if the numerical response was in the saturating regime of the hyperbolic function

$$\frac{N}{1+\eta N} P \to 1 \cdot P \qquad \text{for} \qquad N \gg \eta$$

In that case the functional response should, however, also be independent of N. A systematic version would then be

$$\begin{aligned} \frac{dN}{dt} &= N\,(1-N) - P \\ \frac{dP}{dt} &= \sigma P \left(1 - \kappa \frac{P}{N}\right) \end{aligned}$$

This model would be valid as long as N is sufficiently large.

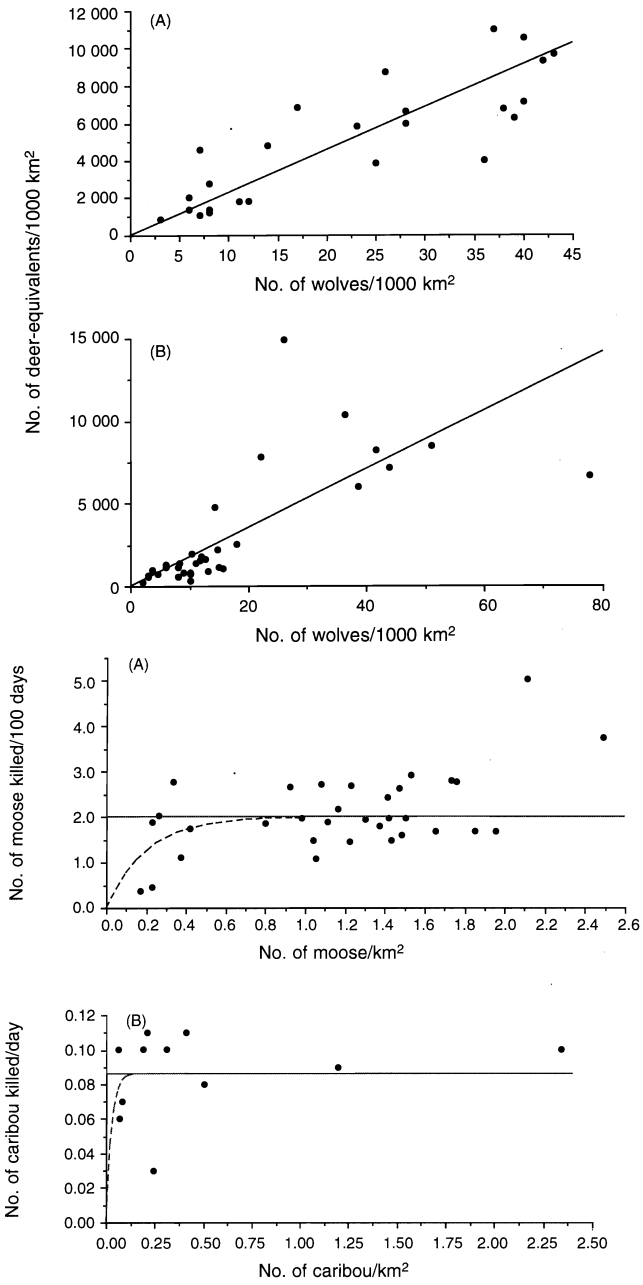

Figure 37: a) Density of wolves as a function of density of 'deer-equivalents'. b) Rate of predation of moose and caribou per wolf is quite independent of the prey density Eberhardt (1997).

2.5 Case Study: Vole Dynamics[9]

"*The affair runs always along a similar course. Voles multiply. Destruction reigns. [...] The experts advise a Cure. The Cure can be almost anything: [...] a Government Commission, a culture of bacteria, poison, prayers denunciatory or tactful, a new god, a trap, a Pied Piper. The Cures have only one thing in common: with a little patience they always work. They have never been known entirely to fail. Likewise they have never been known to prevent the next outbreak. For the cycle of abundance and scarcity has a rhythm of its own, and the Cures are applied just when the plague of voles is going to abate through its own loss of momentum.*" (Charles Elston (1942) cited in *(Barraquand et al., 2017)*)

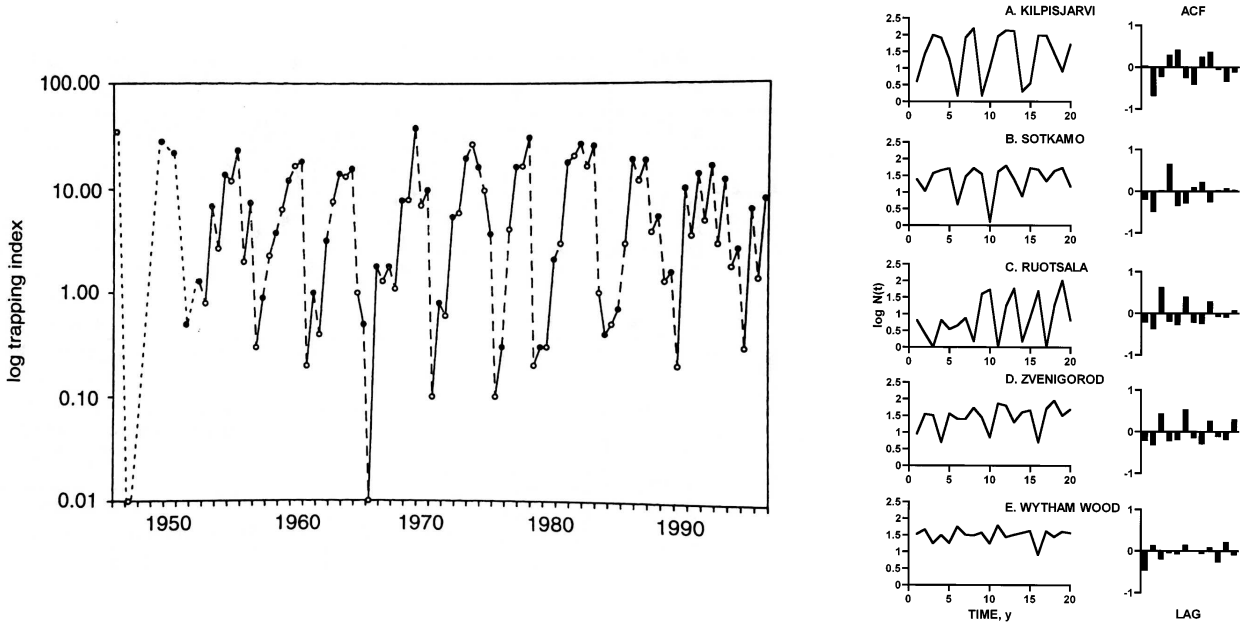

Figure 38: a) Pooled small rodent abundance at Kilpisjarvi, Finnish Lapland. Open symbols (spring), closed symbols (fall), dashed/solid lines denote changes during winter/summer (Henttonen and Hanski, 2000). Measured by trapping. b) Dependence of the oscillations on latitude.

The dynamics of vole populations in Scandinvia show interesting behavior:

- substantial oscillations in areas further north
- almost steady populations in areas further south

One key goal of the modeling is to identify or at least suggest what the key mechanism is that drive the oscillations and why the oscillations die out as one goes south.

Turchin and Hanski Turchin and Hanski (1997) hypothesized this observation is related to the different impact of predation by specialists and by generalists for different latitudes.

[9](Turchin and Hanski, 1997; Turchin and Ellner, 2000; Turchin, 2003)

Presumably the abundance of alternative prey depends on snow cover (duration and depth).

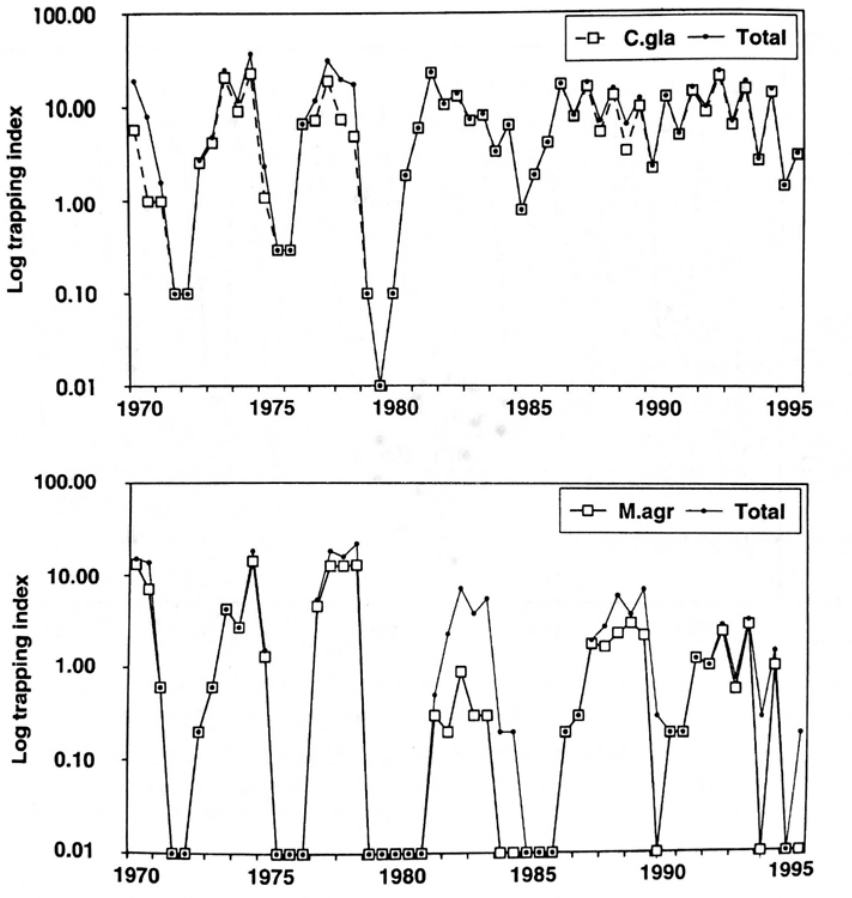

Figure 39: Small rodent abundance at Pallasjarvi for open habitats (lower panel) and forested habitats (upper panel) showing different degree of oscillation Henttonen and Hanski (2000).

Development of the Model

V'oles reproduce 'continuously', no discrete generations $\Rightarrow$ ODE model

Experiments in enclosed fields (40m$\times$40m) in which the density of the voles was controled and varied artificially by removing subadult individuals biweekly Turchin and Ostfeld (1997). They support the assumptions (Fig.40)

- logistic reduction of growth rate with population size
- sort-of sinusoidal variation of growth rate with time of the year (as compared to a discontinuous variation)

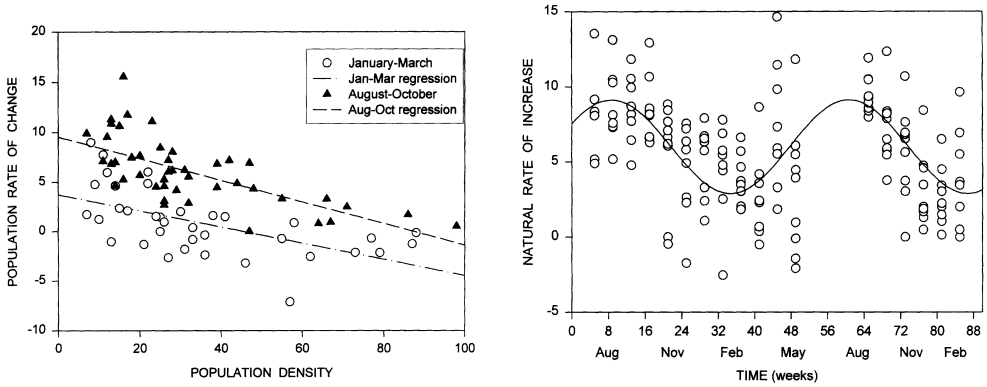

Figure 40: Rate of change of the population depends reasonably linearly on the density and varies with season Turchin and Ostfeld (1997).

Motivated by the change in oscillation amplitude with geography two types of predators are included in the model

- generalists (nomadic avian predators), which tend to stabilize steady states
- specialists (weasels), which tend to induce oscillations through the delay in their population size

$$\begin{aligned} \frac{dN}{dt} &= rN\left(1 - e\sin\omega t - \frac{N}{N_c}\right) - G\frac{N^2}{H^2+N^2} - A\frac{NP}{D+N} \\ \frac{dP}{dt} &= sP\left(1 - e\sin\omega t - Q\frac{P}{N}\right) \end{aligned}$$

Notes:

- Generalist population is not modeled explicitly, since it is assumed that it is relatively constant due to the abundance of other food soureces.
- The carrying capacity of the predator is taken to be proportional to N, since weasels are territorial, which can lead to an N-dependent carrying capacity (cf. discussion of Leslie model in Sec.2.4.2).
- The linear reproduction rate of the predator is taken to be a constant, even though a hyperbolic form for the functional response is taken. They argue
  - weasels produce litters of relatively constant size independent of prey density as long as that density is above a threshold Hanski and Korpimaki (1995); in that regime then reproduction rate would not depend much on food intake. However, no threshold used in the model discussed here $\Rightarrow$ to be a convincing model N has to be large enough.
  - weasels are small: most food may be needed to generate heat [also for predation and competition?]

- seasons assumed to affect both reproduction rates equally and sinusoidally (equality later eased). This term is meant to capture the lack of weasel births when N is too small.

Dimensionless equations:

Introduce

$$n = \frac{N}{N_c} \qquad p = \frac{Q}{N_c}P \qquad 2\pi\hat{t} = \omega t$$

Because of the seasonal variation it is better to make the time dimensionless in terms of that modulation than in terms of the growth rate r of the prey

$$\begin{aligned} \frac{dn}{dt} &= rn\,(1 - e\sin 2\pi t - n) - g\frac{n^2}{h^2+n^2} - a\frac{np}{d+n} \\ \frac{dp}{dt} &= sp\left(1 - e\sin 2\pi t - \frac{p}{n}\right) \end{aligned}$$

with

$$g = \frac{G}{N_c} \qquad h = \frac{H}{N_c} \qquad d = \frac{D}{N_c} \qquad a = \frac{A}{Q}$$

Note:

- Drop again the ˆ on the dimensionless time and the growth rates $r > 0$ and $s > 0$

Estimates for the Parameters

These estimates are all quite rough and robustness with respect to changing the parameters is an important aspect. The estimates are pulling in as much information as can be brought to bear on the problem. To make progress it is essential that one has a good overview of a wide range of experimental facts of the system. This is often a quite challenging task.

- Intrinsic growth rate of voles r: averaged over seasons from Turchin and Ostfeld (1997) $6\,\text{year}^{-1}$
- Amplitude of seasonal forcing e: $0.5 - 1$ Turchin and Ostfeld (1997)
  for weasels the reproduction rate should be negative during the winter, suggesting $e > 1$ for them.
- Carrying capacity N_c: typically observed *peak* densities 300 voles/ha $\Rightarrow N_c \approx 150$ voles/ha.
- Growth rate s of weasels: under good conditions 2 litters per year with 5 pups each per female $\Rightarrow$ per weasel 5 pups/year $s = \ln 5 = 1.6 \Rightarrow$ take $s = 1 \ldots 1.5$.
- Maximum consumption per predator, A:
  Weasels consume food corresponding to 60% of their body weight per day $\Rightarrow$ 1 vole per day. Pregnant weasels eat three times that much.
  Estimate 400 voles per year. In addition, there is some surplus killing. Assume

  $$A \approx 600\text{voles per year per weasel.}$$

  Estimate does not include that weasels may also kill lactating mothers which induces additional death.

- Saturation constant D: for weasels to reproduce the vole density has to be above a threshold of $N_{crit} = \mathcal{O}(10\,\text{voles/ha})$ Erlinge (1974). To barely survive *without* reproduction, a weasel needs to eat about $A_{crit} = 1\,\text{vole/day} = 365\,\text{voles/year}$ (see above: pregnant weasels need ≈3 voles/day). These two minimal values for marginal reproduction should match (per weasel)

$$A_{crit} = A\frac{N_{crit}}{N_{crit}+D} \times 1 \qquad \Rightarrow \qquad D \approx 6 \text{ voles/ha}.$$

- Predator-prey ratio constant Q. In steady-state one has $P = N/Q$, i.e. $Q = N/P$. Thus, Q gives essentially the number of voles that are needed to reproduce enough voles to sustain one weasel.
  Voles reproduce about every 20-30 days. In 20 days the vole population needs to produce 20 voles to sustain 1 weasel. At low vole densities each litter produces 5-7 offspring, at intermediate densities about 2. To produce 20 voles one needs then 10 females (each producing 2 voles per 20 days), i.e. 20 voles per weasle $\Rightarrow Q \approx 20$.
  Weasels are also preyed upon by other predators $\Rightarrow Q$ should probably be chosen larger.

- Generalist predation parameters G, H:
  Generalist predators are mostly nomadic avian predators (owls,...). Estimates are based on proportion of voles in the measured predator diet and on the correlation between number of breeding pairs of the avian predators and the vole density (with a 2 month lag, which showed the strongest correlation)

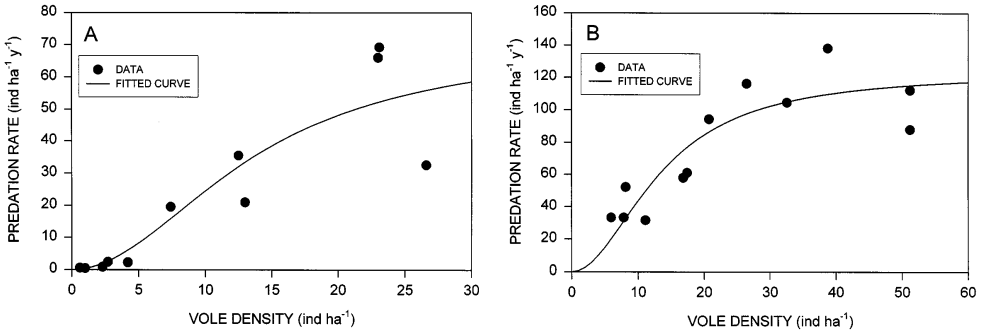

Figure 41: Predation rate of voles by avian predators (generalists) as a function of vole density at Alajoki (latitude $63°$) and Revinge (latitude $56°$). The predation rate is measured via the breeding rate (2 months delayed) and the fraction of voles in the diet Turchin and Hanski (1997).

Data along these lines are available for two locations, Revinge (latitude $56°$) and Alajoki (latitude $63°$). They roughly estimate[10] the density G of generalist predators as a function of the latitude L,

$$G = 700 - 10L.$$

[10]There is a typo in their equation.

The assumption is that the effect of the latitude comes from changes in seasonal snowcover. But vegetation - fields vs woods - will also have its impact on the population dynamics.
They cross-check this linear assumption with two other locations, Grimso and Kilpisjarvi HANSKI et al. (1991). Kilpisjarvi agrees reasonably, but Grimso is quite far off. They argue that the change in landscape from agriculture- to forest–dominated makes a sigificant difference.
They also estimate the switching threshold H from the data in Fig.41 to be $H = 13.8$ and $H = 13.5$, respectively.
Note: It can be discussed whether the data (and their quality) allow to determine H to 3 digits. At Revinge it is not even clear to what extent the data support a sigmoidal rather than a hyperbolic response.

- In the simulations they let the parameters p fluctuate from year to year

$$p_i = p\,(1 + \sigma\xi) \qquad \text{in year } i$$

with ξ Gauss distributed with variance 1.

Dependence of Behavior on Parameters found in Simulations Turchin and Hanski (1997)

Increasing

- a: $\Rightarrow$ specialist predator more important
  - oscillation amplitude increases
  - Lyapunov exponent increases
- d: $\Rightarrow$ reduces impact of specialist predator
  - oscillation amplitude decrease
  - Lyapunov exponent decreases (for larger a that trend is not so clear).
- s: $\Rightarrow$ predator growth faster (but not carrying capacity)
  - period of oscillation decreases
- g: $\Rightarrow$ increases impact of generalist predator
  - oscillation become weaker (see Fig.42)

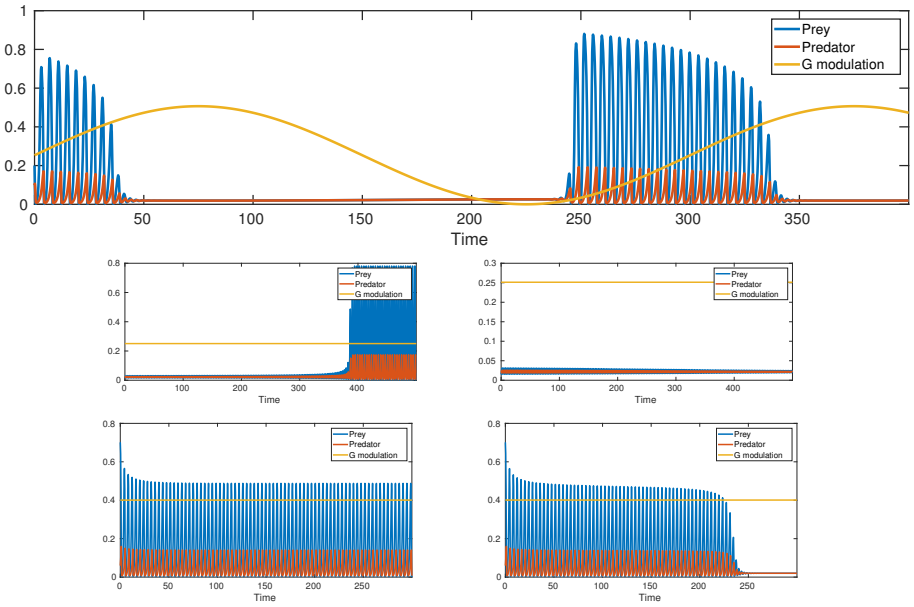

Figure 42: The Hopf bifurcation is subcritial: there is hysteresis when G is varied sinusoidally (top, the hysteresis is exaggered due to temporal ramp in G via a delayed bifurcation). $G = 37.6$ (growing), $G = 37.7$ (decaying), $G = 60.1$ (persisting), $G = 60.14$ (collapsing).

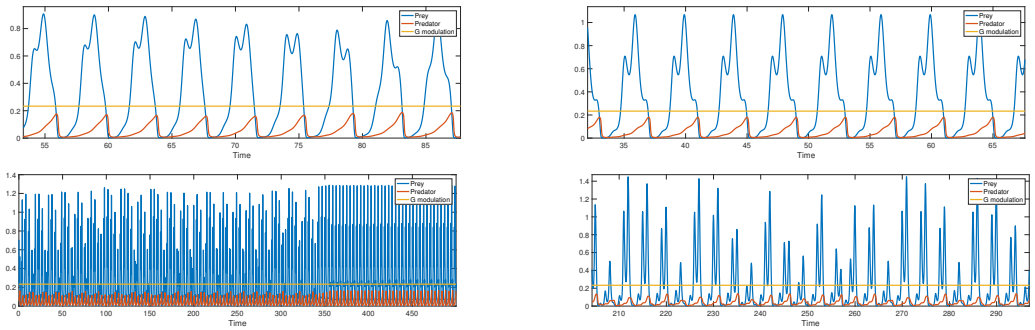

Figure 43: With increasing seasonal modulation the oscillations become more complex. $G = 35$ (fixed point unstable). $e = 0.2$ (not phase-locked), $e = 0.4$ (phase-locked), $e = 0.68$ (complex oscillations only transient), $e = 1.0$ (complex oscillations, persistent chaos)

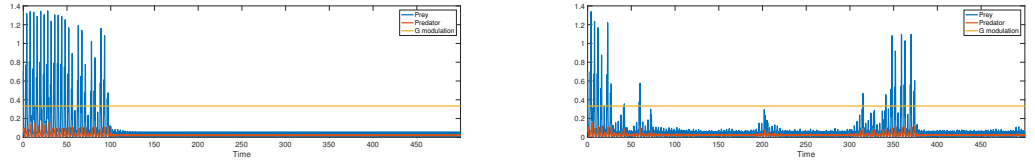

Figure 44: Noise can trigger oscillations repeatedly. $G = 50$ (fixed point linearly stable, without modulation bistable with oscillations) $e = 0.8$. a) $\zeta_n = 0 = \zeta_p$. b) $\zeta_n = 0.05 = \zeta_p$.

Comparison with field data:

- Oscillations have roughly the correct frequency and are increasing with increasing G
- Without noise poor agreement: when increasing G in the model the system goes to the fixed point already at an lower value than corresponds to the field data. This suggests that noise repeatedly excites the oscillations in that regime.
- Oscillation amplitude varies strongly near latitude 60°
  most likely because of subcritical Hopf bifurcation.
- Experimental data suggest a positive Lyapunov exponent. Simulations: without noise chaotic dynamics due to forcing. Lyapunov exponents tend to increase with decreasing G.

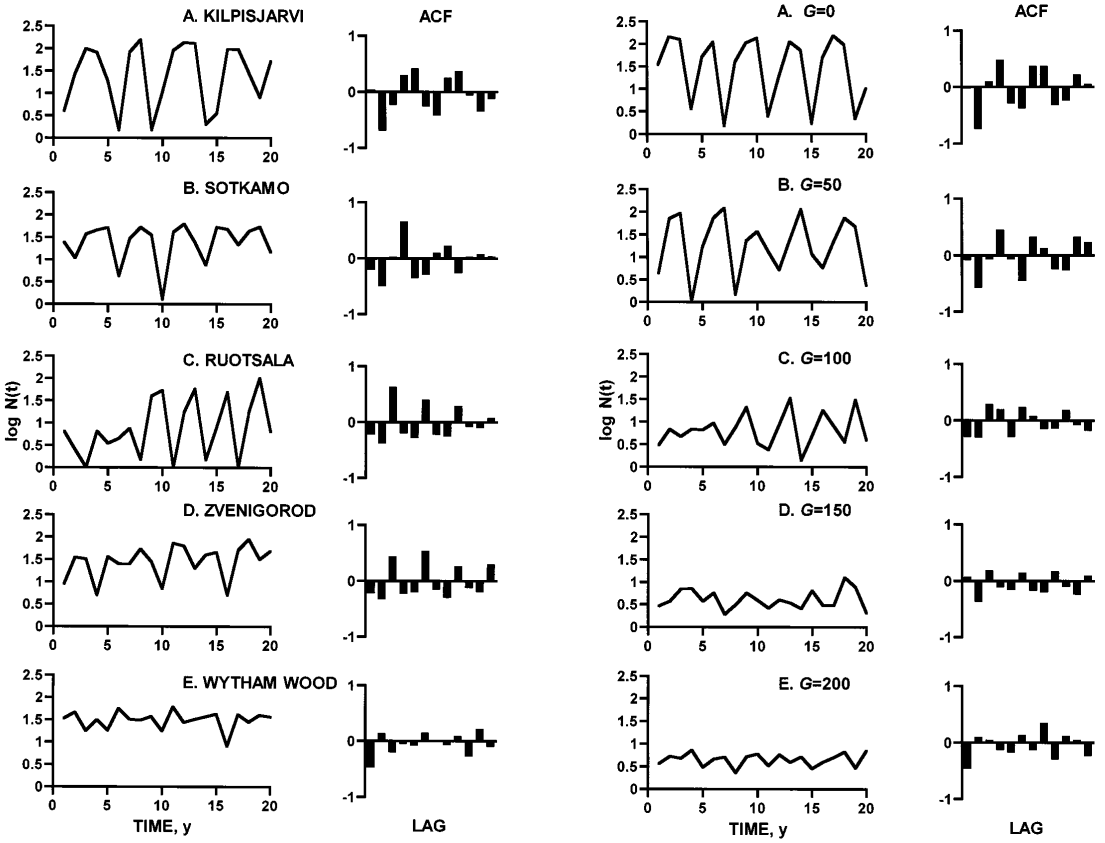

Figure 45: Dependence of oscillations on generalist predator. a) Field data (temporal evolution of vole population and its autocorrelation function) with latitude decreasing from top to bottom (same figure as Fig.38). b) Results from the model with the estimated parameters (and noise added) Turchin and Hanski (1997).

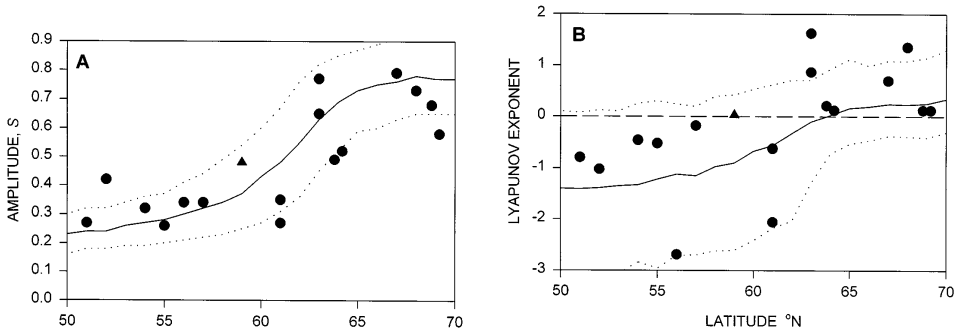

Figure 46: Dependence of oscillation amplitude and Lyapunov exponent on latitude Turchin and Hanski (1997).

Note on Lyapunov Exponents

The key element of chaotic systems is the sensitive dependence of the trajectories on the initial condition. This is quantified via the Lyapunov exponent.

Consider the dynamical system

$$\dot{\mathbf{x}} = \mathbf{f}(\mathbf{x})$$

and two trajectories that start very close to each other at $t = 0$

$$\mathbf{x}(t; \mathbf{x}_0) \qquad \mathbf{x}(t; \mathbf{x}_0 + \delta\mathbf{x}_0)$$

At later times the two trajectories are separated by $\Delta x(t)$,

$$\Delta\mathbf{x}(t) = \mathbf{x}(t; \mathbf{x}_0 + \delta\mathbf{x}_0) - \mathbf{x}(t; \mathbf{x}_0)$$

Measure the distance between these trajectories

$$\|\Delta\mathbf{x}(t)\| = \|\mathbf{x}(t; \mathbf{x}_0 + \delta\mathbf{x}_0) - \mathbf{x}(t; \mathbf{x}_0)\|$$

If $\Delta\mathbf{x}(t)$ is very small one can linearize the differential equation around $\mathbf{x}(t; \mathbf{x}_0, t_0)$ at the time t

$$\begin{aligned} \frac{d}{dt}\Delta\mathbf{x}(t) &= \mathbf{f}\left(\mathbf{x}(t; \mathbf{x}_0 + \delta\mathbf{x}_0)\right) - \mathbf{f}\left(\mathbf{x}(t; \mathbf{x}_0)\right) \\ &= \mathbf{f}\left(\mathbf{x}(t; \mathbf{x}_0) + \Delta\mathbf{x}(t)\right) - \mathbf{f}\left(\mathbf{x}(t; \mathbf{x}_0)\right) \\ &\approx \mathbf{J}\left(\mathbf{x}(t; \mathbf{x}_0)\right) \boldsymbol{\Delta}\mathbf{x}(t) \end{aligned}$$

where $\mathbf{J}\left(\mathbf{x}(t; \mathbf{x}_0)\right)$ is the Jacobian of $\mathbf{f}(\mathbf{x})$ at time t and position $\mathbf{x}(t)$.

Notes:

- If the Jaocbian was constant in time one would expect $\Delta\mathbf{x}$ to grow or decay exponentially
- In general the Jacobian depends on time through the position $\mathbf{x}(t)$ on the attractor

- Over long times $\mathbf{x}(t)$ explores the whole attractor and one could imagine that the growth of $\Delta\mathbf{x}$ is determined by something like an 'average Jacobian'.

Numerically one finds in the limit of long times and small initial distance

$$\|\Delta\mathbf{x}(t)\| \sim \|\Delta\mathbf{x}(0)\|\, e^{\lambda t}$$

Motivated by this observation one defines

$$\lambda \equiv \lim_{t\to\infty} \lim_{\|\Delta\mathbf{x}(0)\|\to 0} \frac{1}{t} \ln\left(\frac{\|\Delta\mathbf{x}(t)\|}{\|\Delta\mathbf{x}(0)\|}\right) \tag{15}$$

Note:

- To stay in the linear regime the limit $\Delta\mathbf{x}(0) \to 0$ is to be taken first before the limit $t \to \infty$.
- In principle, in an n-dimensional system there are n Lyapunov exponents. Each exponent describes the stretching or compression in different directions transverse to the trajectory. (15) results in the largest Lyapunov exponent.

Time Horizon:

The exponential growth of the difference between nearby trajectories limits predictions severely.

Assume we can measure the initial condition with a precision $\delta_0 = \|\Delta\mathbf{x}(0)\|$. If we need to make a prediction with an accuracy δ_{max}, i.e. we require $\|\Delta\mathbf{x}(t)\| < \delta_{max}$, then we can predict the system up to a time t_h

$$\delta_{max} = \|\Delta\mathbf{x}(t_h)\| = \|\Delta\mathbf{x}(0)\|\, e^{\lambda t_h}$$

i.e.

$$t_h(\delta_0) = \frac{1}{\lambda} \ln\left(\frac{\delta_{max}}{\delta_0}\right)$$

The duration for valid predictions grows only logarithmically with the accuracy δ_{max}, which is very slow.

Discrete Time Series

How to obtain reasonable estimates for the (maximal) Lyapunov exponent when only a single noisy time series at discrete times is available?

- We cannot compare multiple trajectories starting with slighly different initial conditions.
  Using (15) actually many such trajectories would be needed, because of the limit $\Delta\mathbf{x}(0) \to 0$. One can follow a given pair of trajectories only as long as they are very near to each other. Once the distance becomes too large, one has to replace one of the trajectories by another one that is again close to the other trajectory.

Having only the time series at discrete time points, we should be considering a map instead of a differential equaion

$$\mathbf{x}_{n+1} = \mathbf{f}(\mathbf{x}_n)$$

Consider the evolution of a slightly perturbed $\mathbf{x}_n$

$$\mathbf{x}_{n+1} + \Delta\mathbf{x}_{n+1} = \mathbf{f}(\mathbf{x}_n + \Delta\mathbf{x}_n) \approx \mathbf{f}(\mathbf{x}_n) + \mathbf{J}(\mathbf{x}_n)\Delta\mathbf{x}_n$$

Thus

$$\Delta\mathbf{x}_{n+1} = \mathbf{J}(\mathbf{x}_n)\Delta\mathbf{x}_n = \mathbf{J}(\mathbf{x}_n)\mathbf{J}(\mathbf{x}_{n-1})\Delta\mathbf{x}_{n-1} = \mathbf{J}(\mathbf{x}_n)\mathbf{J}(\mathbf{x}_{n-1})\mathbf{J}(\mathbf{x}_{n-2})\Delta\mathbf{x}_{n-2}$$

Therefore we consider the eigenvalues of the matrix

$$\mathbf{J}^{(n)} = \prod_{j=1}^{n} \mathbf{J}(\mathbf{x}_j)$$

It has eigenvalues μ_i, $i = 1 \ldots N$ if the system is N-dimensional. They represent *Lyapunov multipliers*.

The Lyapunov exponents are then given by

$$\lambda_i = \lim_{n\to\infty} \frac{1}{n} \ln |\mu_i|$$

and the Lyapunov exponent of interest is $\max_i \lambda_i$.

Note:

- Consider the 1-dimensional case of a constant map

$$x_{n+1} = ax_n = \underbrace{a^n}_{\mu} x_1 = e^{n \ln a} x_1$$

But: we do not have these Jacobian's for the experimental data.

However:

- If the black-box model gives reasonable predictions, we can use it to obtain $\mathbf{J}(\mathbf{x}_i)$ at arbitrary points, since we have an analytic form[11] for the function $\mathbf{F}$.
- In particular, we can compute $\mathbf{J}$ at all the data points of the time series.
- Use the data points $\mathbf{x}_i$
  - if the black-box model was iterated repeatedly, the error in its approximation of the orbit would accumulate and the orbit could diverge from the true orbit substantially - in some cases the iterates actually blow up.

[11] If a non-parametric fit of the response surface is used that would not be so straightforward

  - this captures some aspect of the noise in the system. E.g. if the noise is needed to kick the system every so often onto the slowly decaying oscillatory orbit one would have a chance to characterize that dynamics rather than that of the stable fixed point that would be reached in the absence of noise (cf. Fig.44).

Note:

- The model would be more convincing, if the agreement with the data was compared for different models, e.g. replace ratio for carrying capacity of weasels by hyperbolic numerical response.

2.6 Diversity via Non-Hierarchical Fitness

The 'Paradox of the Plankton' HUTCHINSON (1961): Why are there so many different species? With many of them quite similar, why does not simply the fittest among them win out?

- Extreme case: it has been estimated that in 30g of soil there can be 500,000 different species of bacteria[12].

There are many different ecological niches. But why does the 'best' species not win in a given niche?

- The environmental conditions could keep varying, making different predators best at different times and keeping the system from reaching a 'optimal' state.
- Niches are not only determined by the physical environment (temperature, light, humidity,....), but also by the other species around, with different species contributing to the niche. Niches can be created by other species, which then can change the niches again.

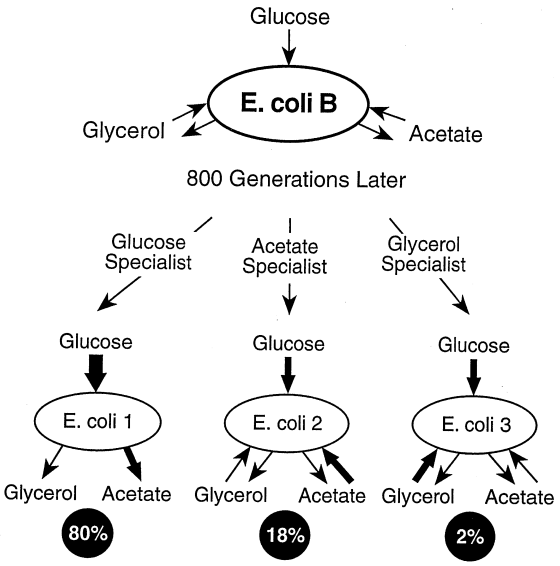

Figure 47: New ecological niches can be created by populations evolving. Dykhuizen (1998)

- There could be no 'best' species: non-transitive competition
  - Overgrowth of sponges and ectoprocts on coral.

[12]Bacteria may be special, since they do not go starve to death and have a high rate of speciation Dykhuizen (1998).

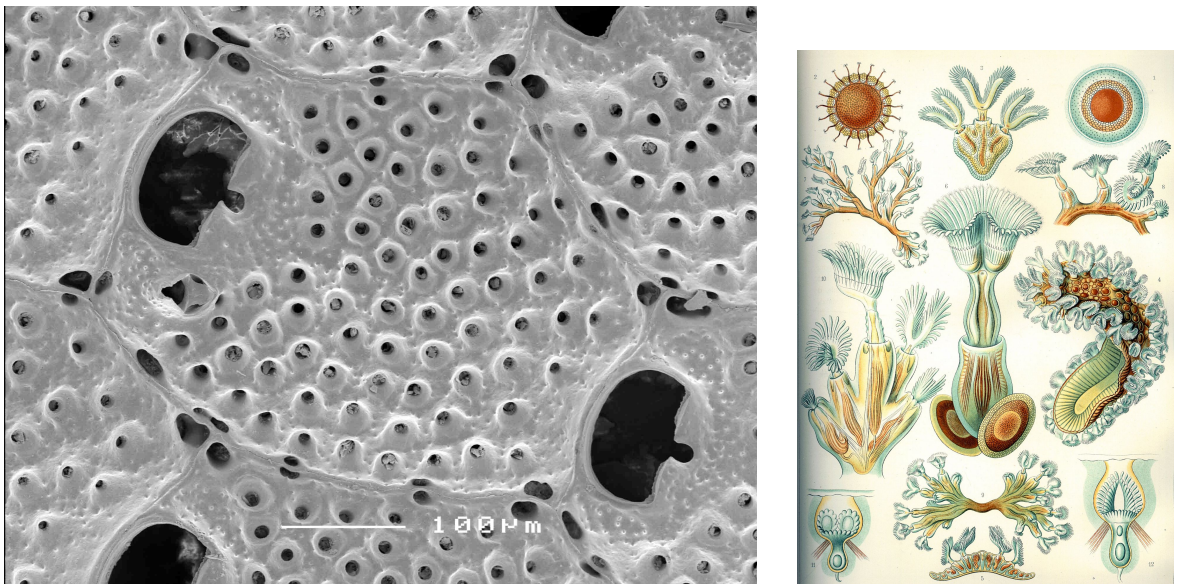

Figure 48: Ectoprocts (bryozoan, moss animals) consist of colonies of individual zooids, which are filterfeeders (Kunstformen der Natur (1904), plate 23: Bryozoa (see here, here and here), Public Domain, https://commons.wikimedia.org/w/index.php?curid=566772.)

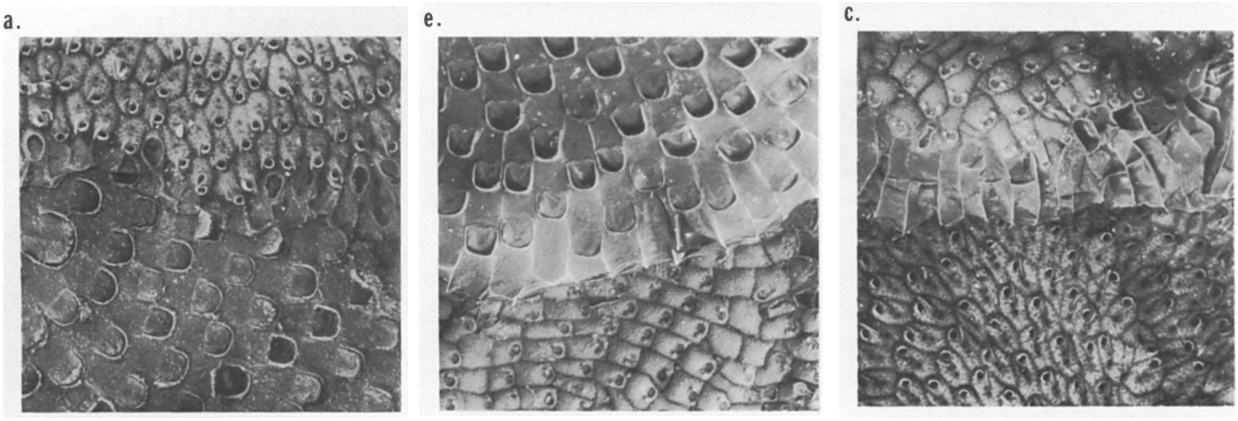

Figure 49: Non-transitive overgrowth patterns of three species of ectoprocts: *Reptadeonella* $\rightarrow$ *Steginoporella* $\rightarrow$ *Stylopoma* $\rightarrow$ Reptadeonlla BUSS and JACKSON (1979).

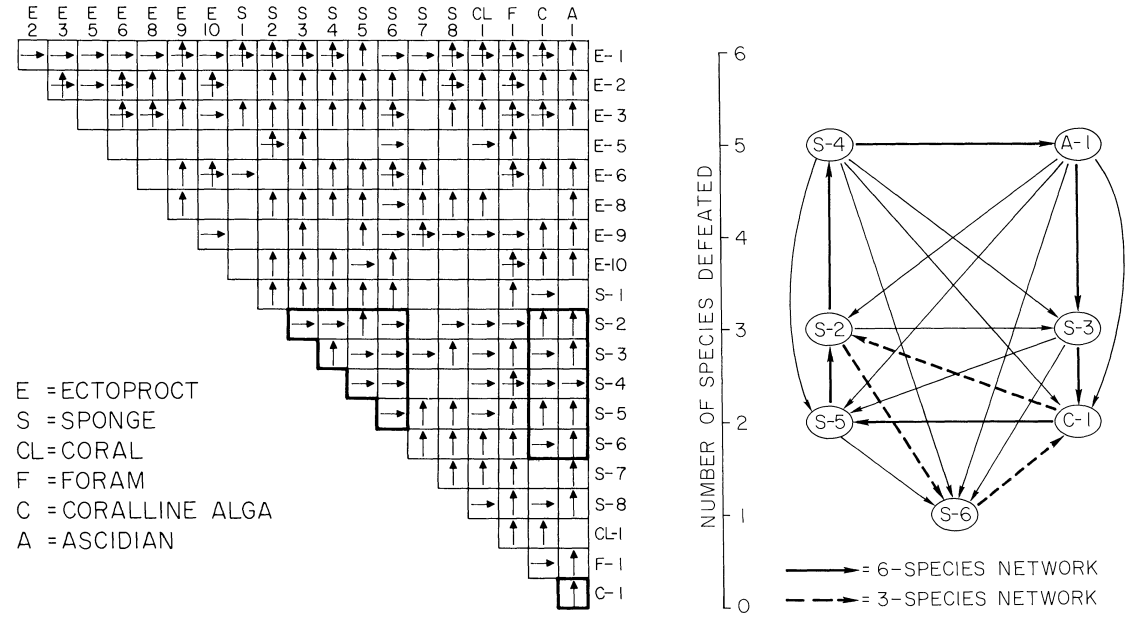

Figure 50: a) Interaction matrix of ectoprocts and sponges on coral. In each square the arrow points to the dominating species in the pair. b) Two cycles of non-transitive interactions. BUSS and JACKSON (1979)

– Interaction of side-blotched lizards hat exhibit throat-color polymorphism.

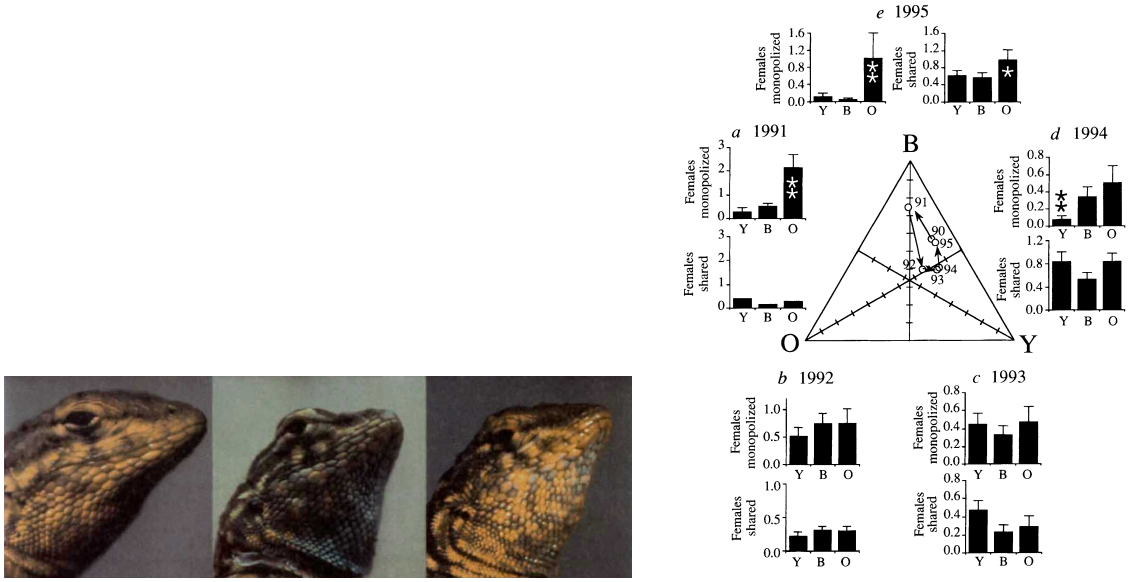

Figure 51: a) Population has lizards with three different morphs, having orange, blue, and yellow throats. They differ in behavior: orange are agressive and defend large territories, blue less so, yellow do not defend territories (look similar to females). b) Indications of an oscillation in the populations of lizards with orange, blue, and yellow throats (loop in the OBY-triangle of population sizes, 0-100% from base to the respectively marked apex Sinervo and Lively (1996)).

- Bacterial warfare:
  interaction between bacteria via toxins: some produce the toxin and are resistant to it, some are only resistant, and others are susceptible
  - The resistant strain R that does not produce toxin has lower metabolic cost than a killer bacterium K. R therefore beats K by faster growth.
  - Susceptible strains S have yet lower metabolic cost since they do not need to invest metabolic cost in the resistance. S beats R by faster growth.
  - The killer strain simply kills the susceptible strain (K beats S) rather than outcompetes it with regard to resource.

These cyclic interactions resemble a rock-paper-scissors game.

We consider here simple models of non-transitive competition. It is, however, not clear whether this plays a significant role in the abundance of species (e.g. Goyal and Maslov (2018)[13])

2.6.1 ODE Model

As a minimal start consider a general rock-paper-scissors game of agents on a lattice:

- two sites are picked at random
- the individual i on the first site invades the individual j on the second site with a probability P_{ij} that depends on the species of the respective occupants

$$\left(\begin{array}{c|ccc} & R & P & S \\ \hline R & 0 & 0 & P_R \\ P & P_p & 0 & 0 \\ S & 0 & P_S & 0 \end{array}\right) \tag{16}$$

Since the sites are picked at random, the probability that a certain species is found is proportional to the density of that species. One then obtains the mean-field equations

$$\frac{dr}{dt} = r\left(P_r s - P_p p\right) \tag{17}$$

$$\frac{dp}{dt} = p\left(P_p r - P_s s\right) \tag{18}$$

$$\frac{ds}{dt} = s\left(P_s p - P_r r\right) \tag{19}$$

Notes:

- For any pair there is always only invasion in one direction, the opposite probability vanishes.

[13] The attractiveness of 'cool dynamics' may be getting in the way of assessing the actual relevance of models.

- In general the invasion probabilities $P_{r,p,s}$ can be different from each other.
- If $P_r = P_p = P_s$ the system has a cyclical (rotation) symmetry in that the equations remain unchanged if one replaces $r \to p$, $p \to s$, $s \to r$.
- Even for $P_r = P_p = P_s$, however, the equations break the chiral symmetry: the interaction between P_r and P_p is different than between P_r and P_s: the invasion matrix (16) is not symmetric.

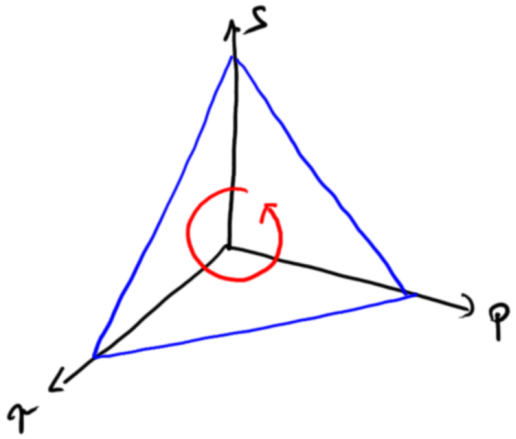

Figure 52: The RPS-dynamics are confined to the blue hyperplane $r+p+s=$ const. They break the chiral symmetry in that surface.

Analyze these equations:

The total number of individuals $n = r + p + s$ is constant

$$\frac{d}{dt}(r + p + s) = 0$$

The total number is therefore a free parameter depending on the initial conditions. All of the dynamics are limited to the two-dimensional hyperplane

$$r + p + s = n.$$

Correspondingly, the population size (r_0, p_0, s_0) at any fixed point is only determined up to a factor.

Trivial fixed point $r = 0$, $p = 0$, $s = 0$

Linear stability:

Writing $r = r_0 + \epsilon r_1(t)$ etc., with $r_0 = 0$ the fixed point leads to

$$\begin{aligned} \frac{dr_1}{dt} &= 0 \\ \frac{dp_1}{dt} &= 0 \\ \frac{ds_1}{dt} &= 0 \end{aligned}$$

Thus, all eigenvalues of the linearization vanish: the trivial fixed point is marginally stable for all values of the parameter. This is not generic. The system is most likely not structurally stable; even small additional terms may be able to change the dynamics qualitatively.

Non-trivial fixed points:

Consider first fixed points in which one population vanishes

$$r = 0 \quad \Rightarrow \begin{cases} s = 0 & \Rightarrow \quad p = n \\ p = 0 & \Rightarrow \quad s = n \end{cases}$$

Thus, there are three fixed points

$$(r = n, 0, 0) \qquad (0, p = n, 0) \qquad (0, 0, s = n).$$

Linear stability:

consider $(r_0 = n, 0, 0)$

$$\begin{aligned} \frac{dr_1}{dt} &= n\left(P_r s_1 - P_p p_1\right) \\ \frac{dp_1}{dt} &= p_1 P_p n \\ \frac{ds_1}{dt} &= -s P_r n \end{aligned}$$

i.e. the Jacobian is

$$\boldsymbol{M} = \begin{pmatrix} 0 & -P_p n & +P_r n \\ 0 & P_p n & 0 \\ 0 & 0 & -P_r n \end{pmatrix}$$

with eigenvalues and eigenvectors

$$\lambda_1 = 0 \quad \begin{pmatrix} 1 \\ 0 \\ 0 \end{pmatrix} \qquad \lambda_2 = P_p n > 0 \quad \begin{pmatrix} -1 \\ 1 \\ 0 \end{pmatrix} \qquad \lambda_3 = -P_r n < 0 \quad \begin{pmatrix} -1 \\ 0 \\ 1 \end{pmatrix}$$

Thus, rock is unstable in the paper-direction, but stable in the scissors-direction. The total population is conserved and arbitrary $\Rightarrow$ perturbations that change n do not relax back, nor do they grow: the eigenvalue in the rock-direction vanishes.

Fixed points with no vanishing component:

$$s_0 = \frac{P_p}{P_r} p_0 \qquad r_0 = \frac{P_s}{P_p} s_0 \qquad p_0 = \frac{P_r}{P_s} r_0$$

Solve the first two equations for r using $n = r + p + s$

$$P_r r_0 = -\left(P_p + P_r\right) p_0 + P_r n_0 \qquad \left(P_p + P_s\right) r_0 = P_s n_0 - P_s p_0$$

Eliminating r between the two equations yields then

$$\frac{p_0}{n} = \alpha P_r \qquad \text{with} \quad \alpha = \frac{1}{P_r + P_p + P_s}$$

Analogously for the other populations by cyclic permutation

$$\frac{r_0}{n} = \alpha P_s \qquad \frac{s_0}{n} = \alpha P_p$$

Note:

- The size of a population is not determined by its own ability to invade the other population, but rather by the invasion ability of the population that it invades:
  - Rock invades scissors and rock's population size is given by the ability of scissors to invade paper:
    The rock-population is large if the scissor-population strongly invades the paper-population, because then there is little invasion by the paper-population into the rock-population.
- Alternatively:
  The population size of species i is proportional to the invasion ability of species $i-2$ in the cycle.
  A large population requires weak invasion into it, which is achieved by strong invasion into that species.

Consider the logarithmic derivatives

$$\begin{aligned}\frac{d\ln r}{dt} &= P_r s - P_p p\\ \frac{d\ln p}{dt} &= P_p r - P_s s\\ \frac{d\ln s}{dt} &= P_s p - P_r r\end{aligned}$$

and note that

$$P_s\frac{d\ln r}{dt} + P_r\frac{d\ln p}{dt} + P_p\frac{d\ln s}{dt} = 0$$

Thus

$$\frac{d\ln r^{P_s}}{dt} + \frac{d\ln p^{P_r}}{dt} + \frac{d\ln s^{P_p}}{dt} = \frac{d}{dt}\ln\left(r^{P_s}p^{P_r}s^{P_p}\right) = 0$$

and

$$r(t)^{P_s}\, p(t)^{P_r}\, s(t)^{P_p} = C$$

For a given total population size n, different initial conditions lead to different orbits. These orbits differ in the value of C, which is constant along each orbit. Writing the equation as

$$\left(\frac{r(t)}{r_0}\right)^{P_s}\left(\frac{p(t)}{p_0}\right)^{P_r}\left(\frac{s(t)}{s_0}\right)^{P_p} = \lambda \tag{20}$$

one has $\lambda = 1$ at the fixed point and $\lambda = 0$ when one of the species is extinct.

Note:

- Thus, both n and λ are conserved during the temporal evolution. That is not expected in general: the equations are not structurally stable; adding small further terms is likely to destroy these invariances. Nevertheless we will stick to this model for now.
- In principle, one should also do a linear stability analysis of this fixed point. However, the continuum of orbits described by (20) encloses the fixed point at an arbitrary distance: this fixed point must be a center, i.e. there must be complex pair of eigenvalues with vanishing real part.

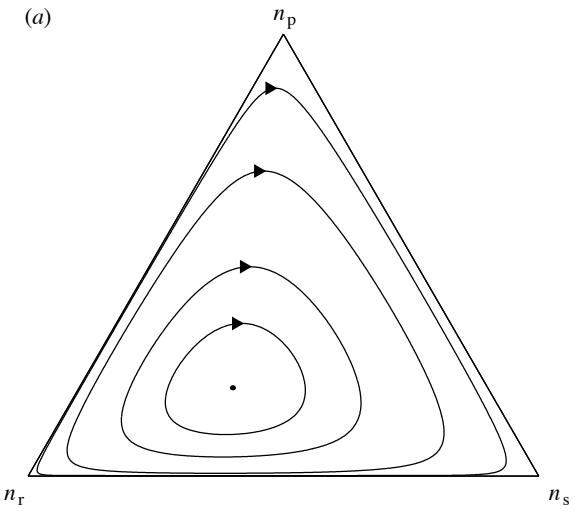

Figure 53: Examples of trajectories and fixed point. Frean and Abraham (2001)

Extinction:

- Within this continuous population model no population will ever go extinct for $\lambda > 0$; they will only oscillate, possibly reaching very small values during part of the cycle. The population will always recover, even after having reached an infinitesimally small value.
- If one species is identically zero, another will go extinct quickly thereafter and the system goes to one of the single-species fixed points. E.g. $r = 0 \Rightarrow s$ will grow rapidly and drive p into extinction.

2.6.2 Discrete Models

For a population to go extinct in the RPS-system, it has to reach 0 exactly. While in the ODE Model this happens only for very special initial conditions (on the edges of the triangle in Fig.53), it will often be the case if discrete populations are considered with invasion probabilities like (16).

For large populations the mean number evolves close to the orbits of the mean-field equations (17,18,19).

However, the discrete dynamics does not preserve the invariant λ (cf. (20)). Therefore under the discrete dynamics λ - and with it the orbits - can grow or shrink (cf. Fig.54) and eventually hit one of the three boundaries $r = 0$, $p = 0$, or $s = 0$, which then yields to the survival of a single species.

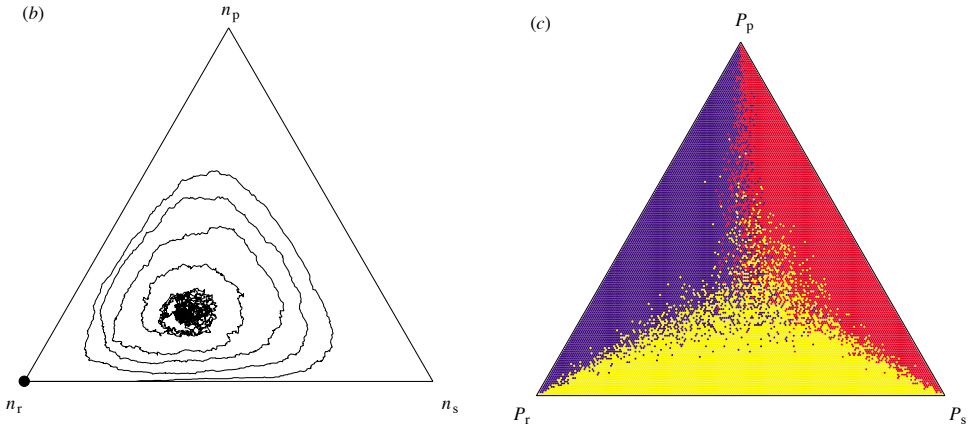

Figure 54: a) RPS-evolution under the discrete dynamics. b) RPS survival: for large system size the weakest species survives best, i.e. the population with the smallest invasion probability. Red: rock survives, blue: scissors survives, yellow: paper survives. The triangle gives the invasion probabilities chosen wth the constraint $P_r + P_p + P_s =$ const.(cf. Fig.52) Frean and Abraham (2001).

How does the survival probability of a population depend on its invasion probability?

The species that is most likely to go extinct is the one that reaches the smallest population size during the oscillations. For the fixed point we have

$$\frac{r_0}{n} = \alpha P_s \qquad \frac{p_0}{n} = \alpha P_r \qquad \frac{s_0}{n} = \alpha P_p$$

One can show Frean and Abraham (2001) that the smallest population size during the oscillation occurs for the population with the smallest size at the fixed point.

How does the survival depend on the invasiveness?

- Species i is smallest and has the highest probability to go extinct, if species $i-2$ has the lowest invasion probability.
- If species i goes extinct, species $i+1$, which is the same as $i-2$, grows, suppressing species $i-1$.
- Species $i-2$ survives.

Thus, the *weakest* population, i.e. the least invasive species, survives.

Is then the non-transitive fitness not able to lead to the co-existence of multiple species?

(c) 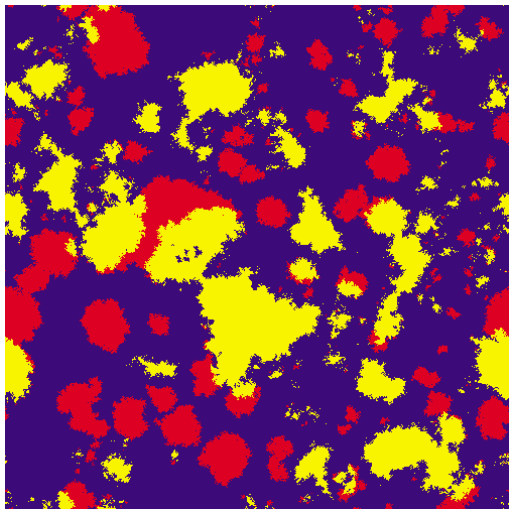

Figure 55: RPS in a large system with only local dispersal sustains persistent multi-species states ($P_r = 0.1$, $P_s = 0.1$, $P_p = 0.8$) Frean and Abraham (2001).

For local rather than global dispersal patches of different species arise and persist.

Experimentally, this was tested using E. coli bacteria that interact via toxins: K>S>R>K (see above).

- When the bacteria were grown undisturbed, i.e. unmixed, the interaction was local and the populations persisted for a long time. Patches with different species arise that invade each other.
- When the solutions were mixed in a flask or transferred from one plate to the other twice at different orientation angles, one population went extinct quite quickly, followed by the second, leaving only the resistant strain.

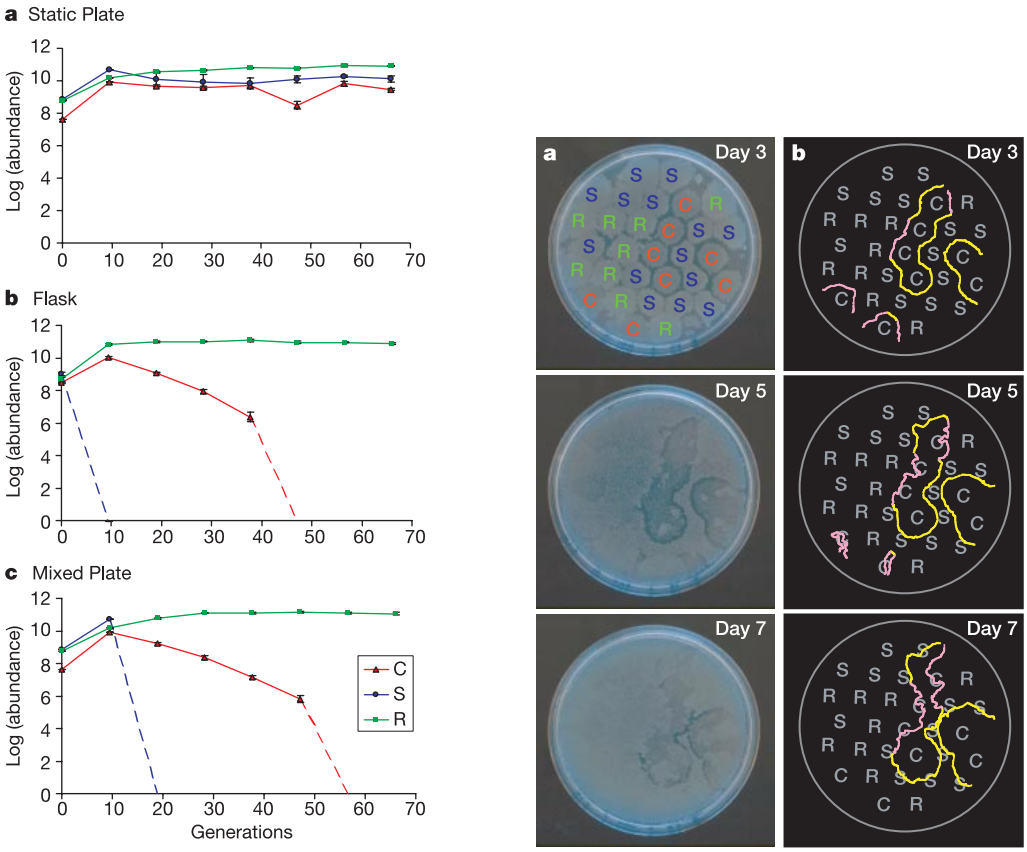

Figure 56: Experimental results for RPS-like dynamics of E. coli bacteria Kerr et al. (2002). Left: population sizes. Right: Inoculation with different strains in a hexagonal pattern. Letter markings the same at the three times, C-S (C=K) fronts in yellow, C-R fronts in pink.

Note:

- Frean and Abraham (2001) also has interesting results about systems in which the invasion rate of a species was allowed to evolve. This leads to an increase in its competitiveness (invasiveness) and at the same timer a *reduction* in its size, because its stronger invasiveness reduces the population $i-2$, which enhances population $i-1$, which then invades the evolved species more strongly. .

2.6.3 Continuum Systems with Dispersal

To understand why the patches of different species persist for so long, it is useful to look at continuum systems with dispersal. For that it is better to look at a more general model that is structurally stable and in which the transition to the oscillations can be controled by a bifurcation parameter.

For instance consider a grid of patches where each patch has N sites on which three species S_i, $i = 1 \ldots 3$, interact with each other in a well-mixed fashion Szczesny et al. (2013). The transitions between the different states occur randomly with probabilities

indicated above the reactions,

$$S_i + S_{i+1} \overset{\sigma}{\rightarrow} S_i + \emptyset, \qquad S_i + S_{i+1} \overset{\zeta}{\rightarrow} 2S_i \qquad S_i + \emptyset \overset{\beta}{\rightarrow} 2S_i \qquad S_i \overset{\mu}{\rightarrow} S_{i\pm1}$$

- σ: S_i kills S_{i+1} and leaves and empty site
- ζ: S_i transforms S_{i+1} to S_i
- β: S_i propagates itself if there is an empty site
- μ: S_i mutates into S_{i+1} or S_{i-1}

In addition there is motion between neighboring patches at locations $\mathbf{r}$ and $\mathbf{r}'$

$$[S_i]_{\mathbf{r}}[\emptyset]_{\mathbf{r}'} \overset{\delta_D}{\rightarrow} [\emptyset]_{\mathbf{r}}[S_i]_{\mathbf{r}'} \qquad [S_i]_{\mathbf{r}}[S_{i\pm1}]_{\mathbf{r}'} \overset{\delta_E}{\rightarrow} [S_{i\pm1}]_{\mathbf{r}}[S_i]_{\mathbf{r}'}$$

- δ_D: hopping into an empty spot
- δ_E: interchange of individuals.

Assuming again that locally the species are well mixed, so that the probability to encounter another individuum of a given species is proportional to its density, one can derive mean-field equations

$$\begin{aligned} \frac{ds_i}{dt} &= s_i\left\{\beta\left(1-r\right) - \sigma s_{i-1} + \zeta\left(s_{i+1}-s_{i-1}\right) + \mu\left(s_{i-1}+s_{i+1}-2s_i\right)\right\} + \\ &\quad +\delta_D \Delta s_i + \left(\delta_D - \delta_E\right)\left(s_i \Delta r - r \Delta s_i\right) \end{aligned} \tag{21}$$

where

$$r = s_1 + s_2 + s_3$$

is the total density.

Notes:

- In this model all three species are equivalent, i.e. 'rotating' the index i cyclically, $i \to i+1$ with 4 being equivalent to 1, does not change the equations.
- As is the case in the RPS-model (16), the system (21) breaks the chiral symmetry and the terms that break the chiral symmetry, σ and ζ, drive the RPS-dynamics.
- The mutation term is a term that couples the different species without breaking the chiral symmetry. It amounts to 'diffusion' in 'species space' (finite-difference approximation for second derivative). It is expected to stabilize the fixed point against the oscillations: μ cannot be too large for oscillations to occur.

  Due to the cyclical symmetry $i \to i+1$, the system must have a solution that reflects that cyclical symmetry, i.e. there must be a fixed point with $s_i = s_0$, $i = 1 \ldots 3$. It is given by

$$\beta\left(1-3s_0\right) - \sigma s_0 = 0$$

$$s_0 = \frac{\beta}{3\beta + \sigma}.$$

One can show that this fixed point becomes unstable to oscillations in a Hopf bifurcation for

$$\mu < \mu_h \equiv \frac{\beta\sigma}{6\,(3\beta + \sigma)}.$$

Thus, as expected the oscillations are suppressed by the mutation term μ; for $\mu = 0$ the fixed point is always unstable.

For small oscillation amplitudes one can, in general[14], derive systematically a simpler equation to describe the oscillations by expanding around the fixed point

$$\begin{pmatrix} s_1(x,t) \\ s_2(x,t) \\ s_3(x,t) \end{pmatrix} = \begin{pmatrix} s_0 \\ s_0 \\ s_0 \end{pmatrix} + \epsilon A(x,t) e^{i\omega t} \underbrace{\begin{pmatrix} v_1 \\ v_2 \\ v_3 \end{pmatrix}}_{\text{eigenvector } \mathbf{v}} + \epsilon A^*(x,t) e^{-i\omega t} \begin{pmatrix} v_1^* \\ v_2^* \\ v_3^* \end{pmatrix} + \mathcal{O}(\epsilon^2).$$

Here ω is the imaginary part of the eigenvalue of the Jacobian obtained by linearizing (21) around the fixed point and $\mathbf{v}$ is the associated, complex eigenvector.

Expanding (21) to cubic order in ϵ one obtains then a condition for the expansion to be valid, which results in a PDE for the complex amplitude $A(x,t)$,

$$\frac{\partial A}{\partial t} = (1 + i\delta_i)\,\Delta A + A - (1 + ic)\,|A|^2\,A. \tag{22}$$

Here, scaling of time, space, and the amplitude A has been used to set coefficients to 1.

Note:

- This equation is the complex Ginzburg-Landau equation, which is the universal equation for generic small-amplitude oscillations

In general, $\delta_i \neq 0$, which leads to interesting dynamics Aranson and Kramer (2002). According to Szczesny et al. (2013) $\delta_i = 0$ for (21).

Important for the current system is the fact that (22) allows spiral waves that rotate clockwise or counterclockwise

$$A_{clockwise} \sim f(r) e^{i\omega t - i\phi - i\psi(r)} \qquad \text{or} \qquad A_{counter} \sim f(r) e^{i\omega t + i\phi + i\psi(r)},$$

where (r, ϕ) are polar coordinates centered at the spiral core.

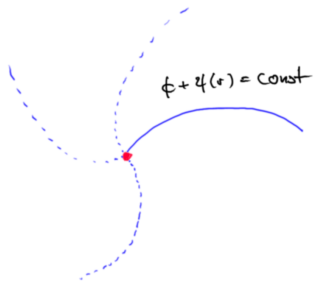

Spirals are relevant for the dynamics for topological reasons:

[14] See, for instance, 322 *Applied Dynamical Systems* [Lecture Notes], Strogatz (2015)

- The phase of the oscillation increases or decreases by 2π when the core of a spiral is encircled once $\Rightarrow$ the phase cannot be defined at the core $r = 0 \Rightarrow f(0) = 0$.
- Since $f(0) = 0$, the core of a spiral represents a 0 of the complex field A, which is given by the intersection between the zero-contours of the real part A_r of A and of its imaginar part A_i.
- $\Rightarrow$ at the core of the spiral the system is at the (unstable) fixed point, i.e. in the vicinity of the core all three species meet.
- $\Rightarrow$ spirals are topologically stable: an intersection between two lines in the plane can only disappear by 'colliding' with another intersection of those lines. $\Rightarrow$ spirals can only be generated and annihilated in pairs (unless they leave the system through the boundaries).

Dynamically, depending on parameters

- spiral pairs can arise from instabilities of the homogeneously oscillating state or of traveling waves
- spirals can disappear in pairs
- the waves emitted by spirals can be unstable, triggering the creation of additional spirals $\Rightarrow$ complex, chaotic dynamics Chaté and Manneville (1996).
  - The instability of the spirals can be weak enough that it is swept along by the outward propagating waves, leaving the core of the spiral untouched and leading to disorder only away from the cores (convective instability).
  - If the instability if stronger it can propagate 'upstream' against the outward traveling waves and destroy also the spiral core (absolute instability).

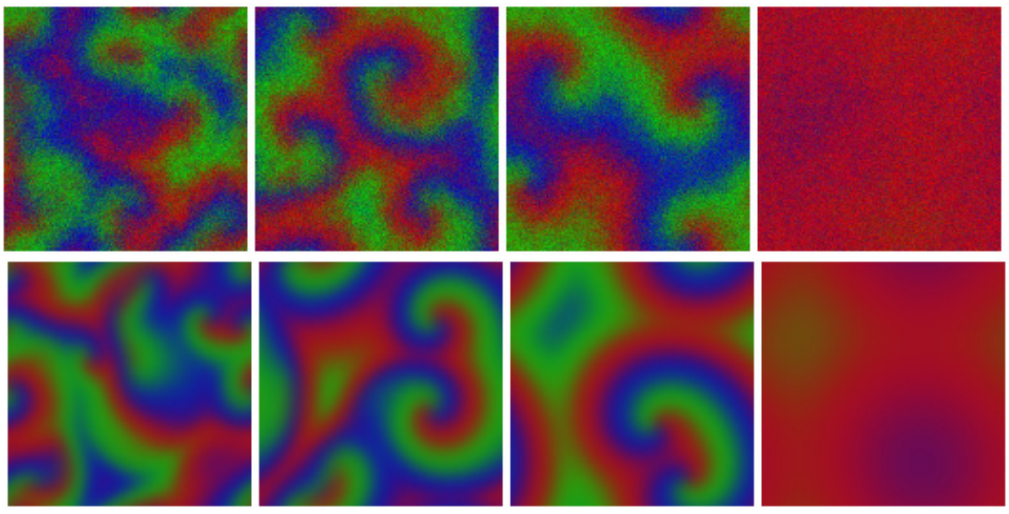

Figure 57: Spiral waves in the stochastic discrete system (a) and in the continuum system (b) for 4 different parameter sets. From left to right: spirals are absolutely unstable, convectively unstable, stable but bound, annihilate each other Szczesny et al. (2013). See also movies at https://figshare.com/articles/Supplementary_material:_When_does_cyclic_dominance_lead_to_stable_spiral_waves_/96949

Thus

- For local interaction between the species patches form in which
  - at a given time one of the three species dominates
  - the dominating species cycle in time
- Patches meet at spiral cores $\Rightarrow$ as long as there is a spiral all three species are present somewhere in the system and can invade the others, none is extinct.
- For extinction all spirals have to annihilate each other. Whether they tend to do that or not depends on the parameters c and δ_i in (22) (for other underlying models $\delta_i \neq 0$ possible)
- Coexistence of the species does not require the oscillations: in more general models than the minimal model (17,18,19) the coexistence fixed point can simply be stable. See, for instance, the model (21) for sufficiently large mutation rate μ.

Note:

- The topological stability of the spirals requires the existence of continuous 0-contourlines of the oscillation amplitude. In the discrete system there are, strictly speaking, no continuous contourlines.
  - In the (stochastic) discrete systems spirals are not topologically stable and individual spirals can dissolve.
  - For sufficiently strong dispersal and interaction between adjacent individuals the continuous oscillation amplitude with continuous contourlines can, however, be a good approximation.

3 Genetic Oscillators and Circadian Clocks

Already in 1729 Jean-Jacques d'Ortous de Mairan observed that certain plants (presumably mimosas) open and close their leaves in a circadian fashion even in the absence of light.

This was one of several reasons why Henri-Louis Duhamel du Monceau (1700–1782) repeated Mairan's experiments in 1758. He went as far as installing his plants in a deep wine cellar where the temperature was very stable and absolutely no sunlight could penetrate, or even in large leather trunks wrapped in blankets. The plants' leaf movements continued, despite the fact that they were far more effectively cut off from daylight.(Klarsfeld, 2013)

Figure 58: Mimosa plant opens and closes leaves in a circadian fashion even at constant light and constant temperature. Movies at `Figures/silk_tree_circadian.mov` and mimosa movie

1516

[15] Article in the Scienfitic American on circadian rhythm in plants: https://blogs.scientificamerican.com/a-blog-around-the-clock/clock-classics-it-all-started-with-the-plants/

[16] TedSMU talk by J. Takahashi at https://www.youtube.com/watch?v=ocqn3wYTCRM

Vor rund 100 Jahren erschien in der Familienzeitschrift „Gartenlaube“ (Jahrgang 1860) unter der Überschrift „Aus dem Leben eines Orang-Outang“ der Bericht über ein drei Jahre altes Affen-Weibchen, das auf einem Segelschiff von Java nach Hamburg gebracht werden sollte. Zu Beginn der Reise erwachte die auf dem Verdeck lebende Äffin bei Sonnenaufgang um 6 Uhr und legte sich gegen 18 Uhr schlafen. Auf dem Wege nach Westen hielt das Tier 12 Std Schlafzeit bei, jedoch unter steter leichter Phasenverschiebung gegen die jeweilige Ortszeit, so daß am Kap der Guten Hoffnung das Erwachen auf 2 Uhr und das Zuruhegehen auf 14 Uhr fiel. Der „physiologische Tag“ der Äffin hatte sich gegen Ortszeit 4 Std verfrüht, gegen Heimatszeit 2 Std verspätet. Mit diesem kurzen Bericht, der wegen des vorzeitigen Todes des Tieres (nach Genuß einer Flasche Rum) unvollständig bleiben mußte, beginnt gewissermaßen die Erforschung der Tagesperiodik bei Primaten — mehr als 100 Jahre nach den ersten Experimenten an Pflanzen, über die BÜNNING kürzlich berichtet hat [3].

Figure 59: Referring to a description in a family magazine in 1860 of the shift in daily rhythm in an orang-utan traveling on a ship westward. The observation came to an end as the orang-utan drank a bottle of rum and passed on (Aschoff and Wever, 1962).

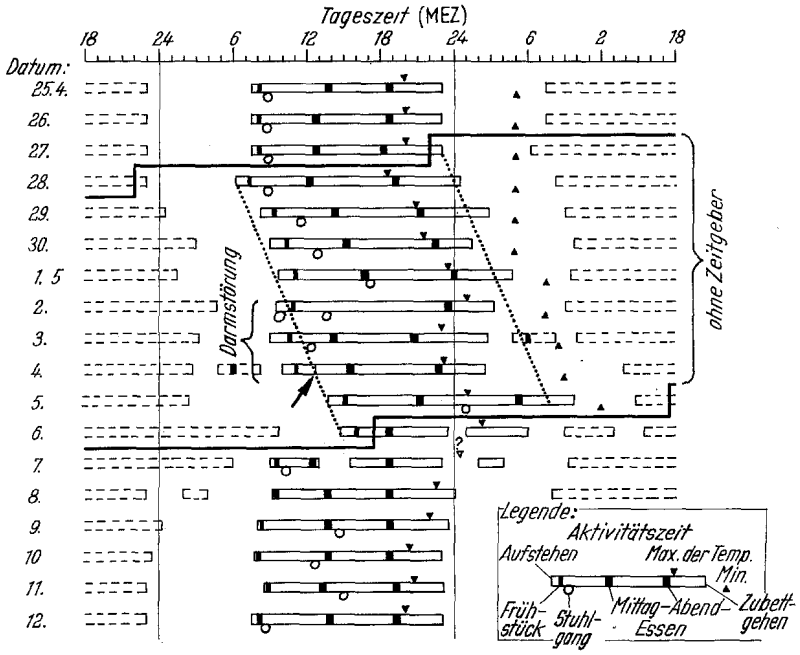

Figure 60: Circadian rhythm in humans. Experiment in sub-basement of University Hospital Munich: '*...an important component of the furniture turned out to be a record player...*'. After three days the subjects had to remove their watches (Aschoff and Wever, 1962).

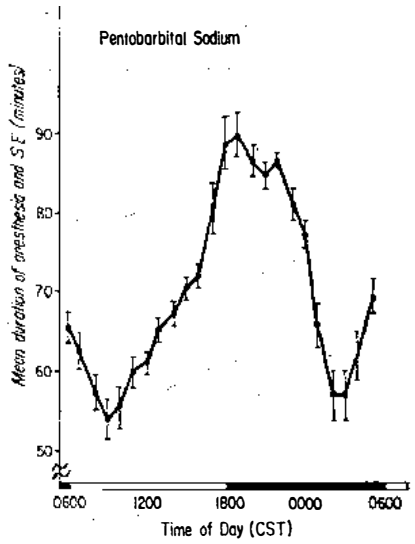

Figure 61: Chronomedicine: the impact, effectiveness, and side effects of medication can depend strongly on the circadian time. E.g. the duration of sleep induced by fixed dosis of anesthetic in rat varies circadianly (Reinberg and Halberg, 1971).

How can the oscillations of the circadian rhythm be so slow? The circadian rhythm is maintained by oscillators built from gene transcription and protein synthesis.

3.1 Negative Feedback during mRNA Synthesis

A key element of the genetic machinery comprising the circadian clocks is negative feedback in the gene transcription. Consider a minimal model for protein synthesis with negative feedback by a repressor.

The proteins are produced by translation from the mRNA, which, in turn, is produced by transcription from the DNA.

For genes to be turned on the RNA polymerase needs to be able to bind to the corresponding promoter site in order to produce the mRNA. This is only possible if there is no repressor bound to the operator.

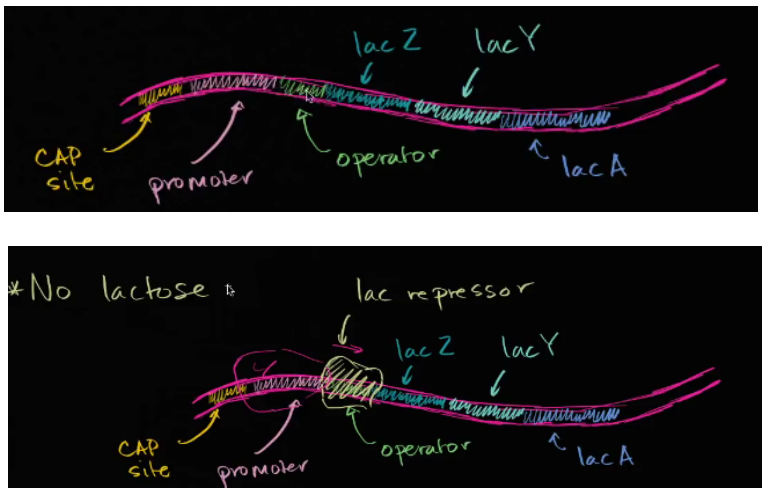

Figure 62: Lac operon controling the genes necessary to process lactose. *lacZ* $\rightarrow$ enzyme to cleave lactose, *lacY* $\rightarrow$ enzyme to allow absorption of lactose through cell membrane, ... When a repressor binds to the operator site the polymerase cannot bind to the promoter site and the downstream genes cannot be transcribed. (Sketch from khanacademy.org)

Assuming that p repressor molecules are needed for the repression of the transcription one has for the repressor R and the operator D

$$p\,R + D \underbrace{\overset{k_R^+}{\rightleftharpoons}}_{k_R^-} DR_p$$

where DR_p is the complex formed by the repressor bound to the operator.

In equilibrium one has then

$$\frac{[DR_p]}{[R]^p[D]} = \frac{k_R^+}{k_R^-} = \frac{1}{K_R^p}$$

with K_R the dissociation constant of the complex.

The total number of operators $[D]_T$ is conserved

$$[D]_T = [D] + [DR_p]$$

Inserting in the equilibrium condition

$$\frac{[D]_T - [D]}{[R]^p[D]} = \frac{1}{K_R^p} \qquad \Rightarrow \qquad [D] = \frac{[D]_T}{1 + \left(\frac{[R]}{K_R}\right)^p}$$

In a large ensemble of cells $[D]$ represents the concentration (fraction) of cells in which the operator is free of repressor. Since the process is stochastic, for a single cell $[D]/[D]_T$ is the probabiility that its operator is free. The time-averaged rate of mRNA production is then

$$V_{mRNA} = \beta \frac{[D]}{[D]_T} = \beta \frac{1}{1 + \left(\frac{[R]}{K_R}\right)^p}$$

where β is the production rate without repressor.

3.2 The Goodwin Oscillator

The minimal model Goodwin considered first is

$$\begin{aligned} \frac{d[X_1]}{dt} &= \frac{\nu_0}{1+\frac{[X_2]}{K_R}} - b_1 \\ \frac{d[X_2]}{dt} &= \nu_1[X_1] - b_2 \end{aligned}$$

He solved these equations on a Philbrick Analogue Computer at MIT.

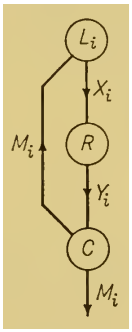

Figure 63: Sketch of reaction network (Goodwin, 1963)

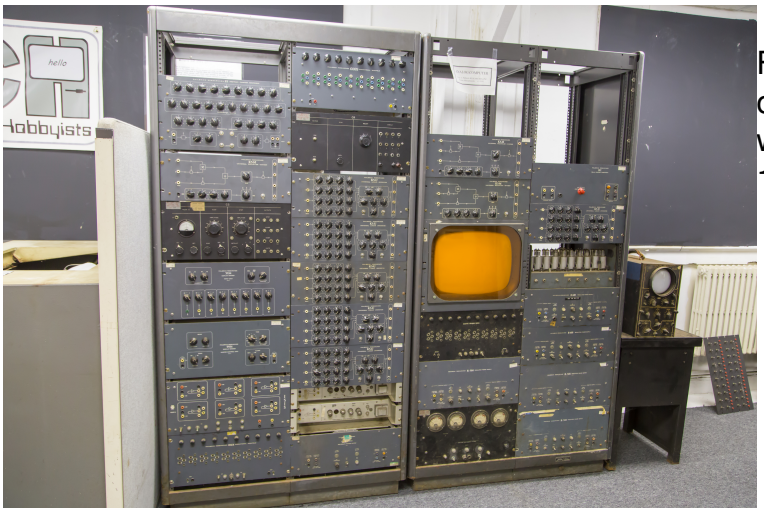

Figure 64: Philbrick analog computer at MIT (www.analogmuseum.org).

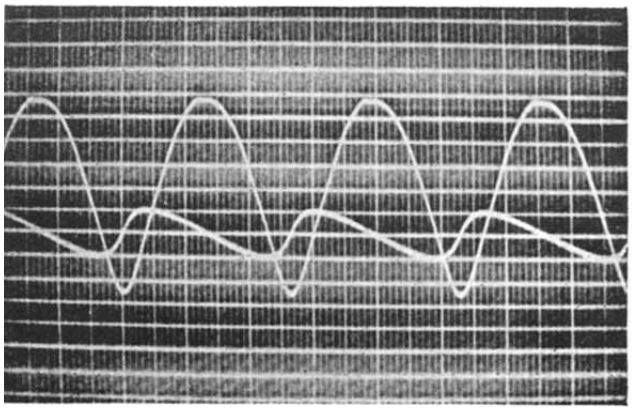

Figure 65: Analogue computer results for Goodwin's minimal model (Goodwin, 1965).

Since the X_1-equation only depends on X_2 and the X_2-equation only on X_1 one can combine the two equations by multiplying with the right-hand sides

$$(\nu_1[X_1] - b_2)\,\frac{d[X_1]}{dt} - \left(\frac{\nu_0}{1+\frac{X_2}{K_R}} - b_1\right)\frac{d[X_2]}{dt} = 0,$$

which allows a separation of variables

$$(\nu_1 X_1 - b_2)\, d[X_1] = \left(\frac{\nu_0}{1 + \frac{X_2}{K_R}} - b_1 \right) d[X_2]$$

This implies for all times t

$$\frac{1}{2}\nu_1 [X_1(t)]^2 - b_2[X_1(t)] = \nu_0 K_m \ln\left(1 + \frac{[X_2(t)]}{K_R}\right) - b_1[X_2(t)] + C$$

Here C is an arbitrary integration constant, which depends on the initial conditions $\Rightarrow$ the solutions do not approach a limit cycle attractor, but there is a continuum of solutions corresponding to the continuum of C.

Thus, this model is structurally not stable. Need to include also an approach to the limit cycle.

The degradation can reasonably depend on the concentration

$$\begin{aligned} \frac{d[X_1]}{dt} &= \frac{\nu_0}{1 + \frac{[X_2]}{K_R}} - k_1[X_1] \\ \frac{d[X_2]}{dt} &= \nu_1[X_1] - k_2[X_2] \end{aligned}$$

However, this system cannot support any oscillations. Write it as

$$\begin{aligned} \frac{dx}{dt} &= f(x,y) \\ \frac{dy}{dt} &= g(x,y) \end{aligned}$$

and assume there is a periodic solution $(x(t), y(t))$. It describes a closed contour $\mathcal{C}$ in the phase plane. Use Green's theorem for that contour

$$\int\int_D \frac{\partial f}{\partial x} + \frac{\partial g}{\partial y}\, dxdy = \int_{\mathcal{C}} -gdx + fdy$$

Along the contour we have

$$\frac{dx}{dt} = f \qquad \Rightarrow \qquad dx = fdt$$

$$\frac{dy}{dt} = g \qquad \Rightarrow \qquad dy = gdt$$

implying

$$\int_{\mathcal{C}} -gdx + fdy = \int -gfdt + fgdt = 0.$$

Therefore we have the **Bendixson-Dulac Theorem**:

If $\frac{\partial f}{\partial x} + \frac{\partial g}{\partial y}$ has the same sign everywhere in a two-dimensional domain D, the dynamical system cannot have a periodic orbit that lies completely in D.

In the model above

$$\frac{\partial f}{\partial x} + \frac{\partial g}{\partial y} = -k_1 - k_2 < 0.$$

Notes:

- The Bendixson-Dulac theorem is valid *only* in 2 dimensions.
- It can be generalized. It is sufficient if

$$\frac{\partial \left(\phi(x,y) f\right)}{\partial x} + \frac{\partial \left(\phi(x,y) g\right)}{\partial y}$$

  does not change sign for some $\phi(x,y)$.

Goodwin considered then the model

$$\begin{aligned}
\frac{d[X_1[}{dt} &= \frac{\nu_0}{1 + \left(\frac{[X_3]}{K_m}\right)^p} - k_1[X_1] \\
\frac{d[X_2]}{dt} &= \nu_1[X_1] - k_2[X_2] \\
\frac{d[X_3]}{dt} &= \nu_2[X_2] - k_3[X_3]
\end{aligned}$$

The analysis of this model is a bit more involved. One can show that the fixed point is asymptotically stable and no oscillations arise unless $p \geq 8$ (Griffith, 1968). Such high values for the cooperativity of the reaction are unrealistic; it would require that at least 8 molecules are needed to form the activated complex leading to the mRNA.

What does the additional linear equation $\frac{d[X_2]}{dt} = \nu_1[X_1] - k_2[X_2]$ do compared to the 2-dimensional model? For illustration purposes assume that $[X_1]$ oscillates harmonically, $[X_1] = \cos t$. Then the equation is like

$$\frac{dy}{dt} = -\lambda y + \cos t.$$

We showed before (36) that after a transient the solution approaches

$$y = \frac{\lambda}{\lambda^2 + 1} \cos t + \frac{1}{\lambda^2 + 1} \sin t = \frac{1}{\sqrt{\lambda^2 + 1}} \cos\left(t - \phi\right)$$

with

$$\phi = \arctan\left(\frac{1}{\lambda}\right)$$

Thus, $y(t)$ lags behind $\cos t$. The lag increases the smaller the decay rate λ; in the opposite limit, $\lambda \to \infty$, y follows the driving adiabatical.
Analogously, $[X_2]$ lags behind $[X_1]$ and $[X_3]$ in turn lags behind $[X_2]$. The additional equation therefore increases the delay with which the suppression on $[X_1]$ acts.

In general, delayed inhibition tends to foster oscillations:

- large $[X_1]$ implies large suppression at later time
- the resulting reduced $[X_1]$ leads in turn to reduced suppression yet later
- which allows large $[X_1]$ later again.

Increasing the 'delay line' by adding further intermediate steps $[X_j]$ reduces the degree p of cooperativity needed to get oscillations (Fall et al., 2002).

Goodwin got periodic oscillations with $p = 1$. He must have an error in his simulations. **Never trust your computer results blindly.**

The model can be modified to obtain oscillations much more generally, particularly even for $p = 1$ (Bliss et al., 1982; Fall et al., 2002)[17],

$$\begin{aligned}\frac{d[X_1]}{dt} &= \frac{\nu_0}{1+\frac{[X_3]}{K_m}} - k_1[X_1] \\ \frac{d[X_2]}{dt} &= \nu_1[X_1] - k_2[X_2] \\ \frac{d[X_3]}{dt} &= \nu_2[X_2] - \frac{k_3[X_3]}{K+[X_3]}\end{aligned}$$

Note:

- How does the nonlinear reaction term in the equation for X_3 come about?

3.3 Michaelis-Menten Kinetics

Consider an enzymatic reaction that *irreversibly* produces a product P from an *abundant* substrate S via a complex ES

$$E + S \underset{k_1^-}{\overset{k_1^+}{\rightleftharpoons}} ES \qquad ES \xrightarrow{k_2^+} P + E$$

The reaction step from the complex to the product is assumed to be irreversible.

This leads to the mass-action equations

$$\begin{aligned}\frac{d[S]}{dt} &= -k_1^+[E][S] + k_1^-[ES] \\ \frac{d[ES]}{dt} &= k_1^+[E][S] - k_1^-[ES] - k_2^+[ES]\end{aligned}$$

In principle, there are also equations for $[E]$ and $[P]$

$$\frac{d[E]}{dt} = \dots \qquad \frac{d[P]}{dt} = \dots$$

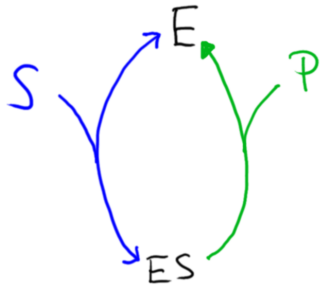

Figure 66: Sketch of enzymatic reaction.

[17] In (Bliss et al., 1982) the equations also include delays.

However, in this reaction the total amount of enzyme E is converved,

$$[E]_T = [E] + [ES] = const.$$

Therefore $[E]$ can be expressed in terms of $[E]_T$

$$[E] = [E]_T - [ES].$$

This leads to

$$\begin{aligned} \frac{d[S]}{dt} &= -k_1^+[E]_T[S] + \left(k_1^- + k_1^+[S]\right)[ES] \\ \frac{d[ES]}{dt} &= k_1^+[E]_T[S] - \left(k_1^- + k_2^+ + k_1^+[S]\right)[ES]. \end{aligned}$$

The total amount of substrate - combined with the product - is also conserved

$$[S]_T = [S] + [ES] + [P] = const.$$

This would allow us to express $[P]$ in terms of $[S]$, $[ES]$ and and $[S]_T$. However, because of the irreversibility the product concentration does not appear in the evolution equations for $[S]$ and $[ES]$. We therefore do not need an equation for P.

We would like to have an equation only for $[S]$ (and $[P]$) without $[ES]$, i.e. without referring to the enzyme any more.

The key assumption in the Michaelis-Menten kinetics is that the enzyme concentration is much smaller than the concentration of the substrate,

$$\frac{[E]_T}{[S]_T} \equiv \epsilon \ll 1$$

Nondimensionalize the concentrations with $[E]_T$ and $[S]_T$, respectively,

$$s = \frac{[S]}{[S]_T} \qquad \hat{es} = \frac{[ES]}{[E]_T}$$

$$\begin{aligned} \frac{ds}{dt} &= -k_1^+[E]_T s + \left(k_1^- \frac{1}{[S]_T} + k_1^+ s\right)[E]_T \hat{es} \\ \frac{d\hat{es}}{dt} &= k_1^+[S]_T s - \left(k_1^- + k_2^+ + k_1^+[S]_T s\right)\hat{es}. \end{aligned}$$

The rate of change of s is set by $[E]_T$, while that for $\hat{es}$ is set by $[S]_T \gg [E]_T$. We are interested in the rate at which s is produced, which is much slower than the change in $\hat{es}$. We therefore introduce a dimensionless time associated with the slower time scale

$$\hat{t} = t\, k_1^+[E]_T$$

and get

$$\begin{aligned} \frac{ds}{d\hat{t}} &= -s + \left(\frac{k_1^-}{k_1^+}\frac{1}{[S]_T} + s\right)\hat{es} \\ \frac{d\hat{es}}{d\hat{t}} &= \frac{1}{\epsilon}\left\{s - \left(\frac{k_1^- + k_2^+}{k_1^+[S]_T} + s\right)\hat{es}\right\}. \end{aligned}$$

Since $\epsilon \ll 1$ $\hat{es}$ evolves much faster than s and will very quickly reach its nullcline, i.e. which is given by $\{\} = 0 \Rightarrow$

$$\hat{es} = \frac{s}{\frac{k_1^- + k_2^+}{k_1^+ [S]_T} + s}$$

Inserting this into the equation for s

$$\begin{aligned}
\frac{ds}{d\hat{t}} &= -s + \left(\frac{k_1^-}{k_1^+} \frac{1}{[S]_T} + s \right) \frac{s}{\frac{k_1^- + k_2^+}{k_1^+ [S]_T} + s} \\
&= -s + \left(\frac{k_1^- + k_2^+}{k_1^+} \frac{1}{[S]_T} + s - \frac{k_2^+}{k_1^+ [S]_T} \right) \frac{s}{\frac{k_1^- + k_2^+}{k_1^+ [S]_T} + s} \\
&= -s + s - \underbrace{\frac{k_2^+}{k_1^+ [S]_T}}_{\hat{V}_{max}} \underbrace{\frac{s}{\frac{k_1^- + k_2^+}{k_1^+ [S]_T} + s}}_{\hat{K}_m} \\
&= -\hat{V}_{max} \frac{s}{\hat{K}_m + s}
\end{aligned}$$

Going back to the original variables

$$\frac{1}{[S]_T k_1^+ [E]_T} \frac{d[S]}{dt} = -\frac{k_2^+}{k_1^+ [S]_T} \frac{[S]}{\frac{k_1^- + k_2^+}{k_1^+ [S]_T} [S]_T + [S]}$$

$$\frac{d[S]}{dt} = -k_2^+ [E]_T \frac{[S]}{\frac{k_1^- + k_2^+}{k_1^+} + [S]}$$

$$\frac{d[S]}{dt} = -V_{max} \frac{[S]}{K_m + [S]}$$

with

$$V_{max} = k_2^+ [E]_T \qquad K_m = \frac{k_1^- + k_2^+}{k_1^+}$$

Thus,

- An irreversible enzymatic reaction that is limited by the availability of the enzyme has a sigmoidal reaction rate.
- The reaction saturates already at low substrate concentrations (K_m small), if the complex lives long and therefore a lot of the enzyme is bound in the complex, i.e. for $k_1^- + k_2^+$ small compared to k_1^+.

3.4 Circadian Oscillator

Now more specifically: what are the genes that are involved in the circadian oscillator?

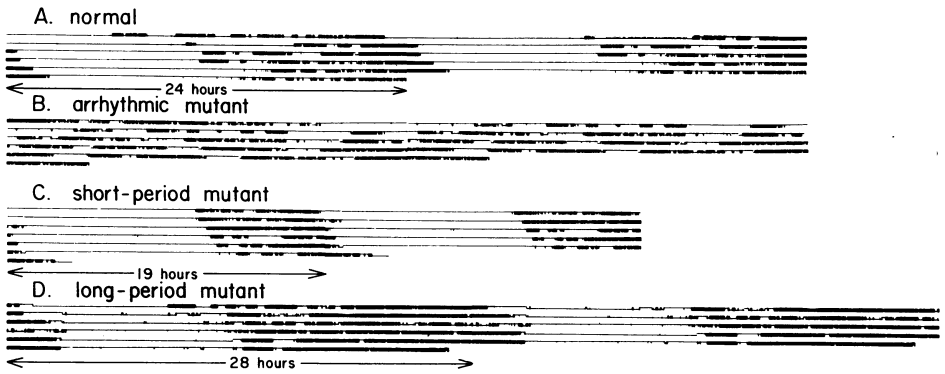

Figure 67: Drosophila: circadian locomotor behavior. Mutations resulting in arrhythmia or rhythms with longer or shorter period. The rhythm seems to depend on a single gene, *per*. (Konopka and Benzer, 1971).

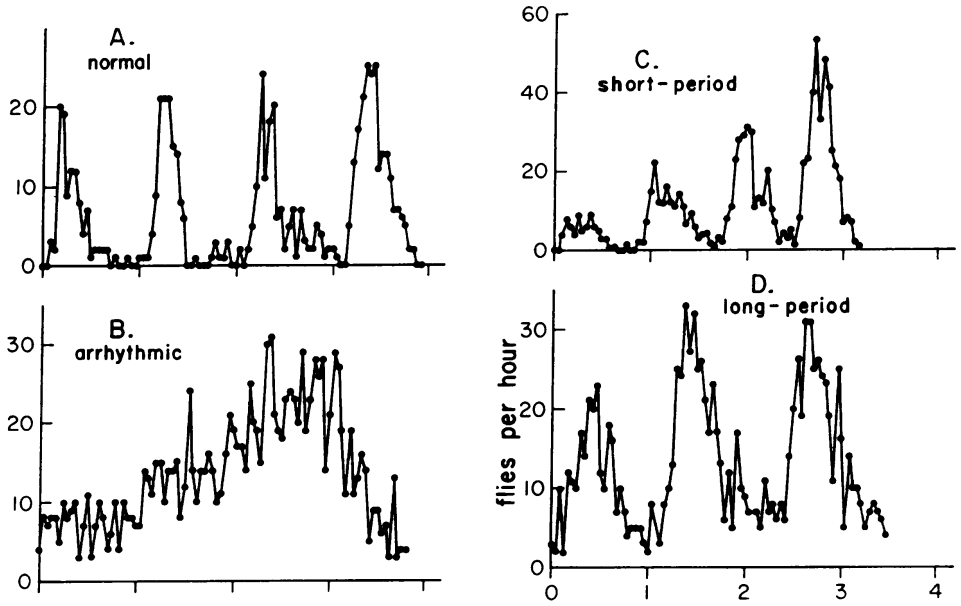

Figure 68: Drosophila eclosion rhythms: circadian emergence of adults from their pupal cases (population of pupae was synchronized by 12:12 light-dark cycle) (bottom, axis is time in days). The same mutations that lead to changes in locomotor rhythm lead to corresponding changes in eclosion rhythms (Konopka and Benzer, 1971).

Experimental findings

- *per* (=period) gene is a key element of the circadian oscillator. It is found to be necessary for circadian locomotor behavior and for the emergence of adult flies from their pupal cases and for the entrainment to the light cycle $\Rightarrow$ this suggests a relatively centrally positioned clock that controls many different functions of the organism or at least functions as a central pacemaker that entrains other clocks.
- PER protein - resulting from translation based on *per* messenger RNA (mRNA) and transfer RNA (tRNA) - becomes multiply phosphorylated by kinases. The phospho-

rylation is reversible (reverse via phosphatases) (Edery et al., 1994).
Phosphorylation of proteins is a key mechanism to switch specific functions of proteins on or off. The attached phosphate group changes the conformation of the protein and with it its function. A protein can have many different phosphorylation sites.

- the degradation and the entry into the cell nucleus depends on the degree of phosphorylation of PER.
- in the nucleus PER represses the transcription of *per* mRNA (Hardin et al., 1990)

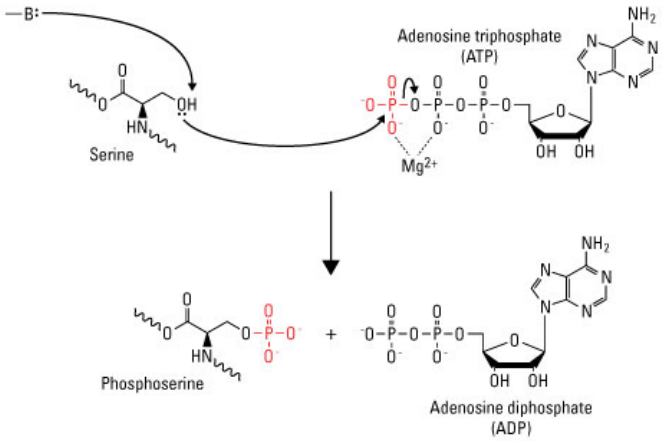

Figure 69: Serine becomes phosphorylated by transfer of the γ-phosphate group on ATP. The reaction is catalyzed by an enzyme (marked -B:). Breaking the phosphate-phosphate bond in ATP releases a large amount of energy and makes the reaction unidirectional. ATP needs to be regenerated, which requires metabolic energy. Figure from ThermoFisher

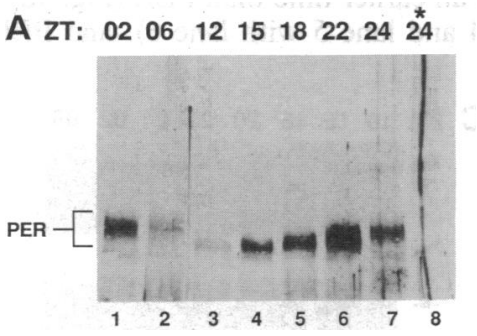

Figure 70: Western blot of PER protein at different circadian times ('Zeitgeber' time ZT, ZT=0 corresponds to onset of light) shows different expression levels (darkness) and increase in size (vertical shift) from ZT12 to ZT02. Western blots measure the size of molecules via electrophoresis in a gel using the dependence of the molecule mobility on its size. Using phosphatase that completely dephosphorylizes the PER showed that the change in molecular size is due to phosphorylation. (Edery et al., 1994)

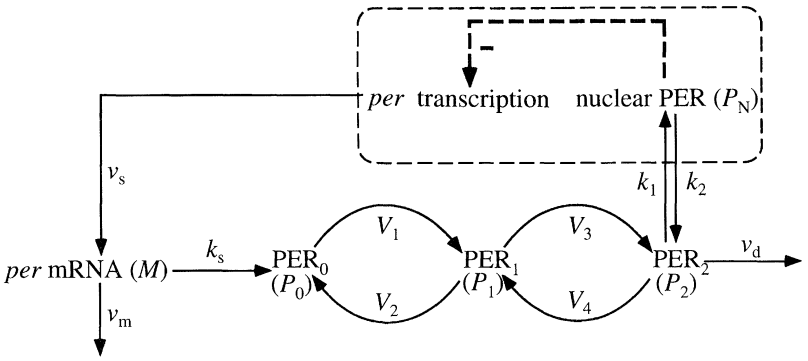

Figure 71: Reaction scheme underlying the Goldbeter model (Goldbeter, 1995). The subscript on PER$_{0,1,2}$ indicates the phosphorylation level of the PER protein.

Based on the experimental evidence Goldbeter proposed the following 'simple' model

$$
\begin{aligned}
\frac{dM}{dt} &= \nu_s \frac{K_1^n}{K_I^n + P_N^n} - \nu_m \frac{M}{K_m + M} \\
\frac{dP_0}{dt} &= k_s M - V_1 \frac{P_0}{K_1 + P_0} + V_2 \frac{P_1}{K_2 + P_1} \\
\frac{dP_1}{dt} &= V_1 \frac{P_0}{K_1 + P_0} - V_2 \frac{P_1}{K_2 + P_1} - V_3 \frac{P_1}{K_3 + P_1} + V_4 \frac{P_2}{K_4 + P_2} \\
\frac{dP_2}{dt} &= V_3 \frac{P_1}{K_3 + P_1} - V_4 \frac{P_2}{K_4 + P_2} - k_1 P_2 + k_2 P_N - \nu_d \frac{P_2}{K_d + P_2} \\
\frac{dP_N}{dt} &= k_1 P_2 - k_2 P_N
\end{aligned}
$$

where M is the *per* mRNA, $P_{0,1,2}$ represents the concentration of the PER protein at different phosphorylation levels, P_N is the concentration of nuclear PER protein.

Notes:

- The enzymatic phosphorylation is modeled by Michaelis-Menten kinetics.
- The model is in some sense an elaborated Goodwin model
  - negative feedback: repression of the first step (mRNA transcription) by the product (PER protein)
  - multiple phosphorylation steps lead to delay
- Only the doubly-phosphorylated PER degrades.
- Only the doubly-phosphorylated PER enters the nucleus. This introduces an additional delay compared to the case in which nuclear entry is also possible for monophosphorylated PER.
- As in the Goodwin model, the cooperativity of the negative feedback ($n > 1$) widens the parameter regime in which oscillations arise.

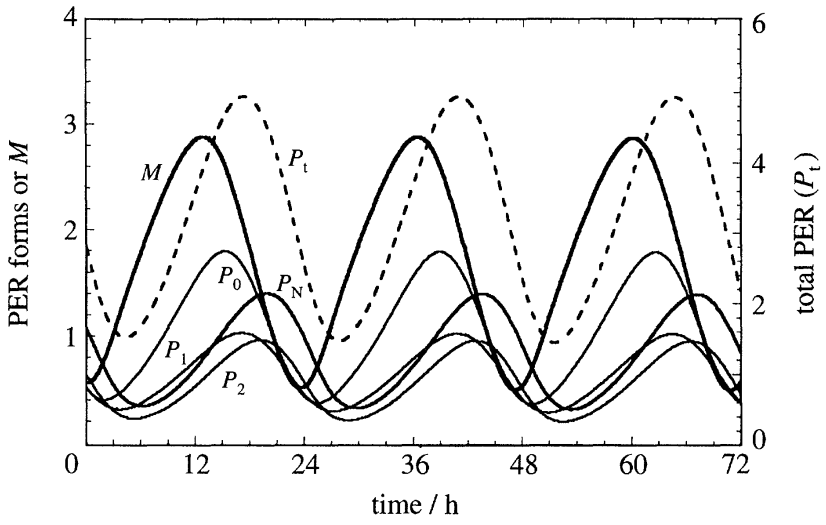

Figure 72: Circadian oscillations in the Goldbeter model (using $n = 4$). Note the delays with which concentrations of the phosphorylated PER rise. $P_t = P_0 + P_1 + P_2 + P_N$. (Goldbeter, 1995).

Mutations:

- One possible interpretation of the variation of the period with mutations of the *per* gene is via the degradation of the PER protein (by changing its structure):
  - with faster degradation it will take longer for enough *per* to accumulate to repress the transcription of its mRNA $\Rightarrow$ the period goes up in the model
- Other interpretations are possible. It is not clear whether the mechanism how the mutations change the period is understood yet.

More genes are involved in the circadian rhythm (e.g. *tim* ('timeless')) and other models capturing other aspects have been developed (e.g. Tyson model (Tyson et al., 1999)).

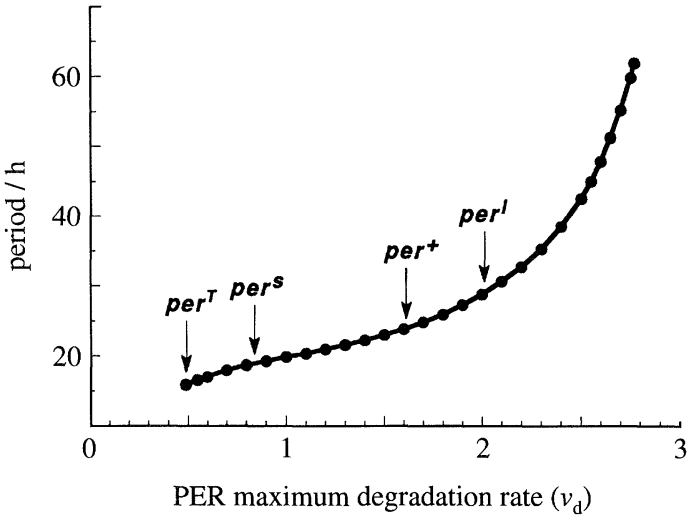

Figure 73: The period of the oscillation in the model increases with increasing degradation rate of PER. The arrows indicate putative values for the various mutants (Goldbeter, 1995).

If PER is a key part of the circadian clock it has to reflect the impact of the day-night cycle, its expression has to depend on light.

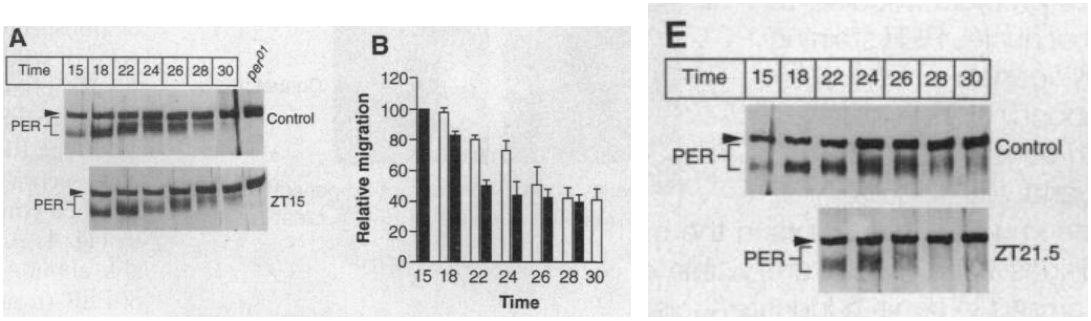

Figure 74: Western blot of PER protein at different circadian times and the impact of a 1-hour light pulse. A) Without light an increase in molecular weight is seen between T15 and T22 (upper border shifted up) and disappearance of smaller PER at T22 (bottom border disappears). Arrow head shows cross-reaction standard. B) Relative migration (in % of the distance between size standard and PER marks) for control (solid bars) and light-pulsed flies (open bars), showing the *delay* induced by the light pulse given at ZT15. E) A light pulse ZT 21.5 induces an *advance* of the phase (earlier disappearance of the band). (Lee et al., 1996).

How does the circadian clock know about daylight? How does it get entrained? TIM (=timeless), which interacts with PER, is degraded by light.

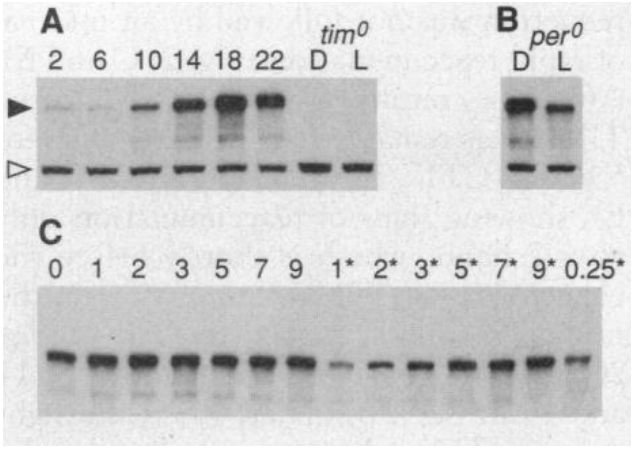

Figure 75: TIM is expressed circadianly and is degraded by light. (A) Solid arrow points to *tim* showing circadian expression. In *tim* null-mutant TIM is expressed neither at ZT19 nor at ZT7. (B) TIM is expressed also in *per* null-mutant. Its abundance is reduced with light (L vs. D), probably by degradation. (C) Even in the absence of *per* (in per^0-mutant), TIM is degraded by light (constant dark up to the starred numbers, which indicate the time since brief light exposure). Recovery from degradation within 5 hours (Myers et al., 1996).

Leloup and Goldbeter developed an enhanced model based on the reactions shown in Fig.76, which involve PER/TIM dimers. It is assumed that

- TIM is also phosphorylated in two steps with similar rates
- only the biphosphorylated forms of TIM and of PER are degraded
- only the biphosphorylated forms of PER and TIM dimerize
- only the PER-TIM complex enters the nucleus

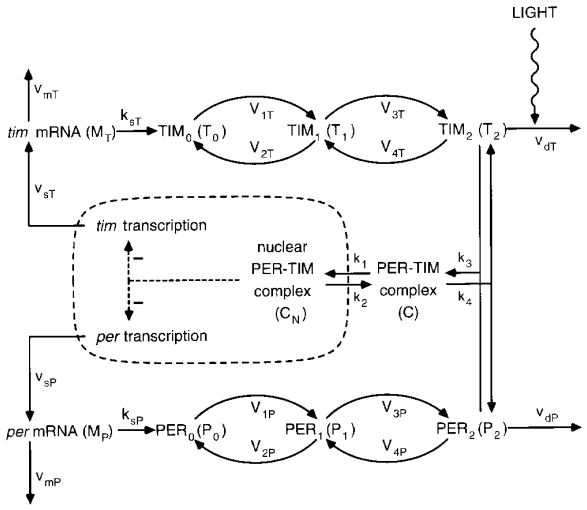

Figure 76: Model for circadian rhythm for Drosophila including TIM and PER. Light response via rapid degradation of TIM by light (Leloup and Goldbeter, 1998).

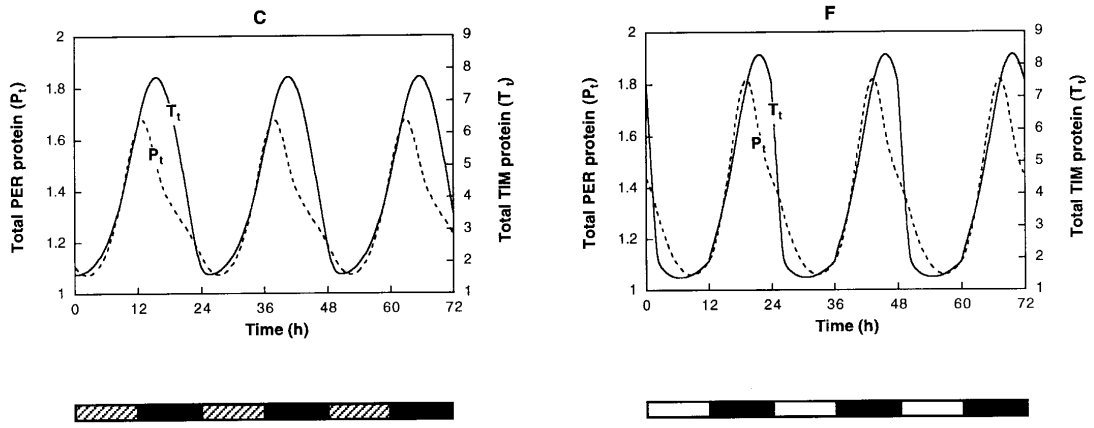

Figure 77: Comparison of model oscillations in PER and TIM without (c) and with L:D=12:12 light modulation. Note the faster degradation of TIM in the morning (Leloup and Goldbeter, 1998).

The impact of light on the circadian oscillator is commonly measured in terms of a phase-response curve $\Delta\phi(\phi_0)$:

- a brief light stimulus is given to the system at a given phase ϕ_0 during the oscillation
- the shift $\Delta\phi$ in the oscillation phase induced by the stimulus is measured as a function of ϕ_0

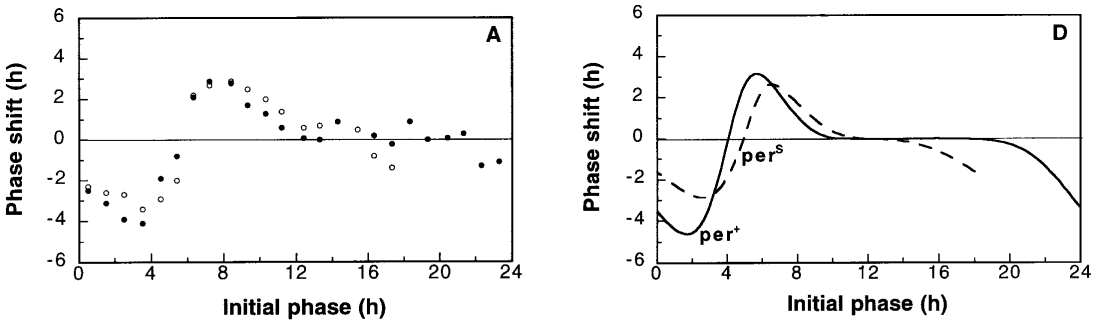

Figure 78: Phase-resetting curves for wildtype Drosophila (solid) and per^S Drosophila (open) (Hall and Rosbash, 1987) and in the PER-TIM model (solid/dashed) (Leloup and Goldbeter, 1998). Phase 0 corresponds to the beginning of the subjective night. Light early in the night (TIM is rising during that phase) delays the rhythm, later at night (TIM decreasing) it advances the rhythm; during the free-running subjective day (i.e. no light) light stimuli have little effect (TIM is close to its minimum anyway).

3.4.1 Jet Lag

The adjustment to a shift in the light-dark cycle takes time during which the different circadian rhythms of the body can get out of synchrony to some extent. This affects not only

travelers, but also shift workers and weekend party animals (social jet lag).

TABLE 1 Home team winning percentage depends on the direction of visitor's transcontinental travel

Visitor's direction of travel	No. of games	Games won	Winning %
No travel	712	385	54.1
East→west	194	109	56.2
West→east	175	110	62.9
Totals	1,081	604	55.9

	Home jet lag					Away jet lag				
Offense	West	West *P* value	Average	East	East *P* value	West	West *P* value	Average	East	East *P* value
Winning, %	−0.02 ± 0.016	0.112	0.539 ± 0.002	−0.035 ± 0.019	0.0335*	−0.01 ± 0.013	0.2295	0.461 ± 0.002	−0.021 ± 0.015	0.075
Runs scored	−0.098 ± 0.104	0.173	4.787 ± 0.015	−0.15 ± 0.121	0.1065	−0.018 ± 0.087	0.4165	4.652 ± 0.015	−0.011 ± 0.096	0.456
Batting average	−0.001 ± 0.003	0.372	0.265 ± 0.0004	−0.004 ± 0.003	0.074	−0.001 ± 0.002	0.2425	0.254 ± 0.0003	−0.001 ± 0.002	0.408
On-base, %	−0.001 ± 0.003	0.419	0.334 ± 0.0004	−0.003 ± 0.003	0.191	−0.002 ± 0.002	0.195	0.319 ± 0.0004	−0.00009 ± 0.002	0.486
Slugging, %	−0.002 ± 0.005	0.327	0.420 ± 0.0007	−0.01 ± 0.006	0.0415*	−0.002 ± 0.004	0.3215	0.400 ± 0.0007	−0.001 ± 0.004	0.412

Figure 79: Jet lag and baseball. a) Eastward travel reduces number of home runs (data 1991-1993) (Recht et al., 1995). b) Impact of jetlag on winning different for home and away jet lag (Song et al., 2017)

Figure 80: a) 'It is actually quite remarklable to me that the word "correlation" does not appear even once in the paper.....' writes (Joly, 2017) about (Song et al., 2017). *b) Spurious Correlations* by Tyler Vigen `http://www.tylervigen.com/spurious-correlations`

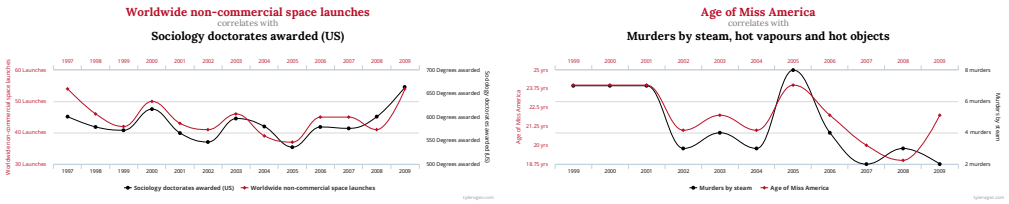

Figure 81: Correlations:
space launches/sociolgy PhD $r = 0.79$; Miss America/murders $r = 0.87$.
Spurious Correlations by Tyler Vigen.

Issue

- to what extent can other factors, i.e. non-circadian factors, be controled for?

- can one see a mechanism that could account for the correlation?
- can one modify that mechanism and confirm that this modifies the outcome as predicted?

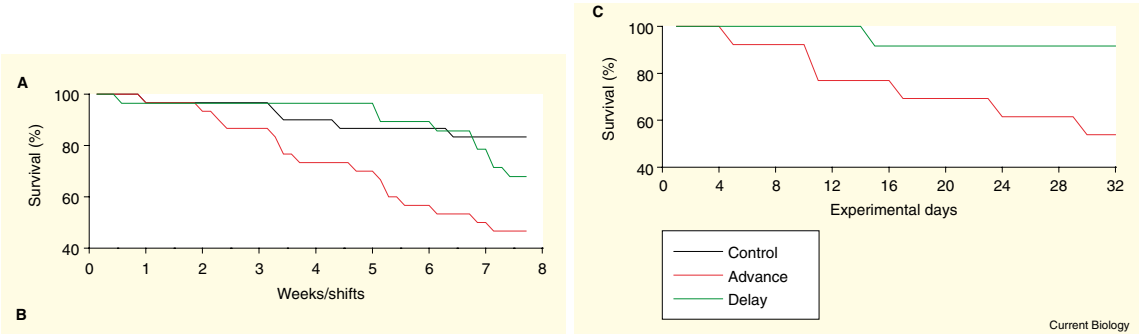

Figure 82: Effect of persistent jet lag on survival in mice. a) Weekly shift by 6 hours. b) Increased stress for more frequent shifts by 6 hours (every 4 days) (Davidson et al., 2006).

Other aspects

- the circadian clock is quite robust
- the period of the clock is quite independent of the temperature, even though all reaction rates vary with temperature; i.e. the circuit somehow compensates for temperature changes.

How is this robustness achieved?

3.5 Repressilator

To understand the behavior of natural genetic circuits is difficult, since they can involve many components, not all of which may be known. What are there design principles? What are the key elements? A different approach is to design synthetic circuits that involve only components that are not naturally present in the cell and study their properties.

An influential early example of this is the repressilator (Elowitz and Leibler, 2000), which consists of 3 sets of repressor-protein systems with the protein $i+1$ repressing the mRNA of protein i cyclically

$$\frac{dm_i}{dt} = -m_i + \frac{\alpha}{1+p_{i+1}^n} + \alpha_0 \tag{23}$$

$$\frac{dp_i}{dt} = -\beta\,(p_i - m_i)\,. \tag{24}$$

The principle is quite similar to that of the rock-paper-scissors system.

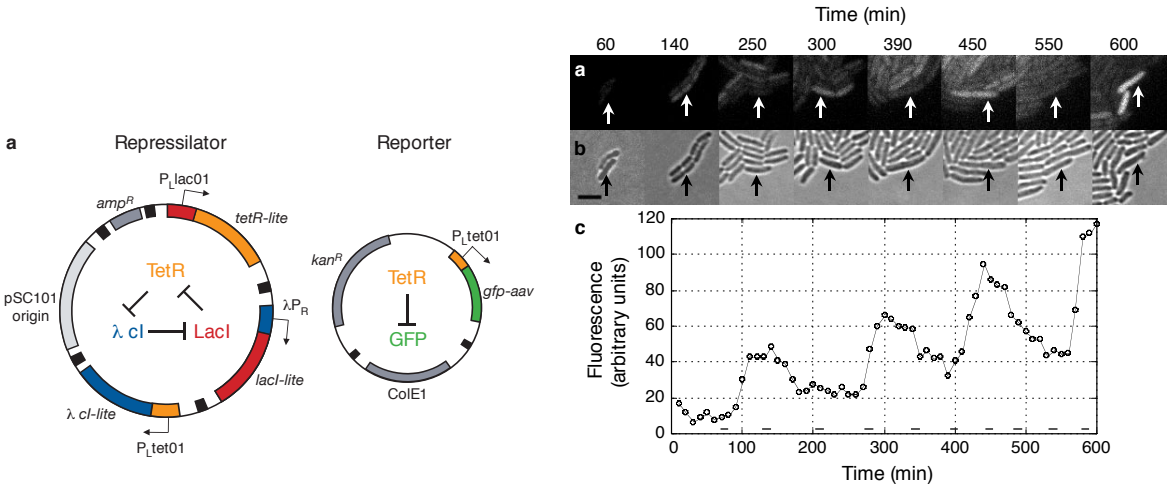

Figure 83: Repressilator designed in E. coli. Visualization of oscillations with GFP; signal from a single cell in bottom graph (Elowitz and Leibler, 2000).

In (23,24) it is assumed, for simplicity, that all three mRNA-protein sets are equivalent. In that case there is a fixed point with $m_i = m^{(0)}$ and $p_i = p^{(0)}$. Its linear stability can be determined relatively easily, because the Jacobian is cyclical, i.e. it does not change when indices are cyclically rotated.

Consider first a simpler case: for $\beta \to \infty$ the p-equation yields $p_i = m_i$ and the m-equation becomes

$$\frac{dm_i}{dt} = -m_i + \frac{\alpha}{1 + m_{i+1}^n} + \alpha_0$$

with linearization

$$\mathbf{L}^\infty = \begin{pmatrix} -1 & -\hat{\alpha} & 0 \\ 0 & -1 & -\hat{\alpha} \\ -\hat{\alpha} & 0 & -1 \end{pmatrix}$$

where

$$\hat{\alpha} = \frac{n\alpha \left(p_{i+1}^{(0)}\right)^{n-1}}{\left(1 + \left(p_{i+1}^{(0)}\right)^n\right)^2} < 0 \qquad p_{i+1}^{(0)} = m_{i+1}^{(0)}.$$

Because of the rotation symmetry shifting the eigenvector components cyclically must result in an eigenvector with the same eigenvalue, i.e. it must be a multiple of the unshifted vector

$$\begin{pmatrix} x \\ y \\ z \end{pmatrix} \to \begin{pmatrix} y \\ z \\ x \end{pmatrix} = \mu \begin{pmatrix} x \\ y \\ z \end{pmatrix}$$

The eigenvector therefore has the form

$$\begin{pmatrix} x \\ y \\ z \end{pmatrix} = \begin{pmatrix} 1 \\ \mu \\ \mu^2 \end{pmatrix}$$

For the eigenvector one gets then the conditions

$$\begin{aligned} -1-\hat{\alpha}\mu &= \lambda \\ -\mu-\hat{\alpha}\mu^2 &= \lambda\mu \\ -\hat{\alpha}-\mu^2 &= \lambda\mu^2 \end{aligned}$$

Eliminating λ one gets

$$-\hat{\alpha}-\mu^2=\left(-1-\hat{\alpha}\mu\right)\mu^2 \qquad \Rightarrow \qquad \mu^3=1 \quad \mu=e^{i\frac{2\pi}{3}j}\; j=0,1,2$$

and

$$\lambda_j=-1-\hat{\alpha}e^{i\frac{2\pi}{3}j} \qquad j=1\ldots 3$$

With $e^{i\frac{2\pi}{3}}=-\frac{1}{2}+i\frac{\sqrt{3}}{2}$ the fixed point is unstable to oscillations for

$$\hat{\alpha}>2.$$

For finite β, the full system is also cyclic and the linearization and the eigenvector have the form

$$\mathbf{L}=\begin{pmatrix} -1 & 0 & 0 & -\hat{\alpha} & 0 & 0 \\ \beta & -\beta & 0 & 0 & 0 & 0 \\ 0 & 0 & -1 & 0 & 0 & \hat{\alpha} \\ 0 & 0 & \beta & -\beta & 0 & 0 \\ 0 & \hat{\alpha} & 0 & 0 & -1 & 0 \\ 0 & 0 & 0 & 0 & \beta & -\beta \end{pmatrix} \qquad \mathbf{v}=\begin{pmatrix} u \\ v \\ \mu u \\ \mu v \\ \mu^2 u \\ \mu^2 v \end{pmatrix}$$

leading to

$$\mu^3=1$$

and

$$\lambda_j^2=\frac{(\beta+1)}{2}\left(-1\pm\sqrt{1-\frac{4\beta\left(1+\hat{\alpha}\mu_j\right)}{(\beta+1)^2}}\right)$$

which recovers for $\beta\to\infty$ the three eigenvalues above, while the other three eigenvalues diverge.

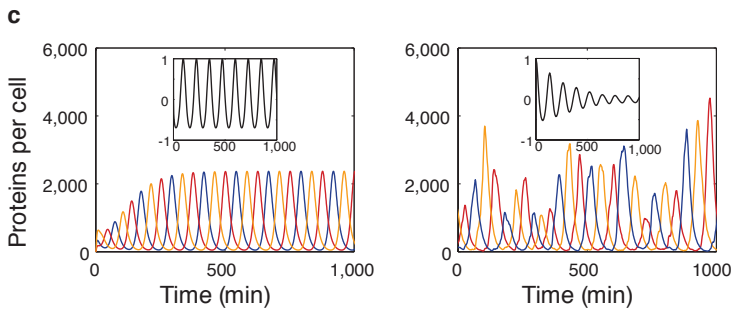

Figure 84: Simulations of the ODEs and of a stochastic version (using Gillespie algorithm), showing strong fluctuations (Elowitz and Leibler, 2000).

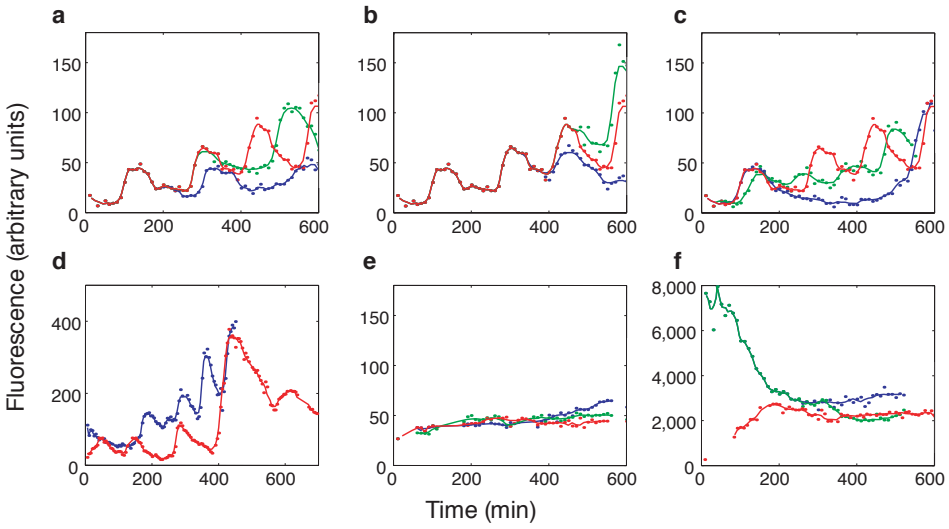

Figure 85: Oscillation period (160 ± 40 minutes) is longer than the cell cycle ($50 - 70$ minutes) and oscillations often remain correlated for some time in daughter cells (cf. Fig.83) before they diverge in phase and/or amplitude (Elowitz and Leibler, 2000).

Note:

- The oscillations in the repressilator are quite noisy
  - circadian oscillators seem to be more robust: what additional design elements do they have?

4 Calcium Oscillations[18]

Calcium in the cytoplasm plays an important role in controling a wide range of cell functions. It controls many aspects of cell dynamics

- muscle contractions
- gene transcription
  - plasticity in neuronal cells for learning and memory
- enzyme secretion
- apoptosis

In many cases it does so by binding to proteins and modifying their enzymatic properties. Its concentration within a cell is therefore very low most of the time to avoid interference with those enzyme functions. Signaling with calcium is achieved with well-controled, very brief changes in calcium concentration that are also quite localized within the cell. An important component of that control is binding of calcium to buffers and sequestering it into intra-cellular stores like the encoplasmatic reticulum (ER) (sarcoplasmatic reticulum in muscle cells).

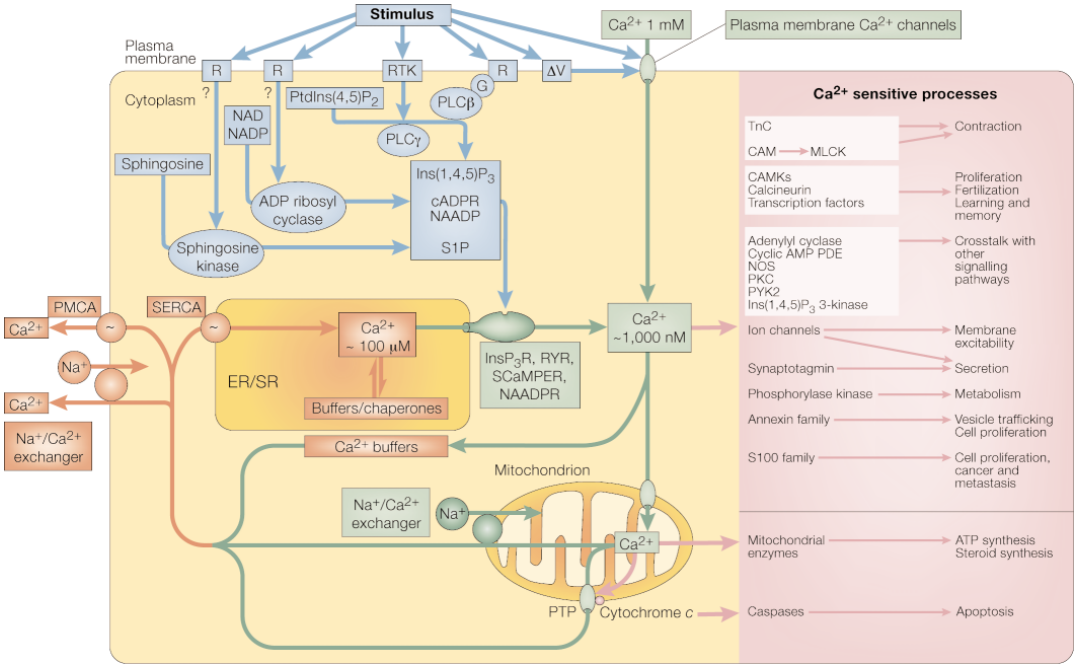

Figure 86: Very busy overview of the multiple functions of calcium in cells Berridge et al. (2000). One central feature is the storage of calcium in the endoplasmatic reticulum (ER) or the sarcoplasmic reticulum (SR) with calcium being pumped by SERCA and PCMCA pumps and released from the stores via RyR and other receptors.

[18](Fall et al., 2002) Ch.5

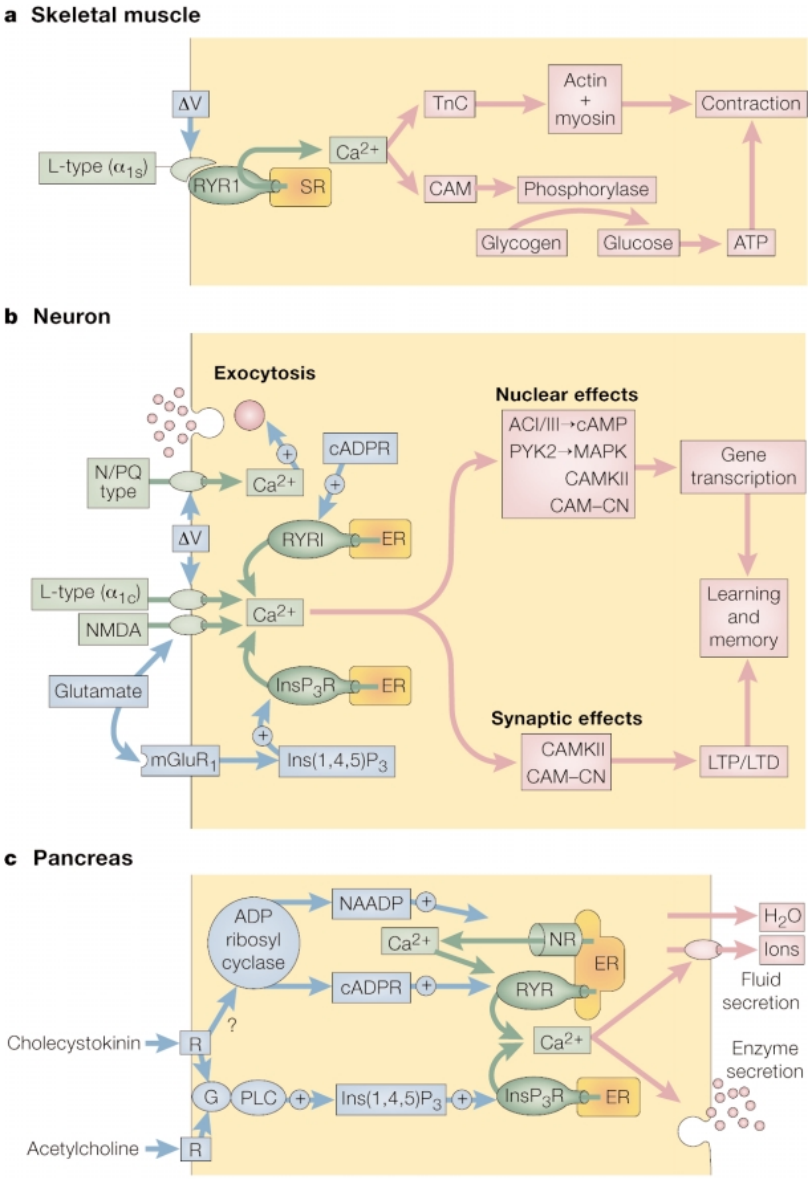

Figure 87: Some more details of specific functions of calcium Berridge et al. (2000).

Calcium can also be involved in communication between cells Leybaert and Sanderson (2012).

Calcium often exhibits oscillatory dynamics that reflect the release of calcium from the intracellular stores in response to an increase of the calcium concentration (calcium-induced calcium release).

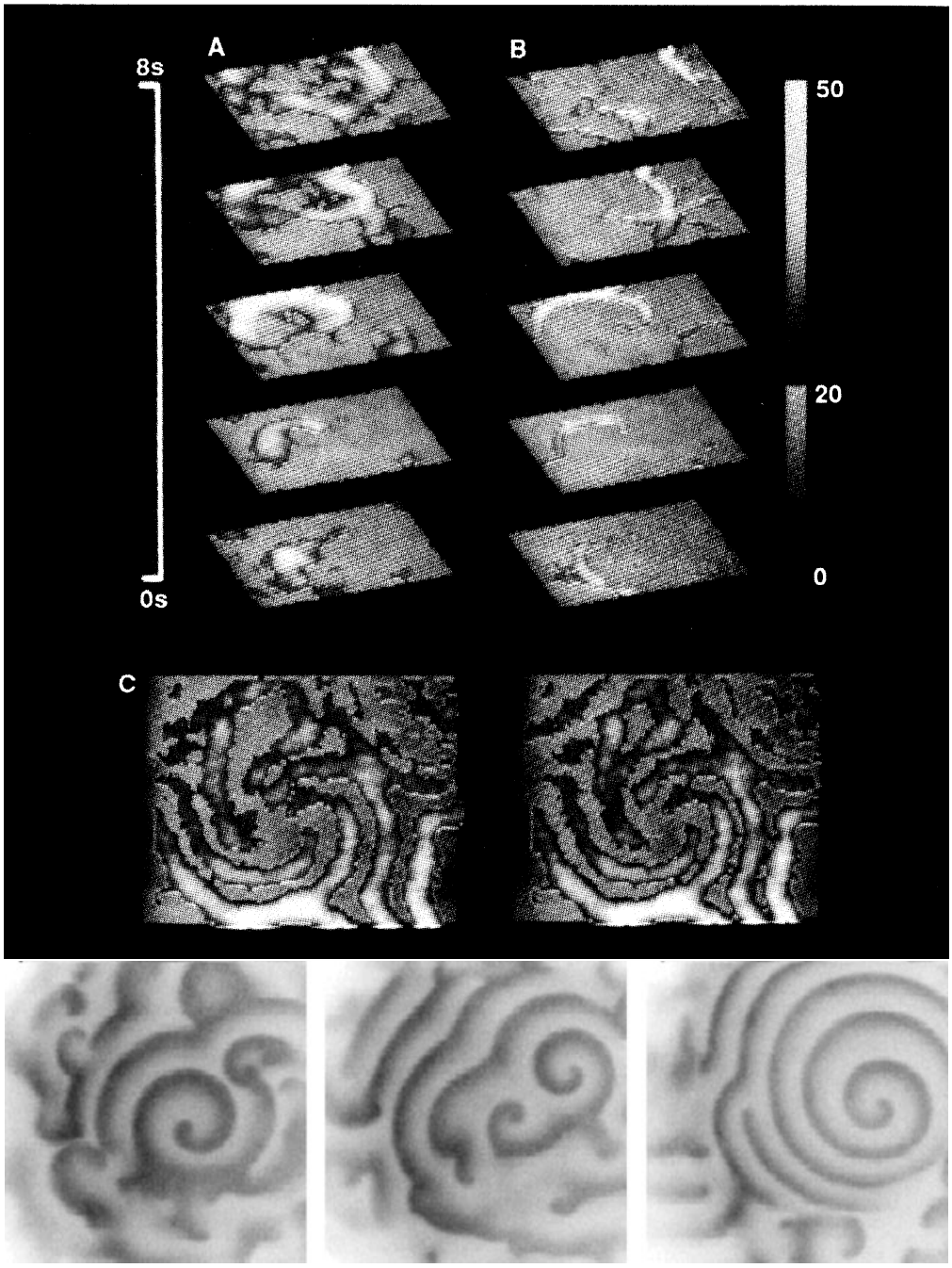

Figure 88: Oscillations in calcium concentration can take the form of spiral waves. a) Time sequence of waves within Xenopus oocyte cells, also shown as 3d image at the bottom (original paper) Lechleiter et al. (1991). b) Snapshots in later paper McGeown (2010).

To model calcium dynamics we need to model the buffering and the sequestering. The latter involves receptors (IP3R and RyR) that release calcium from the stores and pumps that pump it into the stores against a strong concentration gradient.

Consider a cell that contains a cytosolic compartment and an ER. We want to model the calcium dynamics in these interacting cell components

4.1 Rapid Buffering and Flux Balance

The cytosol of a cell as well as the ER contain buffers to which the calcium binds quickly. Therefore, when calcium enters that compartment a certain fraction of that calcium gets bound and only the remaining calcium is free calcium that is available for other reactions. We aim to get a relationship between the change in total calcium and in free calcium.

Consider the cytosol first (subscript i for inside the cytosol)

$$[Ca^{2+}]_i + [Ca^{2+}B]_i = [Ca^{2+}]_i^{tot} \tag{25}$$

$$[B]_i + [Ca^{2+}B]_i = [B]_i^{tot} \tag{26}$$

The buffer reaction is given by

$$[Ca^{2+}]_i + [B]_i \underbrace{\overbrace{\rightleftharpoons}^{k^+}}_{k^-} [Ca^{2+}B]_i$$

leading to the equations

$$\begin{aligned}
\frac{d[Ca^{2+}]_i}{dt} &= k^-[Ca^{2+}B]_i - k^+[Ca^{2+}]_i[B]_i \\
\frac{d[B]_i}{dt} &= k^-[Ca^{2+}B]_i - k^+[Ca^{2+}]_i[B]_i \\
\frac{d[Ca^{2+}B]_i}{dt} &= -k^-[Ca^{2+}B]_i + k^+[Ca^{2+}]_i[B]_i
\end{aligned}$$

Being linear, these equations have a single fixed point (steady state), at which the concentrations satisfy

$$[Ca^{2+}]_i = \frac{k^-}{k^+}\frac{[Ca^{2+}B]_i}{[B]_i} = K_i\frac{[Ca^{2+}B]_i}{[B]_i} \tag{27}$$

with

$$K_i \equiv \frac{k^-}{k^+}.$$

the dissociation constant of that reaction.

Note:

- For $K_i \gg 1$ the affinity of calcium to the buffer is small.

This fixed point is reached from any initial condition. The time it takes to do so depends on $k^{\pm}$: for large k^- and k^+ that time is short. If calcium influxes, say, are small, the concentrations can adjust fast enough to satisfy the equilibrium condition (27) very well at all times. Using (27) to eliminate $[Ca^{2+}B]_i$ from (25) yields then

$$[Ca^{2+}]_i^{tot} = \left(1 + \frac{1}{K_i}[B]_i\right)[Ca^{2+}]_i$$

Using

$$[B]_i^{tot} = \left(1 + \frac{1}{K_i}[Ca^{2+}]_i\right)[B]_i$$

one then gets

$$[Ca^{2+}]_i^{tot} = \left(1 + \frac{1}{K_i}\frac{1}{1+\frac{1}{K_i}[Ca^{2+}]_i}[B]_i^{tot}\right)[Ca^{2+}]_i = \left(1 + \frac{[B]_i^{tot}}{K_i + [Ca^{2+}]_i}\right)[Ca^{2+}]_i$$

The evolution of the calcium concentration is given by conservation laws for the total amount of calcium

$$\frac{d[Ca^{2+}]_i^{tot}}{dt} = \frac{1}{\bar{V}_i}\left(J_{PM}^{in} - J_{PM}^{out} - J_{ER}^{in} + J_{ER}^{out}\right) = j_{PM}^{in} - j_{PM}^{out} - j_{ER}^{in} + j_{ER}^{out}$$

where $\bar{V}_i$ is the volume of the cytosol and j_{PM} is the normalized flux across the cell membrane and j_{ER} the normalized flux across the ER membrane.

Analogously, for the concentration in the ER

$$\frac{d[Ca^{2+}]_{ER}^{tot}}{dt} = \frac{1}{\bar{V}_{ER}}\left(J_{ER}^{in} - J_{ER}^{out}\right) = \frac{\bar{V}_i}{\bar{V}_{ER}}\left(j_{ER}^{in} - j_{ER}^{out}\right),$$

normalizing the fluxes also by the cytosol volume rather than by the ER volume.

Through the fast buffering approximation the derivative of the total calcium can be expressed in terms of that of the free calcium

$$\frac{d[Ca^{2+}]_i^{tot}}{dt} = \frac{d[Ca^{2+}]_i^{tot}}{d[Ca^{2+}]_i}\frac{d[Ca^{2+}]_i}{dt} = \frac{1}{f_i([Ca^{2+}]_i)}\frac{d[Ca^{2+}]_i}{dt}$$

with

$$\frac{d[Ca^{2+}]_i^{tot}}{d[Ca^{2+}]_i} = 1 + \frac{[B]_i^{tot}}{K_i + [Ca^{2+}]_i} - \frac{[B]_i^{tot}[Ca^{2+}]_i}{\left(K_i + [Ca^{2+}]_i\right)^2} = 1 + \frac{K_i[B]_i^{tot}}{\left(K_i + [Ca^{2+}]_i\right)^2}$$

$$f_i([Ca^{2+}]_i) = \left(1 + \frac{K_i[B]_i^{tot}}{\left(K_i + [Ca^{2+}]_i\right)^2}\right)^{-1}$$

Notes:

- Low affinity buffers have large dissociation constants. For $K_i \gg [Ca^{2+}]$ one gets then

  $$f_i \approx \frac{1}{1 + \frac{[B]_i^{tot}}{K_i}}$$

  independent of $[Ca^2+]$.

- For large buffer concentrations f_i is small. Typical values are $f_i = 0.01 \ldots 0.05$.

The flux equation can then be written as

$$\frac{d[Ca^{2+}]_i}{dt} = f_i([Ca^{2+}]_i)\left(j_{PM}^{in} - j_{PM}^{out} - j_{ER}^{in} + j_{ER}^{out}\right) \tag{28}$$

and analogously

$$\frac{d[Ca^{2+}]_{ER}}{dt} = \frac{\bar{V}_i}{\bar{V}_{ER}} f_{ER}([Ca^{2+}]_{ER}) \left(j_{ER}^{in} - j_{ER}^{out}\right). \tag{29}$$

Note:

- With increasing buffer concentration the calcium dynamics become slower.

It is useful to introduce

$$\sigma = \frac{\bar{V}_{ER} f_i}{\bar{V}_i f_{ER}}$$

and write (29) as

$$\frac{d[Ca^{2+}]_{ER}}{dt} = \frac{f_i}{\sigma} \left(j_{ER}^{in} - j_{ER}^{out}\right)$$

Note:

- The buffering reduces the increase in the free calcium concentration arising from an influx. The compartment behaves as if it had a larger effective volume $\frac{\bar{V}_i}{f_i}$ and $\frac{\bar{V}_{ER}}{f_{ER}}$, respectively.
- σ gives the ratio between the effective volumens of the cytosol and the ER.

Combining (28) and σ times (29) yields

$$\frac{d}{dt}\left([Ca^{2+}]_i + \sigma[Ca^{2+}]_{ER}\right) = f_i \left(j_{PM}^{in} - j_{PM}^{out}\right).$$

Thus, the total free calcium concentration can be written as

$$[Ca^{2+}]_T = [Ca^{2+}]_i + \sigma[Ca^{2+}]_{ER}.$$

If there are no fluxes across the membrane $[Ca^{2+}]_T$ is constant and $[Ca^{2+}]_{ER}$ can be eliminated in favor of $[Ca^{2+}]_i$.

Note:

- To complete the dynamics we need to relate the fluxes to concentrations. For that we need models of pumps, leaks and receptors that drive the fluxes.

4.2 Model of the Ryanodine Receptor

The RyR is a key player in calcium-induced calcium release.

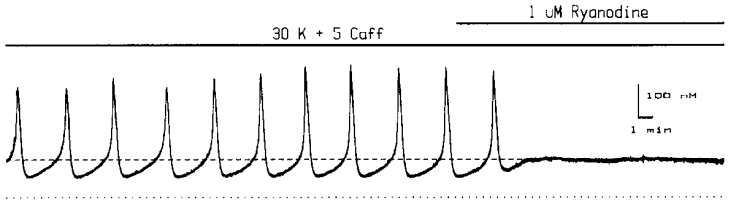

Figure 89: Oscillations in bullfrog sympathetic ganglion neuron involve calcium-induced calcium release (CICR), since they are blocked by applying ryanodine, which blocks the ryanodine receptor. The oscillations require that the ryanodine receptors are activated by caffeine (Friel and Tsien, 1992).

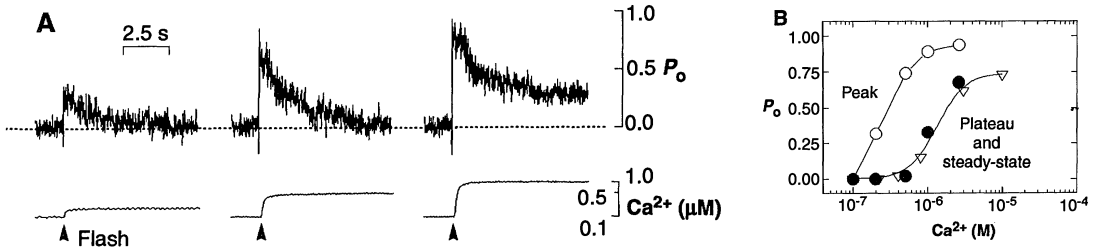

Figure 90: A) RyR respond to a step increase in the calcium concentration with a transient current and a plateau current. B) Dependence of the peak and plateau currents on the step size. (Friel and Tsien, 1992)

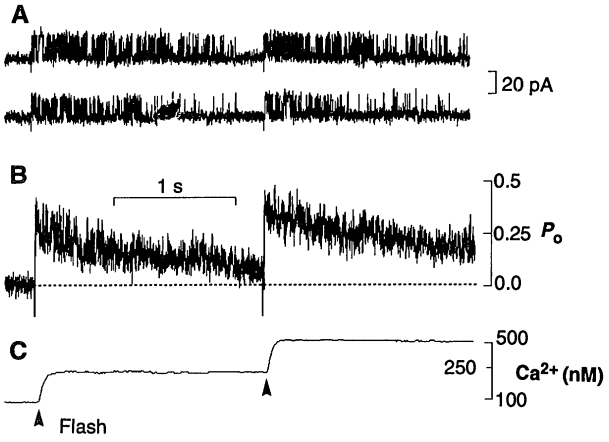

Figure 91: Response of RyR to two sequential puffs of calcium. Traces in A show opening events of a single channel. B: Calcium current averaged over many trials. C: calcium concentration. (Friel and Tsien, 1992)

The transient response of the current to an increase in calcium suggests that the Ryanodine receptor activates quickly but then adapt slowly and becomes inactivated with time.

Keizer and Levine developed a model of the ryanodine receptor that is based on 2 open states and 2 closed states (Keizer and Levine, 1996)[19]. The transitions in and out of the second closed state are slow and represent an inactivation of the receptor.

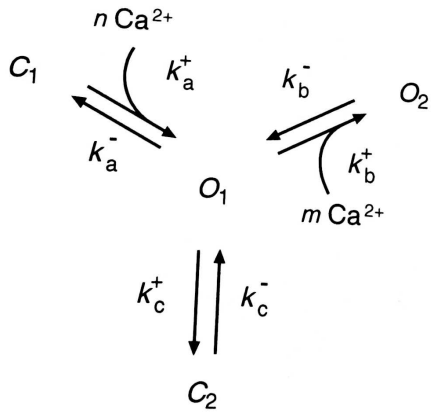

Figure 92: Sketch of the 2 open and 2 closed states of the ryanodine receptor and their transition probabilities (Fall et al., 2002).

Mass action yields equations for the probability of the receptor to be in that state or, equivalently, the mean fraction of the receptors to be in that state,

$$\begin{aligned}
\frac{dP_{C_1}}{dt} &= -k_a^+[Ca^{2+}]^n P_{C_1} + k_a^- P_{O_1} \\
\frac{dP_{O_1}}{dt} &= +k_a^+[Ca^{2+}]^n P_{C_1} - k_a^- P_{O_1} - k_b^+[Ca^{2+}]^m P_{O_1} + k_b^- P_{O_2} \\
&\quad -k_c^+ P_{O_1} + k_c^- P_{C_2} \\
\frac{dP_{O_2}}{dt} &= k_b^+[Ca^{2+}]^m P_{O_1} - k_b^- P_{O_2} \\
\frac{dP_{C_2}}{dt} &= +k_c^+ P_{O_1} - k_c^- P_{C_2}
\end{aligned}$$

The probabilities have to add up to 1 and the equation conserves that sum

$$P_{C_1} + P_{C_2} + P_{O_1} + P_{O_2} = 1 \qquad \frac{d}{dt}\left(P_{C_1} + P_{C_2} + P_{O_1} + P_{O_2}\right) = 0$$

This allows to us to eliminate one variable, e.g. P_{C_1}, from the equations

$$P_{C_1} = 1 - P_{O_1} - P_{O_2} - P_{C_2}.$$

Determine the fixed point for a given constant calcium concentration from the equations for P_{C_1}, P_{O_1}, and P_{O_2}; the equation for P_{C_2} is then automatically satisfied because of the

[19]The paper arose from the undergraduate honors thesis of Leslie Levine

conservation of the probability.

$$\begin{aligned}
\frac{dP_{O_1}}{dt} &= +k_a^+[Ca^{2+}]^n\,(1-P_{O_1}-P_{O_2}-P_{C_2}) - k_a^- P_{O_1} - k_b^+[Ca^{2+}]^m P_{O_1} + k_b^- P_{O_2} \\
&\quad -k_c^+ P_{O_1} + k_c^- P_{C_2} \qquad (30)\\
\frac{dP_{O_2}}{dt} &= k_b^+[Ca^{2+}]^m P_{O_1} - k_b^- P_{O_2} \qquad (31)\\
\frac{dP_{C_2}}{dt} &= +k_c^+ P_{O_1} - k_c^- P_{C_2} \qquad (32)
\end{aligned}$$

Straightforward algebra gives the unique solution to this linear 3×3 system. It is more compact to write the solution in terms the dissociation constants instead of the respective reaction rates $k^{\pm}_{a,b,c}$,

$$K_a^n = \frac{k_a^-}{k_a^+} \qquad K_b^m = \frac{k_b^-}{k_b^+} \qquad K_c = \frac{k_c^-}{k_c^+}.$$

Consider the dimensions of the dissociation constants (using $\{\}$ instead of $[]$ to denote dimensions)

$$\left\{k^-_{a,b,c}\right\} = \frac{1}{time} \qquad \left\{\frac{k_a^-}{k_a^+}\right\} = [Ca^{2+}]^n \qquad \left\{\frac{k_b^-}{k_b^+}\right\} = [Ca^{2+}]^m \qquad \left\{\frac{k_c^-}{k_c^+}\right\} = 1$$

Thus

$$\{K_a\} = \{K_b\} = [Ca^{2+}].$$

Note:

- Consider equilibrium between O_1 and O_2

$$P_{O_2} = \frac{k_b^+}{k_b^-}[Ca^{2+}]^m P_{O_1} = \left(\frac{[Ca^{2+}]}{K_b}\right)^m P_{O_1}.$$

  Thus, K_b gives the calcium concentration for which O_1 and O_2 are equally populated.

One then obtains

$$\begin{aligned}
P_{O_1} &= \frac{1}{\left(\frac{K_a}{[Ca^{2+}]}\right)^n + \left(\frac{[Ca^{2+}]}{K_b}\right)^m + 1 + \frac{1}{K_c}} \qquad (33)\\
P_{O_2} &= \frac{\left(\frac{[Ca^{2+}]}{K_b}\right)^m}{\left(\frac{K_a}{[Ca^{2+}]}\right)^n + \left(\frac{[Ca^{2+}]}{K_b}\right)^m + 1 + \frac{1}{K_c}} \qquad (34)\\
P_{C_2} &= \frac{\frac{1}{K_c}}{\left(\frac{K_a}{[Ca^{2+}]}\right)^n + \left(\frac{[Ca^{2+}]}{K_b}\right)^m + 1 + \frac{1}{K_c}} \qquad (35)
\end{aligned}$$

Important:

- The transitions to and from the inactivated state C_2 are slow, it therefore takes quite a while to reach this fixed point. That fixed point depends on $[Ca^{2+}]$.
- Does one have to solve the full 4 equations to describe the approach to this fixed point when $[Ca^{2+}]$ changes?
- Since the transition rates among O_1, O_2, and C_1 are fast, one can obtain a simplified description of the dynamics that results from changes in $[Ca^2+]$ using the rapid equilibrium approximation.

Consider explicitly the limiting situation

$$k_a^+[Ca^{2+}]^n \sim k_a^- \sim k_b^+[Ca^{2+}]^m \sim k_b^- \gg k_c^+ \sim k_c^-$$

Then P_{C_2} evolves much more slowly than P_{O_1} and P_{O_2} (and P_{C_1}).

Eq.(30) shows that P_{O_1} depends also on the slowly evolving P_{C_2} although it has high reaction rates. To get an idea of how to make use of this consider first a much simpler situation

$$\frac{dy}{dt} = -\lambda y + \cos t \qquad \lambda \gg 1. \tag{36}$$

Calculate the exact solution

$$y = y_h + y_p \qquad y_h = ae^{-\lambda t}$$

and

$$y_p = A\cos t + B\sin t$$

$$-A\sin t + B\cos t = -\lambda A\cos t - \lambda B\sin t + \cos t$$

$$A = \lambda B \qquad B = -\lambda A + 1 \qquad \Rightarrow \qquad A = \frac{\lambda}{\lambda^2+1} \quad B = \frac{1}{\lambda^2+1}$$

For any fixed time t

$$y = ae^{-\lambda t} + \frac{\lambda}{\lambda^2+1}\cos t + \frac{1}{\lambda^2+1}\sin t \quad \underbrace{\rightarrow}_{\lambda\to\infty} \frac{1}{\lambda}\cos t + \mathcal{O}\left(\frac{1}{\lambda^2}\right)$$

Thus, after the decay of the exponentially decaying transient, i.e. for $t \gg \frac{1}{\lambda}$, the solution is given to leading order by the balance between the terms on the r.h.s of (36), i.e. by the quasi-static fixed point

$$\lambda y = \cos t.$$

After a short transient of duration $\mathcal{O}\left(1/k_a^-\right)$, the fast variables P_{O_1} and P_{O_2} will reach the quasi-static fixed point given by

$$\frac{dP_{O_1}}{dt} = 0 = \frac{dP_{O_2}}{dt}$$

with P_{C_2} fixed.

Note that (30) includes also reaction terms $k_c^{\pm}$, which are small compared to the rest. We can ignore those terms when calculating the fixed point.

Simple algebra then gives

$$P_{O_1}^{(0)} = \frac{1}{1+\left(\frac{[Ca^{2+}]}{K_b}\right)^m + \left(\frac{K_a}{[Ca^{2+}]}\right)^n} \cdot w \qquad P_{O_2}^{(0)} = \frac{1}{1+\left(\frac{[Ca^{2+}]}{K_b}\right)^m + \left(\frac{K_a}{[Ca^{2+}]}\right)^n} \left(\frac{[Ca^{2+}]}{K_b}\right)^m \cdot w \tag{37}$$

with

$$w(t) = 1 - P_{C_2}$$

the fraction of receptors that are not inactivated.

We still need to determine $w(t) \equiv 1 - P_{C_2}(t) = P_{C_1} + P_{O_1} + P_{O_2}$. From (32) we get

$$\frac{dw}{dt} = k_c^-(1-w) - k_c^+ P_{O_1}$$

Since w evolves much more slowly than P_{O_1}, P_{O_1} is essentially always at the fixed point given by (37).

$$\begin{aligned}
\frac{dw}{dt} &= k_c^-(1-w) - k_c^+ \frac{1}{1+\left(\frac{[Ca^{2+}]}{K_b}\right)^m + \left(\frac{K_a}{[Ca^{2+}]}\right)^n} \cdot w \\
&= k_c^- \left\{ 1 - \left(1 + \frac{1}{K_c} \frac{1}{1+\left(\frac{[Ca^{2+}]}{K_b}\right)^m + \left(\frac{K_a}{[Ca^{2+}]}\right)^n} \right) w \right\} \\
&= k_c^- \left\{ 1 - \left(\frac{1+\left(\frac{[Ca^{2+}]}{K_b}\right)^m + \left(\frac{K_a}{[Ca^{2+}]}\right)^n + \frac{1}{K_c}}{1+\left(\frac{[Ca^{2+}]}{K_b}\right)^m + \left(\frac{K_a}{[Ca^{2+}]}\right)^n} \right) w \right\}
\end{aligned}$$

This can be written as

$$\frac{dw}{dt} = \frac{w_\infty - w}{\tau}$$

with

$$w_\infty = \left(\frac{1+\left(\frac{[Ca^{2+}]}{K_b}\right)^m + \left(\frac{K_a}{[Ca^{2+}]}\right)^n + \frac{1}{K_c}}{1+\left(\frac{[Ca^{2+}]}{K_b}\right)^m + \left(\frac{K_a}{[Ca^{2+}]}\right)^n} \right)^{-1} \qquad \tau = \frac{w_\infty}{k_c^-}.$$

The probability for the ryanodine receptor to be open is then given by

$$P_O(t) \equiv P_{O_1}(t) + P_{O_2}(t) = \frac{1+\left(\frac{[Ca^{2+}]}{K_b}\right)^m}{1+\left(\frac{[Ca^{2+}]}{K_b}\right)^m + \left(\frac{K_a}{[Ca^{2+}]}\right)^n} \cdot w(t) \tag{38}$$

where $[Ca^{2+}]$ is in general also a function of time.

Fitting to the experiments (Gyorke and Fill, 1993) leads to $n = 4$ and $m = 3$ and values for the reaction constants.

Dependence of the receptor on $[Ca^{2+}]_i$ in the steady state (33,34,35)

- For low $[Ca]_i^{2+}$

  - most receptors closed, very few inactivated since very few in O_1

$$P_{O_1} \sim [Ca^{2+}]_i^n \qquad P_{O_2} \sim [Ca^{2+}]_i^{n+m} \qquad P_{C_2} \sim [Ca^{2+}]_i^n \qquad w_\infty \sim 1$$

- For high $[Ca]_i^{2+}$
  - most receptors in O_2-state, very few inactivated since very few in $O_1$and C_2 cannot be reached from O_2

$$P_{O_1} \sim [Ca^{2+}]_i^{-m} \qquad P_{O_2} \sim 1 \qquad P_{C_2} \sim [Ca^{2+}]_i^{-m} \qquad w_\infty \sim 1$$

- Intermediate $[Ca]_i^{2+}$
  - significant fraction of receptors in $O_1$and therefore also significant fraction in C_2,

$$w_\infty < 1$$

Dependence of adaptation on $[Ca^{2+}]_i$

- Steps to large $[Ca^{2+}]_i$ should not lead to significant adaptation since $w_\infty \sim 1$
- Steps to intermediate $[Ca^{2+}]_i$ will lead to adaptation (i.e. overshoot in $[Ca^{2+}]_i$-flux) because a large fraction of receptors quickly go to O_1 and quickly equilibrate with O_2 (the relative populations of O_1 and O_2 depend on the dissociation constant K_b). The fraction that stays in O_1 equilibrate with C_2 on a longer time scale

Note:

- The rapid equilibrium approximation is valid as long as $[Ca^{2+}]$ does not change too fast to allow the fast variables to be close to the quasi-static fixed point (33,34,35).
- After brief, rapid changes in $[Ca^{2+}]$ there will be a transient during which the fast variables reach the fixed point (33,34,35) .

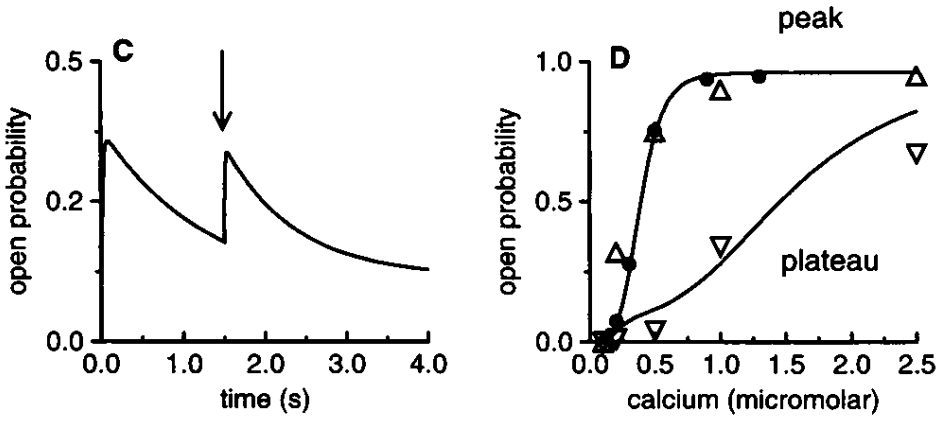

Figure 93: Keizer-Levine model for the RyR: response of Ryanodine receptor model to step increases in $[Ca^{2+}]$ Keizer and Levine (1996).

4.3 Bullfrog Sympathetic Ganglion Neuron Model: Closed Cell

The sympathetic ganglia are part of the autonomous (non-conscious) nervous system, which deals with food and breeding (para-sympathetic nervous system) and with stress response 'fight or flight' (sympathetic nervous system).

Many aspects of these basic functions are conserved among species. The bullfrog sympathetic ganglion neuron was apparently a good model system top study the effect of caffeine on neurons in the sympathetic nervous system Kuba and Nishi (1976).

The calcium concentration in the cytosol satisfies (cf. (28))

$$\frac{d[Ca^{2+}]_i}{dt} = f_i \left(j_{RyR}\left([Ca^{2+}]_i, w\right) + j_{leak}\left([Ca^{2+}]_i\right) - \underbrace{j_{SERCA}\left([Ca^{2+}]_i\right)}_{\text{pump}} \right)$$

The flux through the leak is driven simply by diffusion, i.e. by the difference in concentration in the cytosol and the ER,

$$j_{leak} = \nu_{leak}\left([Ca^{2+}]_{ER} - [Ca^{2+}]_i\right).$$

The ryanodine receptor releases calcium from the ER when its channel is open

$$j_{RyR} = \nu_{RyR} P_O([Ca^{2+}]_i, w)\ \left([Ca^{2+}]_{ER} - [Ca^{2+}]_i\right)$$

with $P_O([Ca^{2+}]_i, w)$ given by (38).

Here it is assumed that the RyR acts symmetrically , i.e. calcium is transported as easily out of the ER as into the ER. That results in the flux being proportional to the concentration gradient (difference).

The SERCA pump pumps calcium into the ER against a very large concentration difference. Its flux can well fitted by a Hill function

$$j_{SERCA} = \nu_{SERCA} \frac{[Ca^{2+}]_i^2}{[Ca^{2+}]_i^2 + K_{SERCA}^2}.$$

Together with

$$\frac{dw}{dt} = \frac{w_\infty\left([Ca^{2+}]_i\right) - w}{\tau\left([Ca^{2+}]_i\right)}$$

and the conservation of calcium

$$[Ca^{2+}]_{ER} = \frac{1}{\sigma}\left([Ca^{2+}]_T - [Ca^{2+}]_i\right)$$

we have a closed system of equations for w and $[Ca^{2+}]_i$

$$\begin{aligned} \frac{d[Ca^{2+}]_i}{dt} &= f_0\left([Ca^{2+}]_i; [Ca^{2+}]_T\right) + w \cdot f_1\left([Ca^{2+}]_i; [Ca^{2+}]_T\right) \\ \frac{dw}{dt} &= g_0\left([Ca^{2+}]_i\right) + w \cdot g_1\left([Ca^{2+}]_i\right) \end{aligned}$$

with $f_{0,1}$ depending on $[Ca^{2+}]_T$ as a control parameter.

Having 2 coupled ODEs allows a phase plane analysis.

The nullclines are given by

$$\begin{aligned} 0 &= f_0 + w f_1 \\ 0 &= g_0 + w g_1 \end{aligned}$$

The intersections of the nullclines give fixed points of the dynamics.

Depending on $[Ca^{2+}]_T$ the equations have 1 or 3 fixed points with saddle-node bifurcations changing the number of fixed points.

In particular, for intermediate $[Ca^{2+}]_T$ there is bistability:

- for low $[Ca^{2+}]_i$ only few RyR are open
- increasing $[Ca^{2+}]_i$ opens more RyR, which leads to more release of calcium from the ER, increasing $[Ca^{2+}]_i$ further, opening yet more RyR.

A linear stability analysis of the fixed points shows the stability as indicated in the bifurcation diagram.

There is also an oscillatory instability (Hopf bifurcation) near the lower saddle-node bifurcation point leading to *unstable* oscillations. For somewhat different parameters (of the SERCA pump) they can be made stable.

However

- The oscillations exist only over a very small range of $[Ca^{2+}]_T$.
- The period of the oscillations tends to be too short. It is controlled by $1/k_c^- = \mathcal{O}(10\text{s})$

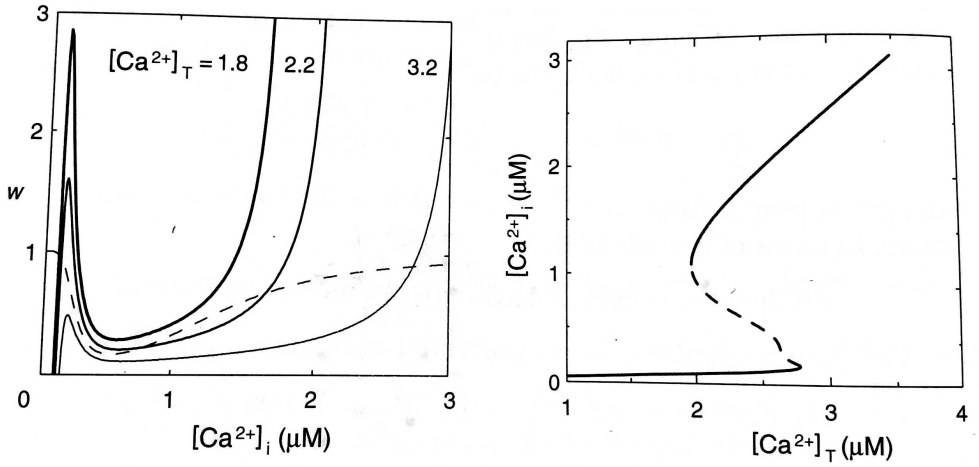

Figure 94: Phase plane and bifurcation diagram for the closed-cell model Fall et al. (2002).

4.4 Bullfrog Sympathetic Ganglion Neuron Model: Open Cell

Consider extension of the model to obtain robust oscillations.

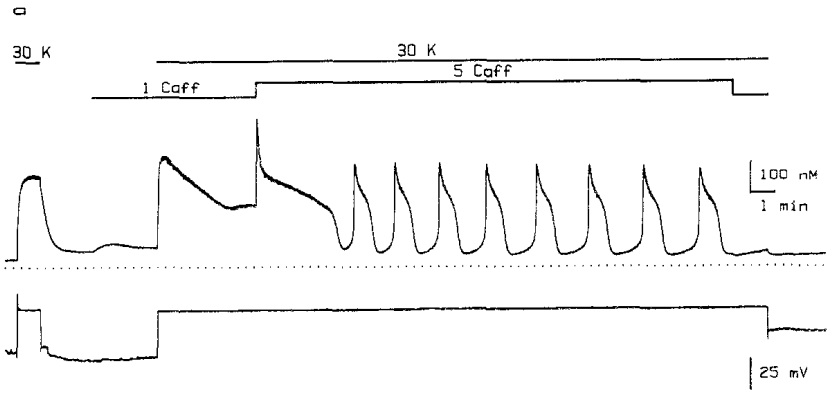

Figure 95: Oscillations require some depolarization of the cell (by reducing the impact of the hyperpolarizing K-conductance) and the application of caffeine. The membrane voltage is held constant Friel and Tsien (1992).

Since the oscillations require some depolarization of the cell, voltager-dependent calcium channels in the external cell membrane could play a role. Since the oscillations persist, when the membrane voltage is fixed (voltage clamp), it may be sufficient to allow a steady influx of calcium.

Consider the total calcium concentration

$$\frac{d[Ca^{2+}]_T}{dt} = f_i \left(\underbrace{j_{in}}_{\text{calcium channel}} - \underbrace{j_{PMCA}}_{\text{pump}} \right)$$

The PMCA pump (plasma membrane Ca^{2+}-ATPases) can reasonably modeled like the SERCA pump

$$j_{PMCA} = \nu_{PMCA} \frac{[Ca^{2+}]_i^2}{K_{PMCA}^2 + [Ca^{2+}]_i^2}.$$

For fixe membrane voltage j_{in} is just a fixed current.

The equation for $[Ca^{2+}]_i$ needs to be extended to include the membrane fluxed

$$\frac{d[Ca^{2+}]_i}{dt} = f_i \left(j_{RyR} + j_{leak} - j_{SERCA} + j_{in} - j_{PMCA} \right)$$

Together with the equation for $w(t)$ one has then three equations. Can they be simplified?

Experimentally, the oscillations have a period of $\mathcal{O}(1\text{min})$. The time constant for $w(t)$ is $\mathcal{O}(10\text{s})$. It is therefore reasonable to assume that $w(t)$ relaxes to w_∞ and follows it quite closely $\Rightarrow$ replace $w(t)$ by w_∞,

$$j_{RyR} = \nu_{RyR} P_O([Ca^{2+}]_i, w_\infty) \left([Ca^{2+}]_{ER} - [Ca^{2+}]_i \right).$$

The bifurcation diagram for $[Ca^{2+}]_i$ as a function of $[Ca^{2+}]_T$ can now be considered as the phase plane with the nullclines

$$[Ca^{2+}]_T \quad : \qquad j_{in} - \nu_{PMCA}\frac{[Ca^{2+}]_i^2}{K_{PMCA}^2 + [Ca^{2+}]_i^2} = 0 \quad \Rightarrow \quad [Ca^{2+}]_i = \text{const.}$$

$$[Ca^{2+}]_i \quad : \qquad j_{RyR} + j_{leak} - j_{SERCA} + j_{in} - j_{PMCA} = 0$$

The fixed-point branch of Fig.94 amounts to the nullcline of $[Ca^{2+}]_i$.

When the nullcline of $[Ca^{2+}]_T$ intersects that of $[Ca^{2+}]_i$ on the intermediate branch one obtains a periodic orbit as indicated

- On the lower branch $[Ca^{2+}]_T$ increases and state follows the lower branch until that branch turns around (saddle-node bifurcation)
- Then $[Ca^{2+}]_i$ increases rapidly and the system goes to the upper branch.
- Since the upper branch is on the other side of the nullcline for $[Ca^{2+}]_T$, $[Ca^{2+}]_i$ decreases until it reaches the end of that branch
- There $[Ca^{2+}]_i$ decreases rapidly and the system goes back to the lower branch.

Note:

- Since $\nu_{PCMA} \ll \nu_{SERCA}$ the evolution along the branches is much slower than the jumping between the branches.
- Such Oscillations are called *relaxation oscillations*.
- The separation of time scales of the evolution along the branches and between branches allows an understanding of the oscillations based on the quasi-static bifurcation diagram.

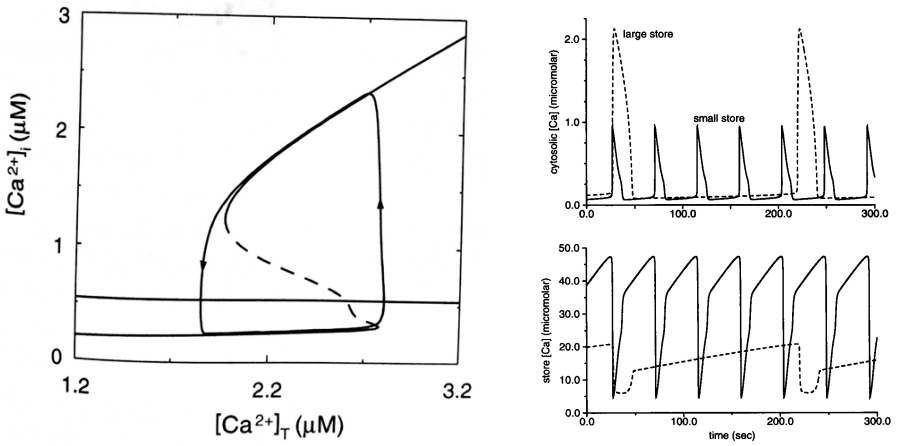

Figure 96: Relaxation oscillations in the open-cell model. a) Nullclines and periodic orbit in the phase plane Keizer and Levine (1996). b) As typical for relaxation oscillations, the oscillations are strongly nonlinear (anharmonic) Fall et al. (2002).